

UCSF

UC San Francisco Electronic Theses and Dissertations

Title

Transcriptomic Dissection of Non-Coding RNA Circuits in Cytotoxic T Cells and Th2 Responses in Human Allergic Asthma

Permalink

<https://escholarship.org/uc/item/0qg0v6hm>

Author

Wheeler, Benjamin David

Publication Date

2023

Peer reviewed|Thesis/dissertation

Transcriptomic Dissection of Non-Coding RNA Circuits in Cytotoxic T Cells and Th2 Responses in Human Allergic Asthma

by
Benjamin Wheeler

DISSERTATION
Submitted in partial satisfaction of the requirements for degree of
DOCTOR OF PHILOSOPHY

in
Biomedical Sciences

in the
GRADUATE DIVISION
of the
UNIVERSITY OF CALIFORNIA, SAN FRANCISCO

Approved:

DocuSigned by:

Alexander Marson

Alexander Marson

7F25CDCE383C4A8...

Chair

DocuSigned by:

K. Mark Ansel

K. Mark Ansel

DocuSigned by:

Jeroen Roose

Jeroen Roose

DocuSigned by:

Adrian Erlebacher

Adrian Erlebacher

F0E47A73FD8E419...

Committee Members

Dedication

The work published here is dedicated to my wife, Zeynep Cakir Wheeler PhD. Without her none of this is possible, and her constant support and pure heart are my inspirations.

Acknowledgements

There are innumerable people who made this work possible and they are endowed with my deepest gratitude. As I look back upon my scientific journey, I am humbled by the support I have received at every turn and how much I have grown as a person and scientist in this process. The little boy fascinated by desert birds in Arizona can scarcely believe he is here writing this document.

From the beginning, my parents David and Sally Wheeler have been instrumental in fostering my curiosity and supporting all of my academic goals. I was extremely lucky to have their support from multiple scientific trips to Wyoming in middle school to multiple degrees at institutions hundreds of miles from St. Louis. My sister Claire Wheeler has always been there for me since day 594, and I am so thankful she has always kept it real with me and when times have been tough she can always bring a smile to my face. One of the happiest occasions of my graduate school career is that my family has now expanded to include my wife and all my in-laws in Turkey. My wife Zeynep Cakir Wheeler PhD has a heart of gold and is always my inspiration to do everything with more compassion. I owe so much of the success of these projects to her unwavering love, support, and partnership. I am so thankful for all the support from my brother-in-law Orhan Saylak, sister-in-law Ayse Cakir Saylak, and mother-in-law Seval Cakir. That they have welcomed me so warmly is a true gift and has made every challenge during my PhD much more bearable.

I also want to thank all those who contributed to my scientific and personal growth prior to graduate school. Peter Searson PhD gave me my first real research experience and through the mentorship of Yu-Ja Huang PhD I learned many foundational wet lab techniques. I was able to build on these skills and begin to gain more independence at Confluence Discovery Technologies. The whole team there was fantastic but I particularly want to thank Joseph Monahan PhD for his encouragement that a PhD was the right career path for me, Heidi Hope

PhD for her mentorship at the bench and encouragement to apply to UCSF, Jeff Hirsch for giving me opportunities to grow, and Sheri Bonar for helping keep my head on straight.

Of course in my time at UCSF there have been many many people who have helped me, taught me, mentored me, and been excellent role models for me to emulate. I would be remiss if this list didn't start immediately with my PhD advisor, Mark Ansel PhD. Mark has been everything a PhD mentor should be. Mark was always understanding of all the challenges involved in completing this work both in and out of the lab. Further, his ability to convey his knowledge while also allowing me to independently derive and test my own ideas has allowed me to grow immensely in the production of this work. The entire Ansel Lab has been a great group of people to weather not only a PhD with but also the COVID-19 pandemic, and for that we will have a lifelong bond. In particular Didi Zhu PhD and Priscila Muñoz-Sandoval (soon to be PhD) have been wonderful colleagues, classmates, and friends. They helped me to contemplate and do a lot of the work presented here and for that I am eternally grateful. Their camaraderie has been indispensable in navigating the challenges of a PhD and without them it would have been much much harder to reach this point. I also want to thank lab managers Simon Wong and Simon Zhou for navigating the lab throughout the years both normal and pandemic times, their help was essential to making progress in an efficient and orderly way. Finally, Eric Wigton PhD and Marlys Fasset MD PhD were always fantastic sources of wisdom and they went above and beyond to keep our mouse colonies in shape during the pandemic, which was probably both literally and figuratively a life saver.

Outside of the Ansel Lab I would like to thank our collaborators in the Spitzer, Fong, and Woodruff labs. Thanks to Larry Fong MD PhD, Matt Spitzer PhD, and Prescott Woodruff MD for their embodiment of the collaborative spirit of UCSF and willingness to contribute to my projects. Rachel Debarge and Marcel Arias-Badia PhD have been wonderfully helpful and I sincerely appreciate all the time and effort they put into the work presented here. Nirav Bahkta MD, Jingming Wang, Srilaxmi Nerella, Stephanie Christenson MD, and Kristina Johansson from the

Woodruff lab have been incredibly gracious for allowing me to get involved in the ACE study and contributing to the study design, sample collection, and analysis for the manuscript that is now in preparation. I would also like to acknowledge the previous Sanjabi Lab and Roan Lab for their willingness to share their supply of LCMV armstrong, which was absolutely a cornerstone to producing this work.

I also thank the members of both my qualifying exam committee and thesis committee. Julie Zikherman MD PhD, Stephen Floor PhD, and Shomyseh Sanjabi PhD all served on my qualifying exam committee and I am so thankful for their help and flexibility in getting all this started exactly in the heart of the pandemic. Adrian Erlebacher MD PhD served as the chair of that committee and has since been a member of my thesis committee and I am extremely thankful for his dedication to my training and his careful approach to scientific investigation that has taught me a lot. Jeroen Roose PhD has been a fixture of my time at UCSF from rotating in his lab, to serving on my committee, and his leadership as part of ImmunoX. I am so thankful for the energy and collegiate spirit he brought to all these endeavors that shaped my experiences at UCSF so much for the better. Finally, Alex Marson MD PhD has served as the chair of my thesis committee and I am very grateful for his service there and his keen perspective for synthesizing engineering and scientific questions has taught me a lot.

Dear reader, thank you. It is an incredible privilege to do work that can benefit or be of use to anyone else. I am honored by your interest in this document, and within it I hope you find inspiration and investigation of note. Please enjoy.

Contributions

The text in chapter 1 is a modified version of a review in preparation for Trends in Immunology. The following authors contributed to the manuscript: Wandi S. Zhu and K. Mark Ansel. Wandi wrote sections focused on RNA binding proteins and created the associated figure, as well as provided brainstorming and editing guidance for the section on lncRNAs. Mark provided brainstorming and editing guidance as well as manuscript writing throughout

The text in chapter 2 is a modified preprint available on bioRxiv and underreview at *eLife* that can be found here: <https://www.biorxiv.org/content/10.1101/2023.04.14.536843v1>. The following authors contributed to the study: John D. Gagnon, Wandi S. Zhu, Priscila Muñoz-Sandoval, Simon K. Wong, Dimitre R. Simeonov, Zhongmei Li, Rachel Debarge, Matthew H. Spitzer, Alexander Marson, and K. Mark Ansel. John derived the miR-15/16^{ΔΔ} mice and in collaboration with Dimitre, Zhongmei, and Alex generated the *Malat1^{scr/scr}* mice. Wandi, Priscila, and Simon facilitated the execution of experiments, in particular the *in vivo* mouse experiments. Rachel and Matthew collaborated with us to do the *Listeria Monocytogenes* infections. Mark helped with experiment design, data interpretation, and manuscript writing.

The text in chapter 3 is a manuscript in preparation. The following authors contributed to the study: Jingming Wang, Srilaxmi Nerella, Stephanie Christenson, Nirav Bhakta, Prescott Woodruff, Priscila Muñoz-Sandoval, Kristina Johansson, Thomas Mazumder, and K. Mark Ansel. Prescott and Nirav designed the clinical study, enrolled subjects, and collected samples. Jingming processed samples, collected data, and analyzed the data for cytof. Srilaxmi, Stephanie, and Kristina analyzed and interpreted RNAseq data. Priscila aided in the sorting and sample preparation for scRNA-seq. Thomas Mazumder aided in the processing and analysis of scRNAseq samples. Mark, Nirav, and Prescott assisted in the design and interpretation of experiments as well as manuscript writing.

Epigraph

“Two there are who are never satisfied: the lover of the world and the lover of knowledge”

-Rumi

Transcriptomic Dissection of Non-Coding RNA Circuits in Cytotoxic T Cells and Th2 Responses in Human Allergic Asthma

Benjamin Wheeler

Abstract

T cells constitute an essential component of the adaptive immune response to immunogenic antigens both endogenous and exogenous such as those from allergens or viral infections. We present here two studies of T cells, one in which we investigate a non-coding RNA circuit in the control of cytotoxic T cells and one in which we characterize allergen reactive T helper cells in human allergic asthmatic subjects. Proper activation of cytotoxic T cells via the T cell receptor and the costimulatory receptor CD28 is essential for adaptive immunity against viruses and intracellular bacteria. Through biochemical analysis of RNA:protein interactions, we uncovered a novel non-coding RNA circuit regulating cytotoxic T cells composed of the long non-coding RNA (lncRNA) Malat1 (Metastasis Associated Lung Adenocarcinoma Transcript 1) and the microRNA family miR-15/16. miR-15/16 is a widely and highly expressed miRNA family important for cell proliferation and survival. miR-15/16 also play important roles in T cell responses to viral infection, including the regulation of antigen-specific T cell expansion and T cell memory. Comparative Argonaute-2 high throughput sequencing of crosslinking immunoprecipitation (AHC) combined with gene expression profiling in normal and miR-15/16-deficient T cells revealed a network of several hundred direct miR-15/16 targets, many with functional relevance for T cell activation, survival and memory formation. Among these targets, the long non-coding RNA Malat1 contained the largest absolute magnitude miR-15/16-dependent AHC peak in T cells. This binding site was also among the strongest lncRNA:miRNA interactions detected in the T cell transcriptome. We used CRISPR targeting with homology directed repair to generate mice with a 5-nucleotide mutation in the miR-15/16 binding site in Malat1. This mutation interrupted Malat1:miR-15/16 interaction, and enhanced the repression of

other miR-15/16 target genes, including CD28. Interrupting Malat1 interaction with miR-15/16 decreased cytotoxic T cell activation, including the expression of IL-2 and a broader CD28-responsive gene program. Accordingly, Malat1 mutation diminished memory cell persistence following LCMV Armstrong and *Listeria monocytogenes* infection. This study marks a significant advance in the study of lncRNAs in the immune system by ascribing cell-intrinsic, sequence-specific *in vivo* function to Malat1. These findings have implications for T cell-mediated immunity, as well as lung adenocarcinoma and other malignancies where Malat1 is overexpressed. Beyond cytotoxic T cells, T helper cells can differentiate into distinct states marked by stereotypical cytokine expression. In the context of allergic diseases type 2 helper T cells which produce the type 2 cytokines, IL-5, IL-4, and IL-13 can become pathogenic and contribute to a consistently elevated level of type 2 inflammation. In asthma, the lung is the primary site of aberrant inflammation and understanding how this tissue responds to allergens is key. In this study, human subjects were locally exposed to allergen via bronchoscopy. We then assayed the immunological and cellular state of these bronchoscopy samples by multiple high dimensional 'omic' technologies: RNAseq, Cytof, and scRNAseq. We then define heterogeneity across these allergic subjects corresponding to type 2 high and type 2 low individuals. In the type 2 high individuals we find that inflammatory monocyte derived populations enter the lung and induce the expression of inflammatory chemokines CCL3, CCL17, and CCL22 likely contributing to increased inflammation in the lung. Further, through scRNAseq we are able to identify Th2 cells recruited specifically by the allergen challenge. In a subset of individuals we could identify TCR clones which were allergen reactive and expanded in the blood post allergen challenge. Indicating that, while these cells are rare in the lung, dampening their function systemically may lead to decreased local inflammation in the lung as well. Understanding all these facets of allergic inflammation in this detailed way is essential for proper clinical understanding of asthma as well as the potential development of novel therapeutic strategies.

Table of Contents

Chapter 1: RNA Circuits in T Cells	1
Abstract	1
Introduction.....	1
RNABinding Proteins.....	2
Long Noncoding RNAs.....	11
Genomic and Transcriptomic Editing Approaches for Dissection of lncRNA and RBP Function	17
Concluding Remarks and Overview of Thesis	19
Figures	21
Chapter 2: The lncRNA Malat1 Inhibits miR-15/16 to Enhance T Cell Activation and Memory Formation	25
Abstract	25
Introduction	26
Results.....	29
Discussion	41
Materials and Methods.....	44
Figures	50
Tables	73
Chapter 3: High Dimensional Profiling Resolves Alveolar Inflammation in Allergen Challenged Allergic Asthmatics	79
Abstract	79

Introduction	79
Results	81
Discussion	92
Materials and Methods.....	95
Figures	100
Tables.....	117
Chapter 4: Conclusion.....	121
References.....	123

List of Figures

1.1 Techniques in dissecting RBP:RNA interactions	21
1.2 Functions of lncRNAs in T cells	23
2.1 Malat1 is highly bound by miR-15/16	51
2.2. Malat1 Inhibits miR-15/16 binding and suppressive activity	53
2.3 The Malat1-miR-15/16 Circuit Increase CD28 Expression and Co-stimulation induced Gene Expression	55
2.4 The Malat1-MiR-15/16 circuit increases functional outcomes of CD28 co-stimulation	57
2.5 Malat1 enhances memory T cell persistence following LCMV infection	59
2.6 Malat1 and miR-15/16 alter memory T cell differentiation following <i>Listeria</i> <i>Monocytogenes</i> infection	61
2.7 Malat1 Enhances Pro-survival Cues Downstream of T cell activation	63
S2.1 <i>Malat1^{scr}</i> allele does not disrupt other miRNA families	65
S2.2 CD28 responsive genes are induced by α CD28 stimulation in all genotypes tested	67
S2.3 Malat1 Regulates Memory Formation in Unchallenged Polyclonal Animals	69
S2.4 Malat1 is epistatic to miR-15/16 in the regulation memory cell expansion following LCMV infection	71
3.1 Allergen Challenge Induces Leukocyte Infiltration into the BAL.....	100
3.2 Cytof Resolves Type 1 – Type 2 Axis of Response to Allergen Challenge.....	102
3.3. IL-13 Responsive Genes are Induced by Allergen Challenge and Highest in Subjects with Type 2 High BAL Infiltration.....	104
3.4 scRNAseq on Enriched CD4+ T cells Resolves Allergen Induced Th2 Cells.....	106
3.5 Expanded Th2 Clones are Allergen Reactive and Expand in the Blood Post-Challenge..	108
3.6 scRNAseq Defines Non-Granulocyte, Non-CD4+ T Cell Populations.....	111

3.7 Allergen Induces T Cell Recruiting Chemokine Expression in Monocyte	
Derived Populations.....	113
S3.1 Sorting strategy for CD4+ enrichment and granulocyte depletion prior to scRNAseq....	115

List of Tables

2.1 lncRNAs with the most AHC reads.....	73
2.2 lncRNAs with the most AHC reads that do not align to rRNA repeat elements.....	74
2.3 T Cell Activation Genes Affected by Malat1-miR-15/16 Circuit.....	75
2.4 Key Reagent Table.....	76
3.1 10X scRNAseq samples assayed.....	117
3.2 SNPs used for sample identification.....	117
3.3 Assigning cells from homogeneous data sets to individuals defined via unbiased demultiplexing of heterogeneous samples.....	117
3.4 Cross referencing assignments of cells from two independent heterogeneous samples containing the same individuals.....	118
S3.1 Key Reagents Used	118
S3.2 Antibodies used for cytof staining and analysis.....	119

List of Abbreviations

AC, Visit 3 allergen challenge samples

AHC, Argonaut 2 high throughput sequencing crosslinking immuno precipitation

α CD28, CD28 crosslinking and stimulating antibody

α CD3, CD3 crosslinking and stimulating antibody

BL, Visit 2 baseline samples

cytof, cytometry by time of flight

DEG, differential gene expression

DIL, Visit 3 diluent samples

FEV1, forced expiratory volume in 1 second

GO, gene ontology

KLRG1, killer cell lectin-like receptor subfamily G member 1

LCMV, lymphocytic choriomeningitis virus

LM, *listeria monocytogenes*

lncRNA, long non-coding RNA

Malat1, Metastasis Associated Lung Adenocarcinoma Transcript 1

Methacholine PC20, the provocative dose of methacholine that results in 20% fall of FEV1

MFI, mean fluorescence intensity

miRNA, micro RNA

RBP, RNA binding protein

SAC, segmental allergen challenge

scRNAseq, single cell RNA sequencing

TDMD, target mediated microRNA degradation

t-TEM, terminal T effector memory cell

UTR, untranslated region

Chapter 1 – RNA Circuits in T Cells

Abstract

RNA is integral to the regulatory circuits that control cell identity and behavior. Cis-regulatory elements in mRNAs interact with RNA binding proteins (RBPs) and microRNAs (miRNAs) that can alter RNA sequence, stability and translation into protein. Similarly, long noncoding RNAs (lncRNAs) scaffold ribonucleoprotein complexes that mediate transcriptional and post-transcriptional regulation of gene expression. Cell programming is fundamental to multicellular life, and in this era of cell therapies, it is of particular interest in T cells. Here, we review key concepts and recent advances in our understanding of the RNA circuits that govern T cell differentiation and immune function.

Introduction

Gene expression programs define cell identity and govern cell behavior. Layered regulatory circuits sculpt spatiotemporal patterns of gene activity to create impressive complexity and environmental responsiveness from a single genomic blueprint. RNA molecules are integral to almost all of these regulatory circuits. RNA is of course the synthetic product of transcription and the template for protein translation, but RNAs also act as substrates for post-transcriptional regulation and as active mediators of regulatory processes. In this review, we discuss RNA circuits that operate in T cells to regulate their development, differentiation, and function in immunity. We discuss messenger RNAs (mRNA), long noncoding RNAs (lncRNA), microRNAs (miRNAs), and others in the context of mechanisms of RNA regulation. We aim to illuminate RNA circuits through the lens of cis-regulatory logic, focusing on the RNA sequence and structural elements that function through interaction with RNA binding proteins (RBPs) and/or

other RNA molecules. Our increasing understanding of RNA circuits sharpens our view of cell programming and may enable their use in genomic and cell therapies.

RNA Binding Proteins

RNA binding proteins (RBPs) bind to linear and structural motifs in the coding region, introns and untranslated regions (UTR) of transcripts to mediate alternative splicing, alternative polyadenylation usage (APA), RNA modifications, localization, stability and translation. Upon exposure to environmental stimuli or internal signaling, RBPs can relocalize and shuttle transcripts to different subcellular compartments to undergo different processes including degradation and translation to generate an appropriate cellular response (Decker and Parker 2012; W. Ma and Mayr 2018). Regulatory circuits involving RBPs and their target transcript(s) modulate T cell differentiation and immune functions. Our expanding knowledge of the RBP repertoire and RNA binding sites in T cells provide an opportunity to deploy RNA-centric approaches for uncovering regulatory circuits that govern T cell function.

Experimental approaches for mapping RBP-RNA interactions

A variety of forward proteomic methods detect interactions between specific RBPs and their target transcripts. RNA immunoprecipitation (RNA IP) pairs immunoprecipitation of a specific RBP with quantitative RT-PCR to identify its associated transcripts (Fig. 1.1A). High throughput sequencing of crosslinking immunoprecipitation (HITS-CLIP) was developed to map the specific binding sites of an RBP (Fig 1.1B). This and many refined methods utilizing UV-crosslinking and RNase digestion to produce small RNA libraries of bound sequences are widely used to produce transcriptome-wide RBP binding profiles at or near nucleotide resolution (Ule et al. 2005; Hafner et al. 2010; König et al. 2010; Van Nostrand et al. 2016)(Hafner et al. 2021). Conversely, RNA-centric reverse proteomics can be used to identify the RBP(s) that bind to

known cis-regulatory regions (Fig. 1.1C). For example, RNA aptamers have been instrumental in identifying RBPs that bind to AU rich elements (AREs) in the 3'UTR of cytokine mRNAs and for uncovering new circuits regulating T cell responses (Leppek and Stoecklin 2014; Salerno et al. 2018).

Recently developed methods profile the entire RBP repertoire and global RBP occupancy on transcripts. Both RNA interactome capture (RNA IC) (Baltz et al. 2012; Castello et al. 2012; Perez-Perri et al. 2018; Garcia-Moreno et al. 2019; R. Huang et al. 2018; Bao et al. 2018) and the organic phase separation methods OOPS and XRNAX (Trendel et al. 2019; Queiroz et al. 2019; Urdaneta et al. 2019) systematically capture RBP:RNA complexes for downstream identification of proteins through mass spectrometry and binding sites through small RNA sequencing (Fig. 1.1D-E). Performed in Jurkat T cell line and in mouse and human primary T cells, these methods expanded the known repertoire of proteins that bind to RNA (Perez-Perri et al. 2018; Hoefig et al. 2021) including non-canonical RBPs such as signal transducer and activator of transcription 1 (STAT1) and STAT4 (Hoefig et al. 2021). Of the RBPs identified through RNA IC and OOPS, 439 were uniquely expressed in primary human T cells when compared to HEK293, U2OS and MCF10a cells (Hoefig et al. 2021). These global RBP interactome data can guide dissection of RBP-mediated post-transcriptional regulatory circuits modulating T cell function.

RBP-mediated post-transcriptional processes

Signal responsive alternative splicing and polyadenylation

Alternative splicing generates mRNA isoforms that can encode proteins with different localization, catalytic activity or stability (Blake and Lynch 2021). Splicing factors, including multifunctional RBPs, regulate splice site usage in a context-specific manner in T cells, forming signal-responsive RNA circuits that modulate T cell activation and immune function. To take a

classic example, CD45, a transmembrane tyrosine phosphatase encoded by *Ptprc*, regulates cell signaling in T cells and other hematopoietic cells. Naive T cells express long isoforms of the protein (e.g. CD45RA), but alternative splicing produces a shorter form (CD45RO) in activated and memory T cells through interaction of Heterogeneous Nuclear Ribonucleoprotein L (HNRNPL) (Rothrock, House, and Lynch 2005; Shankarling et al. 2014) HNRNPL-like (HNRNPLL) (Oberdoerffer et al. 2008) and PTB-associated Splicing Factor (PSF) (Heyd and Lynch 2010) and activation responsive sequences in the *Ptprc* mRNA.

Antigen and costimulatory receptor signaling induce alternative splicing of many transcripts during T cell activation. Activated primary CD4 T cells generate alternatively spliced transcripts involved in apoptosis including *CASPASE9* (*CAS9*), *BIM* and *BAX* (Blake et al. 2022). The short, inactive forms of *CAS9*, *BIM* and *BAX* inhibit apoptosis and instead promote cellular proliferation upon activation (Blake et al. 2022). Binding motifs for CUGBP Elav-Like Family Member 2 (*CELF2*), Serine and Arginine Rich Splicing Factor 5 (*SRSF5*) and Polyprimidine Tract Binding Protein 1 (*PTBP1*) near the splice site in *CAS9* suggest a role for these RBPs (Blake et al. 2022). In murine CD8⁺ OT-I cells, activation with antigen and costimulation via CD134 (*OX40*) and CD137 (*41BB*) induced TAR DNA Binding Protein (*Tardbp*)-mediated alternative splicing (T. A. Karginov, Ménoret, and Vella 2022). *Tardbp*-deficient OT-I cells generated a smaller pool of antigen-specific cells with less cytokine expression (T. A. Karginov, Ménoret, and Vella 2022). Another splicing protein, *SRSF1*, is necessary for thymocyte development (Qi et al. 2021) and regulates T cell cytokine expression (Katsuyama and Moulton 2021; Katsuyama et al. 2019) in mouse models, but whether it regulates these functions through splicing mechanisms remains to be confirmed. RBPs can also regulate their own expression and function through splicing in response to external stimuli. Downstream of TCR engagement, c-Jun N-terminal kinase (*JNK*) pathway regulates *CELF2*, altering splicing of Map Kinase Kinase 7 (*MKK-7*) (Mallory et al. 2015; Martinez et al. 2015). The shorter isoform of *MKK-7*

phosphorylates JNK, which reinforces CELF2 activity (Martinez et al. 2015), generating a positive feedforward loop

In addition to alternative splicing to include or exclude certain exons, transcripts can undergo alternative polyadenylation (APA). In most mRNA and many noncoding RNAs, the newly transcribed transcript is cleaved at the 3' end by a multi-protein complex that recognizes the polyadenylation signal (PAS) composed of an AAUAAA motif and flanking U/G rich sequences (Blake and Lynch 2021). Cleavage is followed by nontemplated addition of adenosines. APA is regulated by RBPs that bind to regions in the 3'UTR to regulate PAS site usage. Activated T cells engage APA to undergo global 3'UTR shortening, eliminating binding sites for trans factors including miRNAs and RBPs (Sandberg et al. 2008; Gruber et al. 2014). The consequences of APA on gene expression and protein expression require further study, as differing conclusions have been drawn. Information on the regulatory circuits modulating APA in cell-type or context specific manner remains limited. CELF2 was shown to regulate APA of certain transcripts upon T cell activation and induce preferential usage of certain PAS sites in Jurkat T cells (Chatrikhi et al. 2019). Within its own 3'UTR, CELF2 induced APA by competing with proteins in the polyadenylation complex at PAS sites (Chatrikhi et al. 2019). Further study is needed to elucidate APA regulatory circuits in T cells.

RNA editing in T cells

Methylation of adenosine at the nitrogen-6 position (m6A) is one of the most abundant RNA modifications, occurring preferentially near the stop codon and in 3'UTRs (Shulman and Stern-Ginossar 2020). The reversible methylation process is mediated by “writer” complexes methyltransferase 3 (METTL3) and METTL14 along with adaptor proteins, “reader” proteins YTH N6-Methyladenosine RNA Binding Proteins (YTHDF1-3) and YTH Domain Containing

proteins (YTHDC1-2) and “erasers” such as AlkB Homolog 5 (ALKBH5) that remove the methyl group (Shulman and Stern-Ginossar 2020).

Studies that modulate m6A expression through removal of the writer or eraser RBPs demonstrate how regulating this modification is crucial for regulating T cell function in different cellular and environmental contexts. Mouse T cells deficient for METTL3 or METTL14, expressed lower levels of m6A, proliferated slower and remained in a naïve state in an adoptive transfer colitis model (H.-B. Li et al. 2017). In this context, m6A expression in naïve T cells was necessary to induce transcript decay of negative repressors of IL-7 mediated STAT5 signaling in CD4⁺ T cells (H.-B. Li et al. 2017) and IL-2 mediated STAT5 signaling in Tregs (Tong et al. 2018). In contrast, CD4 T cells and Tregs deficient in the adaptor protein WT-1 associated protein (Wtap), developed spontaneous gut inflammation and proinflammatory cells in the tissue despite low or no expression of m6A (Ito-Kureha et al. 2022). While both genetic models revealed impaired proliferation, the studies differed in the effects on T cell receptor signaling. While studies on METTL3 deficiency narrowed the effect to IL-7 signaling, the use of Wtap-deficient mouse T cells demonstrates how m6A expression controls stability of transcripts downstream of TCR signaling to inhibit TCR-induced cell death (Ito-Kureha et al. 2022) upon activation. The discrepancy between the two models, both of which lower m6A deposition, may be due to differences m6A deletion efficiency (Ito-Kureha et al. 2022). A comparison of the residual m6A expression levels and the transcripts that remain methylated could provide insight to this difference. Removing the eraser ALKBH5 also alters T cell function. In mouse T cells, ALKBH5 was necessary for removal of m6A on interferon gamma (IFN γ) for transcript stability and generation of an inflammatory response (Zhou et al. 2021).

Other than T cell signaling pathways, m6A expression can also regulate CD4 T cell differentiation through stabilization of transcription factor transcripts. In a Lymphocytic Choriomeningitis Viral (LCMV) infection model, METTL3 and m6A expression was necessary

for stabilization of *Tcf* and other transcripts involved in Tfh differentiation (Yao et al. 2021). In culture, METTL3-deficient naïve CD4 T cells skew towards Th2 over Th1 and Th17 (H.-B. Li et al. 2017). Impaired thymocyte development was also observed in m6A low and Wtap-deficient thymocytes (Ito-Kureha et al. 2022). m6A and the RBP machinery compose an important circuit for regulating transcript stability and various T cell functions. The balance between stabilizing and destabilizing certain transcripts in different cellular contexts in T cells is unknown although studies in human cell lines suggest that YTHDF2 destabilizes (X. Wang et al. 2014) and Insulin-like Growth Factor 2 Binding Protein (IGF2BP) family (H. Huang et al. 2018) stabilizes transcript through m6A binding.

Recent work showed that deposition of RNA 5-methylcytosine by methyltransferase Nsun2 stabilizes *Il17a* in mouse Th17 cells (Yang et al. 2023), demonstrating that at least on additional RNA modification regulates T cell function.

mRNA Stability and Translation

In the cytoplasm, RBPs bind cis-regulatory elements with specific RNA sequence and/or structural motifs to regulate transcript degradation by multiple mechanisms including endonuclease cleavage (Mino et al. 2015, 2019), decapping of the 5' end (Tavernier et al. 2019) and deadenylation of the 3' end (Leppek et al. 2013; Fabian et al. 2013) followed by exonuclease digestion. RBPs can also engage or inhibit translation to further fine-tune protein expression (Salerno et al. 2018; Mino et al. 2015; Essig et al. 2018). The following sections highlight these properties through discussion of 3 RBP families with prominent functions in T cell biology.

AU Rich Elements (ARE) and ARE-BPs

AU rich elements (ARE) and ARE binding proteins (ARE-BP) form complex circuits that modulate the duration and intensity of immune responses. ARE are typically characterized by the canonical pentamer AUUUA, though functional noncanonical sequence motifs also exist. AREs are common in 3'UTRs of cytokines, early activation genes and signal transduction genes (Winzen et al. 2007; C. Y. Chen and Shyu 1994; H. H. Lee et al. 2012; Nicolet et al. 2021), and loss of an individual ARE can lead to hyperinflammation and autoimmunity in mouse models (Kontoyiannis et al. 1999). ARE-BP exert different regulatory mechanisms to modulate T cell effector function in a temporal and cell-type specific manner. Zinc finger protein 36 (ZFP36; also known as tristetraprolin, or TTP) is rapidly upregulated in activated CD4 and CD8 T cells and maintained for several days (Moore et al. 2018). During this time, ZFP36 and its family member ZFP36 like 1 (ZFP36L1) bind to AREs to regulate the stability and translation of mRNAs involved in T cell activation (Moore et al. 2018), and functionally limit proliferation, effector cell function and inflammatory cytokine production (Moore et al. 2018; Petkau et al. 2022). In resting mouse CD8 memory cells, ZFP36 like 2 (ZFP36L2) regulates cytokine production by repressing the translation of ARE containing mRNAs (Salerno et al. 2018). In contrast to the ZFP36 family, HuR (ELAVL1) binding of ARE in certain 3'UTRs can stabilize transcripts. In cultured mouse and human CD4 T cells, HuR extends the half-life of mRNAs encoding GATA-3, IL-4 and IL-13 (Stellato et al. 2011; Casolaro et al. 2008) as well as IL-17 (J. Chen et al. 2013). The mechanisms that determine ARE-BP specificity requires further investigation. In T cell lines, ZFP36 and HuR displayed overlapping but distinct target specificities (Raghavan et al. 2001). Additional ARE-BPs may also contribute to the regulation of ARE-containing mRNAs in T cells. Together, these studies demonstrate the complexity of ARE-directed RNA circuits that regulate T cell responses.

Secondary Structures and RBPs

Other than linear sequences, RBPs can interact with structural motifs in the 3'UTR. Roquin family members (Roquin 1 and Roquin 2) as well as Regnase-1 recognize constitutive decay elements (CDE), alternative decay elements (ADE) and other variations of a stem loop in the 3'UTR of transcripts (Leppek et al. 2013; Janowski et al. 2016) to exert regulatory function. In steady state conditions, Roquin and Regnase bind to motifs in the 3'UTR to initiate transcript decay (Uehata et al. 2013; Mino et al. 2015; Jeltsch et al. 2014) or translational silencing (Mino et al. 2015; Essig et al. 2018). Upon TCR activation, Roquin and Regnase are cleaved by para-caspase MALT1 releasing the regulatory circuits restraining the cells and promoting proinflammatory phenotype (Uehata et al. 2013; Jeltsch et al. 2014). Interestingly, as was demonstrated with mouse *NFκB delta inhibitor (Nfkbid)* 3'UTR, the number of stem loops and interactions with Roquin in the 3'UTR can result in transcript decay or translation inhibition (Essig et al. 2018).

Roquin 1 and 2 have been shown to bind and repress expression of *Icos*, *Ox40* and transcripts in the NF-κB signaling pathway to maintain T cell quiescence (Jeltsch et al. 2014; Vogel et al. 2013; Essig et al. 2017). In mouse CD4⁺ T cells, this regulatory circuit restrains differentiation towards T helper 17 cells (Th17), follicular helper T cells (Tfh) or follicular regulatory T cells (Tfr) through multiple mechanisms including targeting *Icos* itself as well as well as its receptor signaling pathway (Jeltsch et al. 2014; Essig et al. 2017). For CD8⁺ T cells, Roquin restrains proinflammatory and cytotoxic function (Behrens et al. 2021). Regnase1 binds to similar target transcripts as Roquin and restrains hyperinflammatory and autoimmune state (Uehata et al. 2013; Behrens et al. 2021). While Roquin and Regnase can regulate independently, they may also interact and cooperatively regulate T cell function (Behrens et al. 2021), adding a new layer of regulation beyond cis-element and trans-factor interaction.

AT rich interaction domain 5a (Arid5a) similarly binds stem loops in the 3'UTR (Masuda et al. 2016; Hanieh et al. 2018; Zaman et al. 2016) (Masuda et al., 2016; Hanieh et al., 2017; Zaman et al., 2016). In primary mouse T cells, Arid5a stabilizes *Stat3* to direct CD4 naïve T cell differentiation towards Th17 (Zaman et al. 2016) Masuda et al., 2016) along with other targets to control T cell function (Hanieh et al. 2018; Zaman et al. 2016). Arid5a can work antagonistically with Regnase by competing for the same stem loops in transcripts to either stabilize (Arid5a) or destabilize (Regnase-1) the target transcript (Masuda et al. 2013, 2016; Hanieh et al. 2018).

Recent studies have leveraged RBPs, specifically Roquin and Regnase function, to generate new T cell therapies to treat cancer. Deletion of these proteins in human chimeric antigen receptor (CAR) T cells or mouse antigen-specific CD8 T cells increased cytokine and cytotoxic expression in the cells as well as their expansion and persistence in the tumor (Wei et al. 2019; H. Zhao et al. 2021; Mai et al. 2023). Most importantly, transfer of Regnase-1 or Roquin (or double) deficient cells slowed tumor growth. Point mutations in Roquin-1 that disrupted its function showed similar phenotypes in mouse tumor model (Behrens et al. 2021). Together, these studies demonstrate a potential avenue for targeting RBPs and their transcript targets for therapeutic interventions.

MicroRNAs and Argonaute proteins

miRNAs are short noncoding RNA loaded into RBPs of the Argonaute (Ago) family to form the miRNA induced silencing complex (miRISC), which mediates translational repression and transcript instability of target mRNAs. miRNA also interact with other noncoding RNA, RBPs and other proteins in complex RNA circuitry to regulate T cell function. For example, in proinflammatory Granulocyte-macrophage colony-stimulating factor (GM-CSF)+ primary human CD4 T cells, transcriptional repressor Basic Helix-Loop-Helix Family Member E40 (BHLHE40) which inhibits Regnase-4 directly and miR-146 indirectly, releasing the brake on NF- κ B

signaling and cytokine expression (Emming et al. 2020). Individual miRNAs can have multiple target transcripts in the T cell transcriptome as well as multiple binding sites in the same 3'UTR, involved in networks regulating cell function including proliferation and differentiation. Precise targeting of miR-155 binding sites in B cells demonstrate functional impacts of individual miRNA and cis-regulatory region on cell function (Dorsett et al. 2008; Lu et al. 2014). Future studies can dissect individual miRNA binding sites in T cells.

Long noncoding RNAs (lncRNAs)

lncRNAs as a class do not have a specific defined function but can contribute to a variety of regulatory circuits through their interaction with RBPs, other RNAs, and DNA (Wilusz, Sunwoo, and Spector 2009). Here, we will focus on lncRNA-mediated regulatory mechanisms that have been described in T cells: Regulation of transcription, post-translational modification, and miRNA inhibition by acting as competing endogenous RNA (ceRNA) (schematized in Figure 1.2).

lncRNA Annotations and Technological Advances

Long non-coding RNA (lncRNA) are genomically encoded RNAs that do not contain an open reading frame and are not translated into proteins. lncRNAs constitute a large portion of the human transcriptome with 96411 lncRNA genes annotated compared to 19890 coding genes (Nurk et al. 2022; L. Zhao et al. 2021). Mouse annotations are similar with 87890 lncRNA genes annotated compared to 22186 coding genes ("Mus Musculus Annotation Report" n.d.; L. Zhao et al. 2021). lncRNAs have drawn significant research interest due to a high degree of cell type and tissue specificity in their expression (Gibb et al. 2011). Together, these observations suggest that lncRNAs perform important regulatory functions in a variety of cellular contexts.

These insights are direct results of advances in long and short read sequencing technologies (Carpenter 2022). The ability of short read sequencing to deeply and broadly

assay the RNA landscape in many cell and tissue types has led to further interest in lncRNAs (Bu et al. 2015). Long read sequencing has improved annotation of lncRNAs due to its ability to capture whole or nearly whole transcripts (Carbonell Sala et al. 2021). This is important for circular RNAs (circRNA), which are often the result of splicing events where the ends of the removed intron are ligated to create a circular topology (Ashwal-Fluss et al. 2014). Long read sequencing greatly increases the likelihood that the ligated junction will be completely read through and specifically attributed to the circRNA rather than the un-spliced mRNA transcript (Ashwal-Fluss et al. 2014). There are other examples of post-transcriptional processing of lncRNAs, such as the MALAT1-associated small cytoplasmic RNA (scaRNA), which is liberated from the parental MALAT1 transcript by RNase P cleavage (Wilusz, Freier, and Spector 2008). Attention to these details is important when annotating and detecting lncRNAs, especially for assays that rely on aligning short reads.

Transcriptional Regulatory Mechanisms

lncRNA regulation of transcription can act in *cis* (i.e. on local genes) or *trans* (i.e. on genes from any genomic location). Mechanisms acting in *cis* refer to the regulation of genes within the same locus and has been well studied in B cell class switch recombination (Zheng et al. 2015). Malat1, a polyfunctional lncRNA, participates in both *cis* and *trans* mechanisms. A knockout mouse showed that loss of Malat1 increased the expression of nearby genes in *cis*; however, the exact mechanism by which this occurs has not been described (Bin Zhang; Gayatri Arun; Yuntao Mao; Zsolt Lazar; Gene Hung; Gourab Bhattacharjee; Xiaokun Xiao; CarmennbspJ. Booth; Jie Wu; Chaolin Zhang; DavidnbspL. Spector et al. 2012). While the *cis* effect of Malat1 is inhibitory, other lncRNAs are activating in their *cis* interactions. NALT (Notch associated lncRNA in T ALL) is located less than 100 bp from NOTCH1 and both are highly expressed in pediatric T cell acute lymphoblastic leukemia (T ALL) (Y. Wang et al. 2015). shRNA knockdown of NALT led to reduced NOTCH expression in human T ALL cell lines and

slower tumor growth when these lines were implanted into nonobese diabetic/severe combined immunodeficiency (NOD/SCID) mice. A Gal4- λ N/BoxB reporter system showed that NALT could induce the transcription of any proximal gene.

While the cis-regulatory mechanisms of lncRNAs have not been well defined in T cells, trans-regulatory mechanisms have been worked on in great detail. Typically lncRNAs bind transcription factors and epigenetic regulators to affect gene expression. In T and NK cell lymphoma, Malat1 associated with the polycomb repressive complex pathway (Kim et al. 2017). Pulldowns of Enhancer of zeste homolog 2 (Ezh2) and SUZ12 polycomb repressive complex 2 subunit (Suz12) proteins as well as H3K27me3 marks on histones were enriched with Malat1 transcript in human T cell lymphoma cell lines (Kim et al. 2017). Notably, siRNA knockdown of Malat1 did not change the expression of these proteins (Kim et al. 2017). Another recent study confirmed that Malat1 interacts with Ezh2 and H3K27me3 in non-oncogenic CD8⁺ T cells in mice to maintain H3K27m3 marks on memory associated genes (Kanbar et al. 2022). In an adoptive transfer model of the mouse virus lymphocytic choriomeninges virus (LCMV), Malat1-deficiency in P14 viral specific CD8⁺ T cells resulted in greater proportion and number of memory cells. (Kanbar et al. 2022). T helper 17 (Th17) differentiation and cytokine production is regulated by lncRNAs in a similar manner in both mice and humans. In mice, Malat1 is downregulated upon T cell activation and differentiation into the Th17 lineage (S. Ma et al. 2022; Masoumi et al. 2019). As in CD8⁺ T cells, Malat1 binds to Suz12 and enhances H3K27me3 deposition at the *Il17a-Il17f* locus resulting in decreased cytokine expression and colonic inflammation in mice (S. Ma et al. 2022). In contrast, the lncRNA Myocardial Infarction Associated Transcript (MIAT) enhances Th17 differentiation and cytokine production in primary human T cells (Khan et al. 2022). MIAT is highly expressed in T cells isolated from the synovium of rheumatoid arthritis patients and the *IL17A* locus had decreased accessibility upon MIAT targeting. The exact mechanism by which MIAT induces this change is unknown (Khan et al. 2022). Other lncRNAs have been shown to exhibit similar behaviors. For instance, TCLInc1

can modularly scaffold heterogeneous nuclear ribonucleoprotein D and Y-box binding protein 1 complexes to induce the expression of TGF- β in Jurkat cells, a human lymphoma cell line (P. Zhao et al. 2021).

lncRNAs can also regulate post-translational modifications on transcription factors. lncRNA-GM directly targets the phosphorylation of Foxo1 (Yali Chen et al. 2022). In mouse primary cells lncRNA-GM inhibits the dephosphorylation of Foxo1 by PP2A which increases IL23R expression (Yali Chen et al. 2022). This results in enhanced Th17 differentiation and worsening pathology in the mouse model experimental autoimmune encephalomyelitis (EAE) (Yali Chen et al. 2022). The human orthologue of lncRNA-GM similarly enhanced Th17 signature genes in CD4⁺ T cells derived from peripheral blood mononuclear cells (PBMCs) (Yali Chen et al. 2022). lncRNAs can also regulate ubiquitination of proteins. shRNA inhibition of NEAT1 in primary human PBMCs enhanced ubiquitination of Stat3 (Shui et al. 2019). The subsequent reduction in Stat3 resulted in poor Th17 differentiation (Shui et al. 2019). NEAT1 is upregulated in human RA PBMCs and lentiviral delivery of NEAT1 shRNA into the joints of mice in an arthritis model relieved the degree of Type 2 collagen induction, indicating Neat1 may be of clinical relevance in human auto-immune diseases (Shui et al. 2019).

lncRNA Post-Transcriptional and Post-Translational Mechanisms

lncRNAs can regulate cellular functions post-transcriptionally by sequestering RBPs and their regulation of protein-coding mRNAs. For instance, the lncRNA non-coding RNA activated by DNA damage (NORAD) binds to Pumilio family proteins through multivalent interactions to induce subcellular compartmentalization via liquid-liquid phase separation (Elguindy and Mendell 2021).

lncRNAs can also inhibit miRNA binding and function through stoichiometric sequestration, degradation, or some yet to be defined mechanism. In this scenario, the lncRNA contains a seed site for a given microRNA and acts as a decoy or sponge to prevent microRNA

binding and degradation via microRNA-RISC complex of protein coding targets (Xu et al. 2022). This phenomena has gained much interest outside of T cell biology, but increasingly it is being demonstrated in T cells as well. In CD8⁺ T cells Malat1 inhibits the miR-15/16 family to enhance memory cell formation (Gagnon et al. 2019; Wheeler et al. 2023). CRISPR-Cas9 mediated disruption of the miR-15/16 binding site in Malat1 resulted in decreased expression of miR15/16 targets CD28 and Bcl2 (Wheeler et al. 2023). This resulted in poor activation by CD28 and reduced IL-2 production by primary mouse T cells (Wheeler et al. 2023). Other lncRNA:miRNA circuits can regulate apoptosis in T cells. circRNA-1806 sponges miR-126, (L. Zhang et al. 2020), which targets adrenomedullin which induces the phosphorylation of c-Jun and JNK to regulate cell cycle progression (Ouafik, Berenguer-Daize, and Berthois 2009). Targeting circRNA-1806 with siRNA in mice reduced the clearance of the fungus *Cryptococcus neoformans* and decreased mouse survival following infection with the fungus (L. Zhang et al. 2020). lncRNA Lnc-AIFM2-1 sponges miR-330-3p to promote hepatitis B virus immune escape (C. Xie et al. 2023). The key target of miR-330-3p identified in this instance was CD244, which exhibited reduced expression in the human Jurkat cell line targeted with anti-Lnc-AIFM2-1 siRNA (C. Xie et al. 2023). CD244 expression was associated with increased T cell apoptosis and miR-330-3p mimics were associated with poor HBV control in *in vitro* co-cultures (C. Xie et al. 2023).

CD4⁺ T cell differentiation into the Th17 lineage is regulated by the lncRNA:miRNA circuit composed of Lnc-ITSN1-2 and miR-125a (Nie and Zhao 2020). IL-23R is a key target of miR-125a and over expression of Lnc_ITSN1-2 increased IL-17 and RORC mRNA expression in *in vitro* differentiated CD4⁺ T cells derived from both healthy human subjects as well as patients with Crohn's disease or ulcerative colitis (Nie and Zhao 2020). These studies show how a lncRNA:miRNA circuit controls T cell activation, apoptosis, and differentiation. Other work has identified roles for circ-LAMP1 and miR-615-5p (Deng et al. 2019) and circRNA_0000094 and miR_223-3p (Hou et al. 2021) in T cell malignancies.

lncRNAs can also regulate T cell functions via the post-translational regulation of key proteins including phosphorylation of Foxo1 and ubiquitination of Stat3 discussed above (Yali Chen et al. 2022; Shui et al. 2019). Another notable example of lncRNA mediated regulation of protein abundance is the regulation of the vesicular trafficking system by the lncRNA Snhg1 (Y. Zhang et al. 2021). Snhg1 interacts with Vps13D and enhances its function in shuttling CD127 to the surface of the cell. shRNA inhibition of either Snhg1 or Vps13D resulted in lower CD127 protein level as well as reduced memory cell numbers *in vivo* following LCMV infection in mice (Y. Zhang et al. 2021).

Mechanisms of lncRNA:miRNA Sponges

How exactly lncRNA:miRNA interactions lead to the inhibition and/or the degradation of the microRNA in particular remain generally uncharacterized. A notable study involving the lncRNA cyrano demonstrated that extensive 5' and 3' base pairing of cyrano and miR-7 led to the degradation of miR-7 with evidence of tailing (removal of bases from the 3' end of the microRNA) (Kleaveland et al. 2018). Subsequent mechanistic studies have elaborated that extensive 3' binding in addition to 5' seed binding between a microRNA and its targets can lead to target mediated microRNA degradation (TDMD) of Ago2 and the microRNA in a Zswim8 dependent and tailing independent manner (Jaeil Han et al. 2020; Shi et al. 2020). However, many of the lncRNA sponge studies in T cells to date have not indicated extensive 3' binding between the indicated lncRNA and microRNA family (Hou et al. 2021; C. Xie et al. 2023; Deng et al. 2019). How these interactions decrease microRNA abundance is a key open question in the field. Further, some ceRNA lncRNAs do not require the degradation of their target miRNA, so the degree to which stoichiometry alone along with subcellular localization contribute to the ceRNA effect should be resolved in greater detail (Wheeler et al. 2023).

Experimental Approaches to Studying lncRNA Function

The tool kit to study lncRNA function is expanding. Previous genetic approaches have relied on the excision of large portions of the genetic locus of a given lncRNA (Bin Zhang et al. 2012) or the insertion of an early poly-A signal (Nakagawa et al. 2012). These interventions can cause significant disruption to the locus and regulatory regions such as enhancers for nearby or distant genes thus confounding any phenotypes observed. To address this problem many studies have focused solely on the transcript instead and employed RNAi to post-transcriptionally degrade a given lncRNA (Kanbar et al. 2022; C. Xie et al. 2023; L. Zhang et al. 2020; Shui et al. 2019). While this avoids confounding genetic effects, it is limiting in the settings in which lncRNAs can be studied, particularly for T cells. For this reason, mice models where TCR transgenics are available have seen the best application of this technology where virally delivered shRNAs can be stably expressed in transduced cells (Kanbar et al. 2022). Limitations of RNAi include incomplete knockdown of the transcript that may make observation of subtle phenotypes difficult and the inability to identify specific functional sequences within the lncRNA.

Partial fragments of a lncRNA can be transcribed to probe sequence specific binding through methods like RNA-IP (P. Zhao et al. 2021). However, this strategy requires investigators to make *a priori* assumptions or have specific observations about the fragments. The advent of a multitude of CRISPR based technologies will allow a much more directed approach, described below. With these technologies, specific sequences and/or binding site dependent functions can be targeted (Wheeler et al. 2023). This type of approach is amenable to more model systems and functional dissections of lncRNA mediated regulatory circuits will provide molecular mechanisms in greater detail.

Genomic and Transcriptomic Editing Approaches for Dissection of lncRNA and RBP Function

The non-viral targeting of human T cells with CRISPR/Cas systems has opened the door to efficient and rapid genetic editing of T cells (Roth et al. 2018; Mandal et al. 2014; Schumann et al. 2015; Hendel et al. 2015). However, these systems have most often been employed to induce insertions and deletions (indels) in an exon of a coding gene (Garcia-Doval and Jinek 2017). This is often insufficient to change the function of a lncRNA or the global function of a 3' UTR.

There are instances where Cas9 induced indels may have functional outcomes for RBP and lncRNA function. For instance, the miR-15/16 binding site within Malat1 in humans can be directly targeted by Cas9, and introduce indels in this site that disrupts binding similar to the *Malat1^{scr/scr}* mouse line (Wheeler et al. 2023). Where a single guide approach is insufficient, paired sgRNAs can be used to excise portions of the genome with precision (Jinxiong Han et al. 2014; Guo et al. 2023). While this may remove important regulatory elements it can be done more precisely than homologous recombination (Bin Zhang et al. 2012). Further, there is no need for recombinase expression or residual novel sequences, such as LoxP sites (Bin Zhang et al. 2012).

One way to create more controlled mutations is to utilize homology directed repair (HDR) templates, in which the desired new sequence is provided via an exogenous oligonucleotide (Y. Wu et al. 2013). This can be used to disrupt binding sites and maintain the nucleotide content (Wheeler et al. 2023). This can also be used to insert large novel sequences (Iancu et al. 2023). Further genomic base editors (BE) can also be applied, where catalytically dead Cas9 is fused to an adenosine deaminase to only edit adenosines targeted by the sgRNA (McAuley et al. 2023). For instance, CD3 δ was recently targeted in human hematopoietic stem

cells to restore T lymphopoiesis from immunodeficient patients (McAuley et al. 2023). Applicable BE produces higher desired mutation rates with lower indel byproducts compared to HDR strategies (McAuley et al. 2023).

Cas13 systems have also been developed that target RNA transcripts directly (Abudayyeh et al. 2017). Cas13 was employed to show that lncRNA-GACAT3 is a ceRNA for miR-497 (Z. Zhang et al. 2020). This is advantageous because Cas13 has equivalent or better depletion of transcripts compared to RNAi, can be present transiently, and does not alter genome stability (Abudayyeh et al. 2017). Further, being able to understand an RNA transcript's subcellular localization and its interaction partners are outstanding questions in this field. Catalytically inactive Cas13 has been paired with fluorescent labeling to dynamically track specific RNA transcripts in living cells (Yang et al. 2019). This has been used to show dynamics of NEAT1's interaction with paraspeckles and could be paired with orthogonal dCas13 or dCas9 to investigate RNA-RNA or RNA-DNA interactions in a sequence specific fashion (Yang et al. 2019).

Concluding Remarks and Overview of Thesis

The RNA circuits discussed above illustrate the complex mechanisms present in T cells to regulate cell identity, function, and fate. RBPs primarily act in a post-transcriptional fashion to regulate gene expression and these processes. RBPs bind to mRNA transcripts to splice, stabilize, and destabilize these RNAs. Disruption of RBPs can result in alteration of core T cell programs such as expression of cytokines as in ALKBH5 control of IFN γ via m6A removal or altered differentiation as in Roquin 1 and 2 control of Th17, Tfh, and Tfr via repression of *Icos* and *Ox40* (Zhou et al. 2021; Jeltsch et al. 2014; Essig et al. 2017).

While RBPs illustrate how proteins can interface with RNA, lncRNAs function in the reverse fashion in that an RNA species modulates protein function. Subsequently, lncRNAs can

exert regulatory capacity at the transcriptional, post-transcriptional, and post-translational level. Some transcripts can even work in multiple modes simultaneously such as Malat1, which facilitates H3K27me3 deposition via Ezh2 and sponges microRNAs (Kim et al. 2017; Kanbar et al. 2022; Luan et al. 2016; Su et al. 2021; Wheeler et al. 2023).

These layers of regulation mediated by RNA illustrate how precise control of gene expression networks is essential for cellular differentiation, activation, and survival of T cells. The work in this document explores immune networks from the gene expression programs in cytotoxic T cells to cellular heterogeneity in the lung of human asthmatics. Chapter 2 describes how the lncRNA Malat1 inhibits the microRNA family miR-15/16. These together constitute a non-coding RNA circuit that regulates cytotoxic T cell activation and memory cell differentiation during both LCMV and *Listeria monocytogenes* infection. Chapter 3 looks beyond cell intrinsic gene regulation to explore T cell contributions to complex human disease. Namely, through transcriptomic approaches we identify Th2 cells in the bronchoalveolar space after allergen challenge. These Th2 cells contain systemically present TCR sequences and are elevated in subjects with other modules of elevated type 2 inflammatory tone such as eosinophilia and IL-13 responsive gene expression in the lung epithelium. Thus, together these chapters illustrate the importance of precise control of T cells because of their potent effects on inflammation and inflammatory disease.

Figures

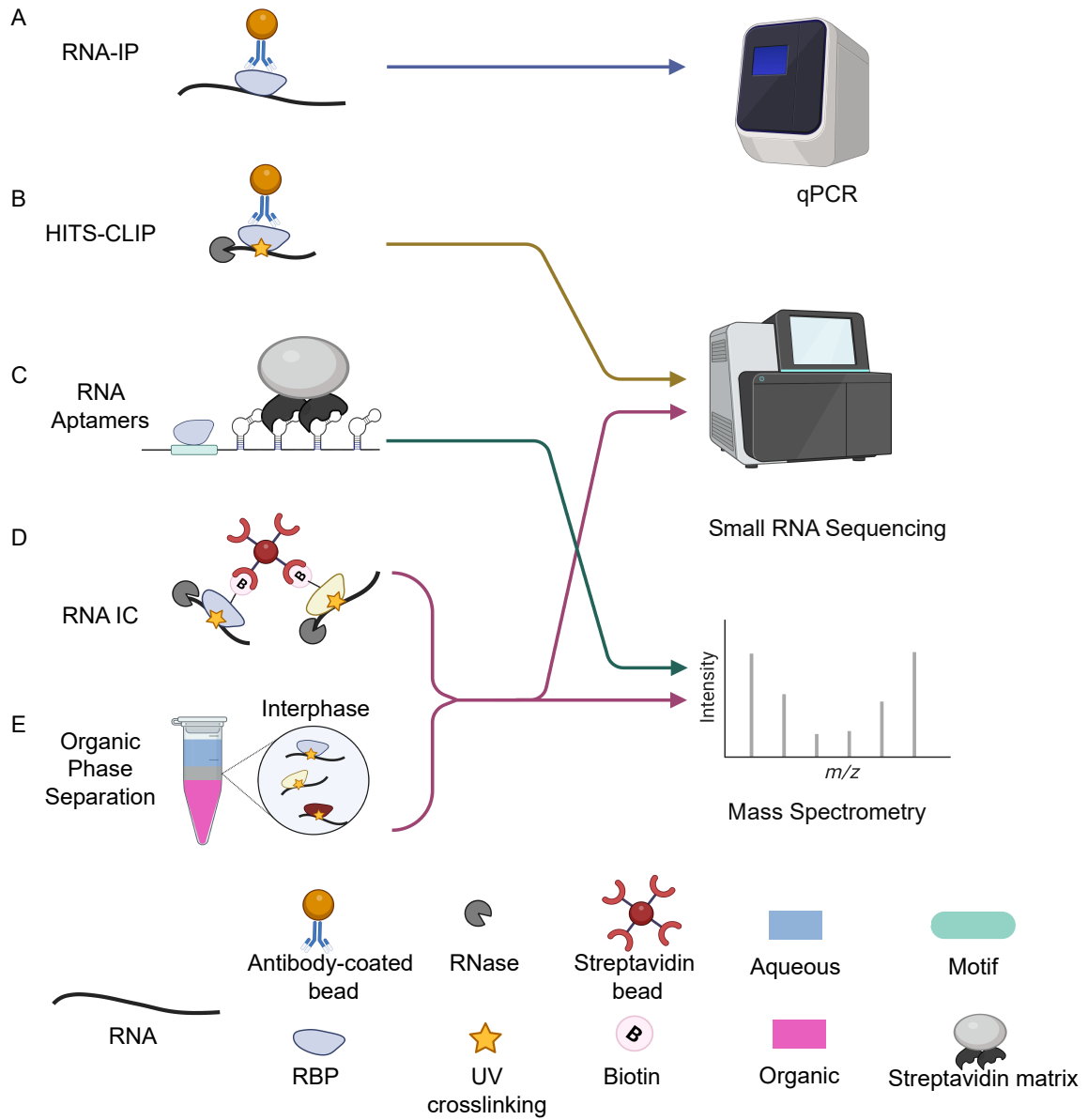


Figure 1.1. Ribonucleoprotein capture methods performed in T cells.

(A) RNA immunoprecipitation (RNA IP) captures RBP-RNA interactions using antibody-coated beads to pull down specific RBPs and their bound transcripts in the cell under native conditions. The bound transcript is released from the protein and processed for quantitative PCR to determine target transcripts by the specific RBP. **(B)** Crosslinking immunoprecipitation with high throughput sequencing methods (HITS-CLIP) use UV radiation to covalently bind RBPs to their transcripts and prevent dissociation of the ribonucleoprotein (RNP) complex. The RNPs are captured using antibody coated beads and undergo RNase digestion to generate small RNAs containing the bound region. These fragments are then sequenced to determine the transcriptomic binding profile. **(C)** RNA aptamers contain small, structured motifs that recognize small molecules and can be used to pull down and identify RBPs that bind to a sequence of interest. The illustration depicts an aptamer with modified streptavidin binding structures (S1m) and the sequence of interest upstream of these regions. Streptavidin matrix is used to pull down the protein-bound aptamer and the proteins are processed for mass spectrometry. **(D)** RNA interactome capture methods (RNA IC) biotinylate the proteins and use streptavidin beads to extract RBP-bound RNA. Captured RPBs are identified using mass spectrometry and RNA undergoes library preparation and sequencing to determine RBP binding sites. **(E)** Organic phase separation similarly can be used to systematically identify RBPs and RBP binding profiles of a cell. Unlike RNA-IC, these methods use phenol phase separation which partitions proteins and RNA into the organic and aqueous phase respectively. RNPs that separate into the interphase are captured and processed for mass spectrometry and/or sequencing.

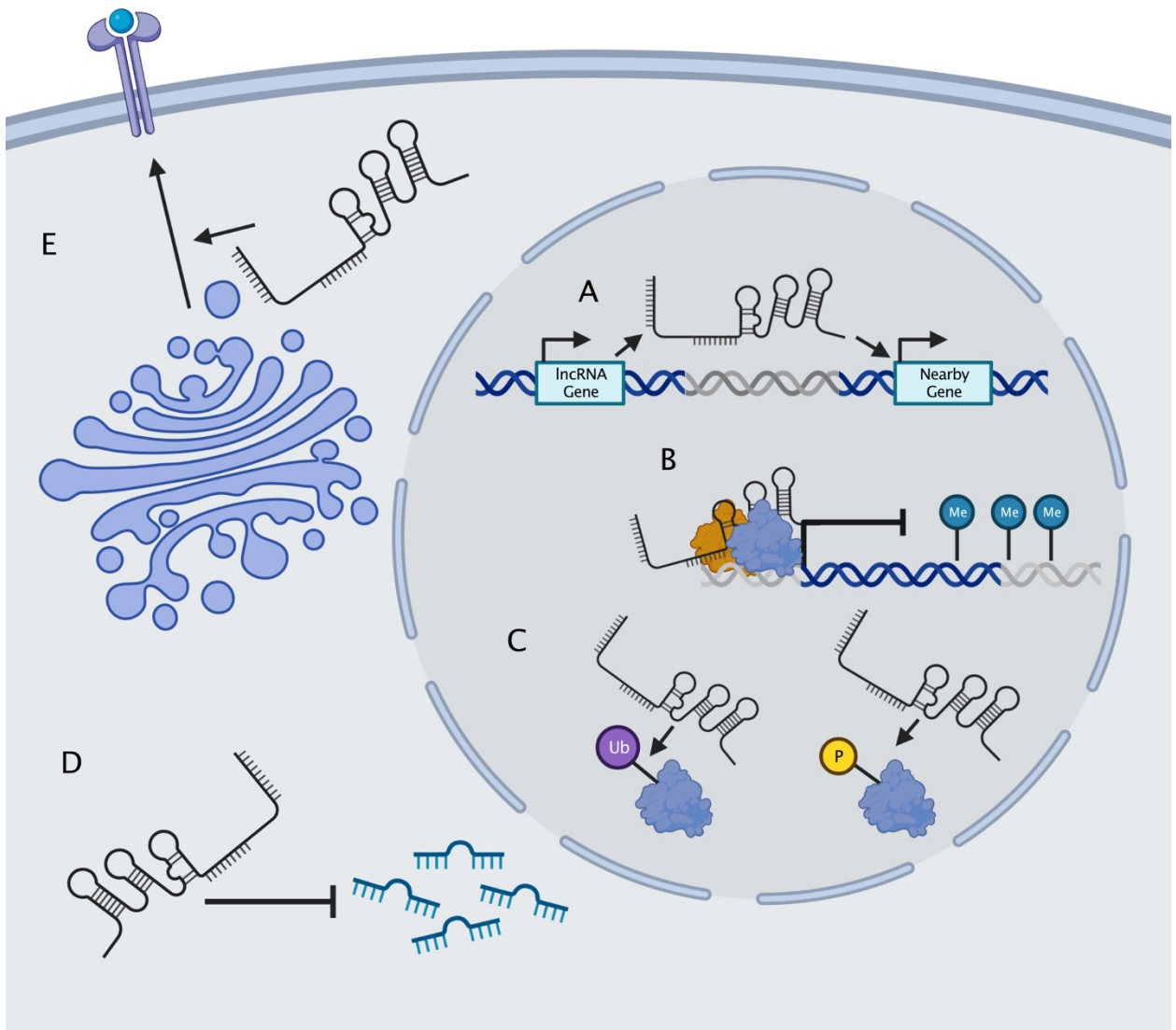


Figure 1.2. lncRNA Functions Identified in T cells

(A) Transcription of lncRNAs has significant impacts on the expression of other genes in the same locus. In T cells the mechanisms of this *cis*-regulatory effects are still not well defined. **(B)** lncRNAs often regulate a host of other protein-coding genes via *trans*-regulatory mechanisms. This is often done via the scaffolding of various transcription or epigenetic factors and facilitating their binding to chromatin. This can influence the deposition of histone regulatory modifications such as H3K27me3. **(C)** lncRNAs can regulate transcription factors in a post-translational fashion by influencing the addition of ubiquitin or phosphoryl groups resulting in degradation, inhibition, or activation of the transcription factor. **(D)** lncRNAs act as ceRNAs for microRNAs which reduces the amount of microRNA induced inhibition of protein coding targets. lncRNA acting as a ceRNA often leads to the degradation of the microRNA but in some cases may inhibit the microRNA solely via stoichiometric means. **(E)** lncRNAs can influence protein activity of the golgi vesicle trafficking network. In particular VPs13d activity is enhanced by the presence of a lncRNA and this is critical for the cell surface expression of important cytokine receptors for T cells such as IL-7R.

Chapter 2 - The lncRNA Malat1 Inhibits miR-15/16 to Enhance T Cell Activation and Memory Formation

Abstract

Proper activation of cytotoxic T cells via the T cell receptor and the costimulatory receptor CD28 is essential for adaptive immunity against viruses, many intracellular bacteria and cancers. Through biochemical analysis of RNA:protein interactions, we uncovered a novel non-coding RNA circuit regulating activation and differentiation of cytotoxic T cells composed of the long non-coding RNA Malat1 (Metastasis Associated Lung Adenocarcinoma Transcript 1) and the microRNA family miR-15/16. miR-15/16 is a widely and highly expressed tumor suppressor miRNA family important for cell proliferation and survival. miR-15/16 also play important roles in T cell responses to viral infection, including the regulation of antigen-specific T cell expansion and T cell memory. Comparative Argonaute-2 high throughput sequencing of crosslinking immunoprecipitation (Ago2 HITS-CLIP, or AHC) combined with gene expression profiling in normal and miR-15/16-deficient T cells revealed a large network of several hundred direct miR-15/16 target mRNAs, many with functional relevance for T cell activation, survival and memory formation. Among these targets, the long non-coding RNA Malat1 contained the largest absolute magnitude miR-15/16-dependent AHC peak in T cells. This binding site was also among the strongest lncRNA:miRNA interactions detected in the T cell transcriptome. We used CRISPR targeting with homology directed repair to generate mice with a 5-nucleotide mutation in the miR-15/16 binding site in Malat1. This mutation interrupted Malat1:miR-15/16 interaction, and enhanced the repression of other miR-15/16 target genes, including CD28. Interrupting Malat1 interaction with miR-15/16 decreased cytotoxic T cell activation, including the expression of IL-2 and a broader CD28-responsive gene program. Accordingly, Malat1 mutation diminished memory cell persistence following LCMV Armstrong and *Listeria monocytogenes* infection. This

study marks a significant advance in the study of long noncoding RNAs in the immune system by ascribing cell-intrinsic, sequence-specific *in vivo* function to Malat1. These findings have implications for T cell-mediated autoimmune diseases, antiviral and anti-tumor immunity, as well as lung adenocarcinoma and other malignancies where Malat1 is overexpressed.

Introduction

Cytotoxic T cells are indispensable for mounting an adaptive immune response against intracellular pathogens and the clearance of mutated cells such as cancer. Over the course of a viral infection, cytotoxic T cells are primed by antigen presenting cells and undergo extensive rounds of intense proliferation (Murali-Krishna et al. 1998). As they clonally expand, these cells differentiate into effector and memory cells and acquire effector functions, including the production of cytotoxins and critical cytokines such as IL-2, TNF α , and IFN γ (Bachmann et al. 1999). As the infection is cleared, the cytotoxic T cell response contracts as many cells die via apoptosis, yielding a long lived pool of memory cells poised for secondary expansion and protection against reinfection with the same pathogen (Wherry and Ahmed 2004; Badovinac, Porter, and Harty 2002). The factors that control this expansion, differentiation, and contraction have been intensely researched in the past decades, focusing in large part on proteins such as transcription factors, signaling enzymes, and cytokines (Yao Chen et al. 2018). However, it is of recent interest to understand how non-protein coding regions of the genome contribute to the regulation of these cells as well. These non-protein coding elements can be regulatory in nature such as enhancers (Roychoudhuri et al. 2016; Shapiro et al. 1997-7), or RNA species that are transcribed but not translated. Two such species of interest to our present study are microRNAs (miRNAs) and long non-coding RNAs (lncRNAs).

MicroRNAs are short (21 nucleotide) RNAs which, when loaded into Argonaute (Ago) proteins, can target mRNAs that contain complementary seed sequences in their 3' UTRs for translation inhibition and degradation (Bartel 2018; Djuranovic, Nahvi, and Green 2012; Eichhorn

et al. 2014). In particular, the miR-15/16 family are potent regulators of cell cycle and survival (Q. Liu et al. 2008). Previous work from our group utilized conditional deletion of the four major miR-15/16 family members (miR-15a, miR-15b, miR-16-1, miR-16-2) driven by CD4-cre transgene (hereafter referred to as miR-15/16^{ΔΔ} mice or T cells) to demonstrate that this miRNA family has important effects on cytotoxic T cells (Gagnon et al. 2019). In response to viral infection, miR-15/16^{ΔΔ} mice generate more viral-antigen specific T cells, and these cells preferentially differentiate into memory cells that express CD127 and CD27 (Gagnon et al. 08/2019).

In contrast to the well-defined roles of miRNAs, lncRNAs as a class do not have a single defined function. They are broadly defined as RNAs transcribed by polymerase II, over 200 nucleotides (nt) in length, that lack a translated open reading frame (Su et al. 2021; Wilusz, Sunwoo, and Spector 2009). Some lncRNAs bind to chromatin and regulate nearby or distant genes, and others scaffold transcription factors and other protein complexes (Kopp and Mendell 2018). Most relevant to the present study, some lncRNAs act as competing endogenous RNAs (ceRNAs) that bind to miRNAs, preventing their binding to and subsequent repression of mRNA targets (Su et al. 2021; Poliseno et al. 2010). However, rigorous connections between lncRNA physiological functions and molecular mechanisms of action has been hampered by the lack of precise tools to facilitate their study (Ponting and Haerty 2022). As lncRNAs lack an open reading frame, insertion or deletion (indel) mutations do not reliably create null alleles. Instead, investigators have frequently deleted large genomic regions around the promoter or excised the genomic locus of the transcript altogether. These approaches risk disrupting cis-regulatory elements or topologically associated domains that control other nearby genes. Other studies that identified physiological roles for lncRNAs rely on RNAi-mediated lncRNA degradation. Both this approach and genetic manipulations that block lncRNA transcription leave a mechanistic gap between sequence features and downstream function. Only a few studies demonstrate

sequence dependent function of lncRNAs (Kleaveland et al. 2018; J. T. Lee, Davidow, and Warshawsky 1999; Elguindy and Mendell 2021).

One lncRNA that has garnered much attention is the Metastasis Associated Lung Adenocarcinoma Transcript 1 (Malat1). Malat1 was first identified as highly expressed in both malignant tumors and healthy lung and pancreas with high interspecies conservation (Ji et al. 2003). Malat1 is mostly localized to the nucleus, where it is found within nuclear speckles, although it is not necessary for their formation (Nakagawa et al. 2012). These characteristics have generated numerous hypotheses about the function of Malat1 including that it scaffolds epigenetic and splicing factors and acts as a ceRNA to inhibit a variety of miRNAs (Tripathi et al. 2010; Su et al. 2021).

In the immune system, Malat1 has been studied in dendritic cells, macrophages, T helper cells, T regulatory cells, and cytotoxic T cells (Hewitson et al. 2020; J. Wu et al. 2018; Masoumi et al. 2019; Kanbar et al. 2022). Malat1 is regulated during cytotoxic T cell differentiation with higher expression in memory precursors and lower expression in short-lived effector cells during LCMV infection (Kakaradov et al. 2017). Similarly, T cells stimulated *in vitro* express decreased levels of Malat1 over time (Masoumi et al. 2019). Early reports using large genetic deletions in the mouse Malat1 locus detected widespread gene expression changes but failed to identify a role for Malat1 in mouse development or cytotoxic T cell responses (Yao et al. 2018; Bin Zhang et al. 2012; Nakagawa et al. 2012), though a recent report using RNAi detected altered T cell responses (Kanbar et al. 2022). Clearly there remains much to learn about the sequence-specific mechanisms by which Malat1 tunes pathways and functions essential to cytotoxic T cells.

In the present study, we present a novel non-coding RNA circuit that regulates the activating signals from CD28 and IL-2, leading to low Bcl-2 expression and loss of memory cells following LCMV infection. We do so by identifying candidate interactions between miRNAs and lncRNAs via a targeted biochemical approach, and by creating CRISPR-targeted transgenic

mice with precise mutation of Malat1 to interrogate the physiological function of the interaction between miR-15/16 and Malat1. We use this novel mouse to identify CD28 responsive gene programs affected by this circuit, and provide a new sequence-specific function of Malat1 *in vivo*.

Results

Malat1 is highly Bound by miR-15/16

To identify candidate noncoding ceRNAs in cytotoxic T cells, we performed Argonaute-2 high throughput sequencing of crosslinking immunoprecipitation (Ago2 HITS-CLIP, AHC). Integrating sequence reads across different classes of transcribed genomic annotations revealed that lncRNAs are bound extensively by Ago2, but the median lncRNA had 7.8 times fewer aligned AHC sequence reads compared to 3' untranslated regions (UTRs) where miRNAs canonically bind to mRNAs (Fig. 2.1A). This difference likely reflects the comparatively low expression of many lncRNAs, and it highlights the relatively low occupancy of Ago2 on most of these transcripts. Nevertheless, there were individual lncRNAs that stood out as highly bound across the transcript. To prioritize lncRNAs for further investigation, we manually curated the transcripts with the largest number of aligned AHC sequence reads. Among the top 10 most highly bound transcripts, 3 overlapped with protein coding genes, 2 were on the mitochondrial chromosome, and 3 were repetitive annotations. Strikingly, all of the top 10 transcripts were either annotated as rRNA or contained an rRNA repeat element, except the 8th most bound transcript, Malat1 (Table 1). When the same analysis was repeated with rRNA repeats masked, Malat1 was the second most highly bound transcript (Table 2).

Malat1 has been proposed to inhibit miRNAs as a ceRNA (H. Xie et al. 2017; Qiao et al. n.d.; L. Chen et al. 2017; J. Wu et al. 2018; Luan et al. 2016; Q.-M. Wang et al. 2019; Xiao et al. 2015). We used the Piranha peak calling algorithm to identify sites with the highest degree of miRNA binding, as indicated by AHC sequence read number and density (Fig. 2.1B). Within

cytotoxic T cells, the algorithm identified 55 AHC peaks in Malat1, the largest of which was extremely pronounced (Fig. 2.1C). Compared with other lncRNA binding peaks, this peak had the 36th most total aligned reads and the 142nd highest read density (15th and 16th respectively when rRNA reads are masked). Even when compared to peaks in 3' UTRs of mRNAs, the largest peak in Malat1 was the 100th most (98th percentile) bound peak in terms of read density (Fig. 2.1B).

miRTarget, the custom miRNA binding prediction algorithm (W. Liu and Wang 2019), identified an 8-mer seed binding sequence of the miR-15/16 family centered within the most densely bound region of the called peak (Fig. 2.1C). miR-15/16 has not been previously shown to interact with Malat1, so to determine whether this peak is miR-15/16 dependent, we performed AHC with cultured CD8⁺ miR-15/16^{ΔΔ} T cells. In the absence of miR-15/16, Ago2 binding to Malat1 was preserved throughout the whole transcript except for the peak containing the predicted miR-15/16 8-mer seed binding sequence (Fig. 2.1C). Further, miR-15/16 binding occurred in a region of high evolutionary conservation (Fig. 2.1D). The corresponding region containing the miR-15/16 binding site in human MALAT1 was highly enriched in two publicly available AHC datasets obtained using the 293 human embryonic kidney (HEK) cell line (F. V. Karginov and Hannon 2013);(Y. Li, Estep, and Karginov 2018) (Fig. 2.1E). We conclude that miR-15/16 bind abundantly to Malat1 in mouse cytotoxic T cells and this interaction is likely to be conserved in human cells.

We hypothesized that Malat1 may inhibit the function of miR-15/16 in cytotoxic T cells. To directly address this question in mice, we used CRISPR-Cas9 with homology directed repair to generate mice in which five nucleotides of the miR-15/16 seed binding sequence within Malat1 were scrambled (Fig. 2.1F). Mice homozygous for this mutation are subsequently referred to as *Malat1*^{scr/scr}. To confirm the targeted functional outcome of this mutation, AHC was performed on cultured CD8⁺ T cells isolated from *Malat1*^{scr/scr} mice. Ago2 binding was preserved across the Malat1 transcript except at the mutated miR-15/16 binding site, where AHC

sequence read density was greatly reduced (Fig. 2.1C). This finding confirmed that miR-15/16 binds to Malat1 at this site in a sequence dependent manner, and provided us with a tool for highly specific investigation of the functional consequences of Malat1:miR-15/16 interaction.

Malat1 inhibits miR-15/16 availability and activity

Malat1:miR-15/16 interaction could lead to regulation and/or degradation of the lncRNA, the miRNAs, or both. To assess whether miR-15/16 degrades Malat1 we compared the expression of Malat1 by mRNA sequencing in primary mouse CD8⁺ T cells. Malat1 expression was unchanged in miR-15/16^{ΔΔ} cells as well as in the *Malat1*^{scr/scr} cells (Fig. 2.2A). Previous studies investigating Malat1 and other lncRNAs as ceRNA inhibitors of miRNAs have suggested that inhibition occurs by either target RNA-directed miRNA degradation (TDMD) or stoichiometric sequestration of the miRNA from protein-coding mRNA targets (Jaeil Han et al. 2020; Su et al. 2021). Therefore, we also tested the possibility that Malat1 lowers miR-15/16 abundance by TDMD or a related mechanism. However, in freshly isolated mouse CD8⁺ T cells, miR-15b and miR-16 were unchanged and only miR-15a, a family member with lower expression, was modestly decreased in *Malat1*^{scr/scr} cells (Fig. 2.2B). We conclude that Malat1 and the miR-15/16 family do not influence each other's absolute abundance in this setting.

To test whether Malat1 affects miR-15/16 function, we examined miR-15/16 target binding in our AHC data. We first defined an experimentally supported list of TargetScan predicted miR-15/16 binding sites with at least 1 AHC read in both WT and *Malat1*^{scr/scr} cells. Using this list, we then examined the read depth at these sites in both *Malat1*^{scr/scr} and WT cells (603 sites contained in 479 genes). In WT cells, these sites constituted on average 3.2% of the binding in each 3' UTR, and this figure increased to 3.4% in *Malat1*^{scr/scr} cells, indicating that Ago2 occupancy preferentially increased at these sites when miR-15/16 binding to Malat1 was eliminated (Fig. 2.2C). To confirm that binding to these target sites was miR-15/16 dependent, we assessed their AHC read depths in miR-15/16^{ΔΔ} cells as well. As predicted, binding was

greatly reduced in miR-15/16^{ΔΔ} cells, representing, on average, 1.0% of binding to a given 3' UTR, a 69% reduction in Ago2 binding compared to WT (Fig 2.2D). In contrast, no significant differences were observed for binding at predicted sites for the highly expressed miRNA families of miR-101, Let-7, miR-21, and miR-142, (Fig. 2.S1). Thus, we conclude that the *Malat1*^{scr} allele specifically negatively regulates the first requirement of miR-15/16 function – binding to mRNA targets.

We next sought to investigate whether this increased binding resulted in decreased target mRNA expression. To do so, we analyzed mRNA-sequencing data from primary CD8+ T cells 24 hours after stimulation. We generated empirical cumulative density fraction (CDF) plots from these data comparing target gene expression in miR-15/16^{fl/fl} to miR-15/16^{ΔΔ} cells as well as WT to *Malat1*^{scr/scr} cells. For each of these comparisons, we then compared the distribution for miR-15/16 target genes, as defined above, to the distribution for all other expressed genes. In the case of WT to *Malat1*^{scr/scr} cells, the distribution was shifted in favor of decreased target gene expression in the *Malat1*^{scr/scr} cells (Fig 2.2E). In the case of miR-15/16^{fl/fl} to miR-15/16^{ΔΔ}, the distribution was shifted in favor of increased target gene expression in the miR-15/16^{ΔΔ} cells, indicating that this gene set is relieved of miRNA-induced repression (Fig. 2.2F). These data indicate that the increased availability of miR-15/16 leads to increased repression of mRNA target genes when Malat1:miR-15/16 interaction is ablated.

We further investigated genes that displayed reciprocal expression changes in miR-15/16^{ΔΔ} and *Malat1*^{scr/scr} cells. Of 479 genes in the bound target list, 432 (90%) were either downregulated in *Malat1*^{scr/scr} cells or upregulated in miR-15/16^{ΔΔ} cells, compared to controls. Among these genes, the expression of 298 (62%) were decreased in *Malat1*^{scr/scr} cells, and 294 (61%) were increased in miR-15/16^{ΔΔ} cells, with 160 (33%) both increased in miR-15/16^{ΔΔ} and decreased in *Malat1*^{scr/scr} cells (Fig 2.2G). Gene ontology enrichment analysis revealed multiple pathways associated with growth factor and antigen receptor signaling affected by the Malat1:miR-15/16 circuit in cytotoxic T cells (Fig. 2.2H). Many of these modules were identified

because they share key signaling proteins. Genes enriched in the T cell activation module are listed in Table 3. Targeting of these genes by miR-15/16 is consistent with their known tumor suppressor role (Cimmino et al. 2005; Gagnon et al. 2019) and with Malat1's association with cancer cell proliferation and metastasis (Ji et al. 2003), providing new mechanistic insight into the regulated genes that underlie those observations.

Malat1 enhances CD28 Expression and Downstream CD8 T Cell Activation

Given that the Malat1:miR-15/16 circuit regulated genes essential to T cell activation, and in particular CD28, we next investigated the functional consequences of perturbing this circuit in cytotoxic T cells. First, we looked directly at CD28. AHC in WT cells detected a prominent peak in the CD28 3'UTR at the TargetScan predicted binding site for miR-15/16. This peak was absent in miR-15/16^{ΔΔ} cells, whereas other binding peaks were preserved, empirically verifying that this binding event is miR-15/16-dependent. AHC in *Malat1*^{scr/scr} cells indicated a modest increase in Ago2 binding at this site compared to WT cells relative to Ago2 binding in the whole 3' UTR (Fig 2.3A). These data, along with our previous demonstration that the CD28 3' UTR is miR-15/16 responsive, indicates that CD28 is part of a module of miR-15/16 target genes that are highly likely to be affected by the *Malat1*^{scr} allele (Gagnon et al. 08/2019).

Indeed, CD28 expression and T cell activation were regulated by the Malat1:miR-15/16 circuit. Flow cytometric measurement in primary splenic CD8⁺ T cells revealed that CD28 protein expression was decreased in *Malat1*^{scr/scr} mice and enhanced in miR-15/16^{ΔΔ} mice (Fig 2.3B-C). To investigate activation-induced gene expression, we performed RNA-seq on splenic CD8⁺ T cells stimulated for 24 hours with plate-bound αCD3 with or without αCD28 cross-linking antibodies diagrammed in (Figure 2.3D). CD28 stimulation enhances distinct activation-induced gene expression changes in T cells (Martínez-Llordella et al. 2013), and these CD28-responsive genes were altered in miR-15/16^{ΔΔ} and *Malat1*^{scr/scr} cells (Fig 2.3E-H). The previously defined set of 164 genes that are upregulated in WT cells stimulated with αCD3 + αCD28 compared to αCD3

alone was also significantly upregulated in the α CD3 + α CD28 condition compared to α CD3 alone for each genotype tested in our experiments (Fig 2.S2A-D). Importantly, the Malat1:miR-15/16 circuit affected this gene set in the α CD3 alone condition, with Malat1^{scr/scr} cells exhibiting decreased expression compared to WT cells, and miR-15/16 ^{Δ/Δ} cells exhibiting increased expression compared to miR-15/16^{mi} cells (Fig 2.3E,G). This trend was preserved, but to a lesser degree, in the α CD3 and α CD28 condition (Fig 2.3 F,H). Thus, Malat1:miR-15/16 interaction enhanced expression of a costimulation-responsive gene expression program in activated T cells, and it further enhanced expression of that module even when CD28 costimulation was directly engaged.

Unsupervised hierarchical clustering of these samples based on the expression of the 164 costimulation-responsive gene set further underscored the costimulatory-like effect of the Malat1:miR-15/16 circuit. In comparing gene expression in Malat1^{scr/scr} and WT samples, 3 major groups emerged. The group with the lowest average costimulation-responsive gene expression contained only samples stimulated with α CD3 alone and primarily Malat1^{scr/scr} samples. The group with intermediate expression was the largest group with an even representation of Malat1^{scr/scr} samples and WT samples. While samples in this intermediate group were from both stimulation conditions, the Malat1^{scr/scr} samples tended to be from the α CD3 + α CD28 condition and the WT samples had an even representation from both stimulation conditions. The group with the highest average expression contained predominantly α CD3 + α CD28 stimulated samples with an even representation of Malat1^{scr/scr} and WT samples (Fig 2.3I). Thus, Malat1:miR-15/16 inhibition and engagement of CD28 signaling additively induced costimulation-responsive genes. This observation is further supported when clustering the miR-15/16 ^{Δ/Δ} and miR-15/16^{mi} samples. The 2 largest clusters were divided nearly exclusively by genotype. The group with lower average expression of costimulation-responsive genes contained predominantly miR-15/16^{mi} samples stimulated with α CD3 alone. The group with the higher average expression contained a majority of miR-15/16 ^{Δ/Δ} samples, and the only miR-15/16^{mi} samples within the group

received α CD3 + α CD28 stimulation. Within the higher expression group, the miR-15/16^{mi} samples stimulated with α CD3 + α CD28 sub-clustered with miR-15/16 ^{$\Delta\Delta$} samples stimulated with α CD3 alone (Fig 2.3J). A third, much smaller cluster was composed of both samples from a single outlier biological replicate. Overall, these data show that miR-15/16 restrict costimulation-responsive gene expression, and that Malat1:miR-15/16 interaction limits this effect.

In addition to the proximal changes in gene expression, downstream functional outcomes of CD28 costimulation were also affected. Early activation genes have been well described in T cells, with CD69 responding to many cues including TCR and CD28 ligation, and Nur77 responding very specifically to TCR signals (Ashouri and Weiss 2017; Vandenberghe et al. 1993). In similar fashion as above, we assessed the expression of these proteins 2 and 4 hours after stimulation with plate bound cross linking antibodies on primary CD8+ T cells. CD69 exhibited decreased expression in *Malat1*^{scr/scr} cells at both 2 and 4 hours post stimulation (2 hr: $p=0.0014$ and 4 hr: $p=0.0598$) and increased expression in miR-15/16 ^{$\Delta\Delta$} cells at 4 hours post stimulation only ($p < 0.0001$) (Fig 2.4 A-B), in accordance with costimulation-responsive gene module expression (Fig 2.3). There was no difference, however, in expression of Nur77 across *Malat1*^{scr/scr}, WT, and miR-15/16 ^{$\Delta\Delta$} cells, indicating that TCR signals were equivalent (Fig 2.4 A,C). Another key consequence of CD28 ligation is the production of IL-2 (Vandenberghe et al. 1993; Fraser et al. 1991; Maggirwar, Harhaj, and Sun 1997). Therefore, we assessed cytokine production in the supernatants of these cultures 16 hours after stimulation. In line with previous findings in LCMV-infected mice (Gagnon et al. 08/2019), miR-15/16 ^{$\Delta\Delta$} cells made significantly more IL-2 and TNF α after α CD3 stimulation both with and without α CD28, with a trend toward increased IFN γ as well (Fig 2.4D-F). *Malat1*^{scr/scr} cells stimulated with α CD3+ α CD28 exhibited a reciprocal trend specifically for IL-2 (23% decrease compared to WT, $p=0.26$) (Fig 2.4D). Together, these data show that the Malat1:miR-15/16 circuit regulates key functional outcomes of CD28-mediated costimulation, from proximal gene expression changes to early activation protein expression and cytokine secretion.

Malat1 enhances Cytotoxic Memory T Cell Differentiation

miR-15/16 restrict memory T cell differentiation, cell cycle, and cell survival during the response to LCMV Armstrong infection (Gagnon et al. 08/2019). CD28 costimulation is essential for IL-2 production, memory cell formation, and memory recall responses *in vivo* (Grujic et al. 2010; Suresh et al. 2001; Fuse, Zhang, and Usherwood 2008; Borowski et al. 2007; Eberlein et al. 2012-2). IL-2 is also essential for these same processes and in particular is required in a CD8⁺ T cell intrinsic nature for the formation of CD127⁺ KLRG1⁺ memory cells (Toumi et al. 2022; Pipkin et al. 2010; Blattman et al. 2003; Kahan et al. 2022; Whyte et al. 2022). Since Malat1 inhibits miR-15/16 activity and this circuit impacts proper T cell activation and IL-2 production after CD28 costimulation, we hypothesized that *Malat1*^{scr/scr} cells would exhibit poor memory formation and survival.

We first examined steady state memory populations of polyclonal T cells in unchallenged, young mice. *Malat1*^{scr/scr} mice had normal naive and central memory T cell populations, but a reduced percentage and number of effector memory (CD44⁺CD62L⁻) cells in the spleen (Fig 2.S3). Therefore, we investigated the cell intrinsic nature of the *Malat1*^{scr/scr} memory cell impairment during a viral challenge known to induce a large memory response. We bred the *Malat1*^{scr/scr} mice with P14 TCR transgenic mice that express an antigen receptor specific for the immunodominant LCMV GP33 peptide. We then transferred *Malat1*^{scr/scr} and WT P14 T cells into congenic CD45.1 hosts followed by LCMV Armstrong infection and tracked the acute and memory responses in the spleen and liver, the sites of primary LCMV infection (Figure 2.5A) (Matloubian et al. 1993).

The total numbers of P14 cells were similar in recipients of transferred WT or *Malat1*^{scr/scr} P14 cells in both the spleen and liver at day 7, and in the spleen at day 31. However, there was a reduction in *Malat1*^{scr/scr} P14 cells in the liver at day 31 (Fig 2.5 B-C). Despite having no effect on cell expansion at the peak of infection and mixed cell number results in the memory phase,

the *Malat1^{scr}* allele had a distinct effect on the cellular phenotype across organs and time points. *Malat1^{scr/scr}* P14 cells preferentially displayed a phenotype associated with terminally differentiated effector memory cells (t-TEM), defined by KLRG1 expression and lack of CD127 expression as shown by (Milner et al. 2020), and a corresponding reduction in the percentage of KLRG1⁺ CD127⁻ memory cells (Fig 2.5 D-F). Previous work has shown that substantial heterogeneity exists in the memory pool and that CD27 and CD43 can be useful in delineating functional differences such as recall potential between different memory cells. For instance, CD27⁻ memory cells tend to produce more IL-2 than CD27⁺ cells (Milner et al. 2020), and CD43⁺ CD27⁻ cells are more effective at clearing *Listeria* upon re-challenge (Hikono et al. 2007; Olson et al. 2013). We therefore assessed these markers on the transferred *Malat1^{scr/scr}* and WT P14 cells. Consistent with increased KLRG1⁺ CD127⁻ t-TEM cells there were proportionally more CD27⁻ CD43⁻ cells in both the spleen and liver at day 31 among the *Malat1^{scr/scr}* transferred cells compared to WT (Fig 2.5 G,I). CD27⁻ CD43⁺ cells were unchanged. The proportional reduction in CD127⁻ KLRG1⁺ cells corresponded with a decreased proportion of CD43⁺ CD27⁻ cells. Notably, the total numbers of all CD27⁻ subsets were unchanged. The proportional differences we observed were primarily driven by a reduction in the number of CD43⁺ CD27⁺ *Malat1^{scr/scr}* P14 cells compared with wild type P14 cells (45% reduction in liver ($p = 0.0058$), 30% reduction in spleen ($p = 0.113$)) (Fig 5 G-I). This phenotype is exactly reciprocal to the increase in CD27⁻ memory cells previously documented in miR-15/16^{ΔΔ} mice (Gagnon et al. 08/2019). To test whether the effect of the *Malat1^{scr}* allele was epistatic to miR-15/16, we bred *Malat1^{scr/scr}* mice to miR-15/16^{ΔΔ} mice to generate triple mutant *Malat1^{scr/scr}* miR-15/16^{ΔΔ} mice. The poly-clonal LCMV response in these mice phenocopied that of miR-15/16^{ΔΔ} with a WT allele of *Malat1*, indicating that the observed effects of the *Malat1^{scr}* allele are epistatic to miR-15/16 (Fig 2.S4). We conclude that *Malat1* inhibits miR-15/16 in responding CD8⁺ T cells during LCMV infection, leading to fewer CD43⁺ CD27⁺ memory cells.

Compared to LCMV, *Listeria monocytogenes* (LM) infection induces lower expression of multiple co-stimulatory ligands so the antigen specific response is more sensitive to the ablation of CD28 co-stimulation (Welten et al. 2015). Therefore, we hypothesized that cytotoxic T cell response may be more impaired by the *Malat1^{scr}* allele during LM infection. We first sought to understand the effect of miR-15/16 on cytotoxic T cells during primary LM infection. To do so, we directly infected polyclonal miR-15/16^{fl} and miR-15/16^Δ mice with LM expressing the LCMV GP33 peptide (LM-GP33) (Fig 2.6A). In contrast to the increased antigen-specific CD8⁺ T cell numbers in LCMV-infected miR-15/16^Δ mice (Gagnon et al. 08/2019), we observed similar cell numbers in LM-GP33 infected miR-15/16^Δ and miR-15/16^{fl} mice (Fig 2.6B). However, the effect on memory cell differentiation was still present with decreased percentages of CD127⁺ KLRG1⁺ t-TEMs and increased percentages of CD127⁺ KLRG1⁺ memory cells (Fig 2.6 C,D). Again, miR-15/16^Δ antigen specific cells had a significantly lower proportion of CD43⁺ CD27⁺ cells and a trend toward proportionally more CD43⁺ CD27⁺ cells ($p = 0.127$) (Fig 2.6 E,F).

Given that antigen-specific miR-15/16^Δ T cells exhibited enhanced memory cell differentiation during LM-GP33 infection, we further tested the role of *Malat1*:miR-15/16 interaction in this model using the P14 adoptive transfer system (Fig 2.6F). Transferred *Malat1^{scr/scr}* and WT P14 cells accumulated in the spleen and the liver to similar numbers at both day 7 and day 31 following LM-GP33 infection (Fig 2.6H). In contrast to LCMV, there was no change in the proportion or number of CD127⁺ KLRG1⁺ *Malat1^{scr/scr}* P14 cells at day 7 in the spleen or liver (Fig 2.6I). However, in LM-GP33 infection at day 7, CD43 and CD27 expression didn't explicitly mirror the phenotype observed by CD127 and KLRG1 expression. In the spleen, there was a proportional and numerical increase in CD43⁺ CD27⁺ P14 cells with the *Malat1^{scr/scr}* genotype (Fig 2.6J). There was a decreased proportion of CD43⁺ CD27⁺ cells ($p = 0.0531$), but this was despite a trend towards increased numbers of these cells ($p = 0.1056$) in the *Malat1^{scr/scr}* P14 cells (Fig 6K). In the liver, there were no significant trends in any of these populations at day 7 (Fig 2.6 J,K).

Although some of the phenotypes observed with LCMV were attenuated or absent during acute infection with LM-GP33 at day 7, Malat1:miR-15/16 interaction had more pronounced effects on memory cell populations at later times post-infection (Fig 2.6 L,M). On day 31, KLRG1⁺ cells were increased in proportion and numbers in the *Malat1^{scr/scr}* P14 cells (Fig 2.6N). In the liver, a similar trend in KLRG1⁺ cell proportion existed ($p = 0.233$), but the numeric effect was entirely absent (Fig 2.6N). Surprisingly, this effect was restricted to the KLRG1⁺ populations, as CD127⁻ KLRG1⁺ memory cells were unaffected in proportion and number in both the spleen and liver (Fig 2.6O). In both organs CD43⁻ CD27⁻ t-TEMs were proportionally increased and CD43⁻ CD27⁺ memory cells were proportionally decreased in *Malat1^{scr/scr}* P14 cells (Fig 2.6P,Q). The numeric underpinnings of these proportional changes were different in each organ, with a 94% increase in CD43⁻ CD27⁻ cells in the spleen, and a 40% loss of the CD43⁻ CD27⁺ population in the liver (Fig 2.6P,Q). Taken together, these data demonstrate that miR-15/16 restrict memory cell differentiation, and reveal the ability of Malat1:miR-15/16 interaction to enhance memory cell differentiation across infection contexts.

Malat1 Enhances Cytotoxic T Cell IL-2 Production and Survival

Finally, we investigated how the Malat1:miR-15/16 RNA circuit regulates memory cell differentiation and accumulation, giving consideration to the many direct targets of miR-15/16 and the subsequent indirect effects on IL-2 and other costimulation-responsive gene expression in CD8 T cells. The pro-survival protein Bcl2 is the first characterized target of miR-15/16 (Cimmino et al. 2005). Higher abundance of Bcl2 in memory cells (as compared with short-lived effector cells) aids their survival and persistence, counteracting their increased expression of pro-apoptotic factors such as Bim (Kurtulus et al. 2011). As such, changes in the balance of pro- and anti-apoptotic factors can have selective effects on the accumulation of memory T cells. Bcl2 expression in *Malat1^{scr/scr}* P14 cells was reduced at day 31 in the CD43⁻ CD27⁻ population in both LCMV and LM-GP33 infection, and also in CD43⁻ CD27⁺ cells in LCMV infection (Fig 2.7A-

C). This reduction is consistent with increased direct miR-15/16 action on the Bcl2 3' UTR in the *Malat1^{scr/scr}* cells, but it may also be affected by IL-2 and other co-stimulation responsive factors. Also consistent with reduced Bcl2 expression, increased proportions of dead *Malat1^{scr/scr}* cells were observed in both the KLRG1⁺ and KLRG1⁻ cell fractions at day 7 during LM-GP33 infection (Fig 2.7 D,E). Very few dead cells were detected among P14 cells of either genotype at day 31.

IL-2 is critical for the induction of Bcl2 in memory T cells to promote their survival (Toumi et al. 2022). Furthermore, IL-2 production by cytotoxic T cells predisposes them to differentiate into a memory phenotype, likely by an autocrine/paracrine mechanism (Kurtulus et al. 2011; Wojciechowski et al. 2007; Kahan et al. 2022). Given the enhanced ability of miR-15/16^{ΔΔ} cells to produce IL-2 and the trend toward impaired IL-2 production in *Malat1^{scr/scr}* cells in vitro (Fig. 2.4D), we assessed IL-2 production by *Malat1^{scr/scr}* T cells in LCMV and LM-GP33-infected mice. Corroborating our in vitro observations, a lower proportion of *Malat1^{scr/scr}* P14 cells produced IL-2 when stimulated ex vivo on day 7 in both infection models (Fig 2.7F,G). This defect was also shared by KLRG1⁺ and KLRG1⁻ populations and limited to this critical early time point. Higher proportions of memory cells were able to produce IL-2 ex vivo at day 31 after infection with either LCMV or LM-GP33 infection, and *Malat1^{scr/scr}* P14 cells produced equivalent amounts of IL-2 (Fig 2.7H).

As CD28 co-stimulation is key to IL-2 production, the observed early defect is consistent with less robust activation while antigen is still present (Shapiro et al. 1997-7). Taken together, these results indicate that *Malat1^{scr/scr}* cells in the context of a viral or bacterial infection receive relatively poor activating cues and subsequently produce less IL-2 early during infection, contributing to a less robust pro-survival and pro-memory state. These findings illustrate how *Malat1* regulation of miR-15/16 and its large target gene network can act through multiple connected nodes to coordinate gene expression programs essential to cytotoxic T cell responses.

Discussion

LncRNAs are a large, diverse class of gene products that perform important physiological functions through a variety of molecular mechanisms. However, functional requirements are typically tested using RNAi to degrade the lncRNA or by disrupting their transcription entirely with no paradigm to dissect sequence specific functions. “Sponging” miRNAs (acting as a ceRNA) is among the most frequently proposed mechanisms of lncRNA function. Networks of noncoding ceRNAs, miRNAs, and target genes likely do shape gene expression programs in many biological contexts. Yet definitive evidence that a lncRNA:miRNA interaction has a physiological effect in a living organism has remained elusive. Guided by a biochemical approach, we investigated the requirements for Malat1 interaction with miR-15/16 by surgically altering just 5 nucleotides within the endogenous 8 kb Malat1 transcript in mice. Using T cells from these animals, we rigorously attribute changes in costimulation-responsive gene expression and in vivo defects in memory T cell formation to this Malat:miR-15/16 circuit.

Malat1 is a pleiotropic lncRNA implicated in a multitude of processes, including scaffolding splicing and epigenetic regulators, binding to chromatin, and interacting with several miRNAs in different cell types (Arun, Aggarwal, and Spector 2020). Its extremely high expression and interspecies conservation nominated Malat1 as a strong candidate to have an impact on the activity of even highly abundant miRNAs like miR-15/16 that have large effects on gene expression and cell behavior. Less abundant miRNAs can also serve essential functions (Wigton et al. 2021), and they are likely to be more susceptible to inhibition by Malat1 and other ceRNAs. The same biochemically-driven sequence-specific approach used here could be applied to probe the physiological effects of other lncRNA:miRNA interactions, and it could also be extended to probe the requirement for interaction with Ezh2 and other proteins.

Another important future direction is to better understand how exactly Malat1 inhibits miR-15/16, given that TDMD does not appear to result from this interaction. Most Malat1 resides in the nucleus, whereas miRNAs reside and function in the cytoplasm. Advances in miRNA

fluorescent in situ hybridization (miR-FISH) or the implementation of proximity-CLIP (Benhalevy, Anastasakis, and Hafner 2018) may help clarify whether Malat1 nuclear sequestration plays a role in its ceRNA function. Detailed mechanistic understanding of this experimentally tractable circuit may illuminate how ceRNAs may be leveraged by the cell or by cellular engineers to manipulate the miRNA pool and target gene expression.

There is a growing interest in Malat1 function within the immune system, where it is highly expressed in many cell types and often regulated in interesting ways, including differential expression in short lived effector and memory precursor cells produced by asymmetric division of activated T cells during LCMV infection (Kakaradov et al. 2017). Malat1 overexpression in dendritic cells promotes IL-10 production by T regulatory cells (J. Wu et al. 2018), and *Malat1*^{-/-} mice exhibited reduced IL-10 and Maf expression by T helper cells in vivo and in vitro (Hewitson et al. 2020). Two prior reports addressed Malat1 function in cytotoxic T cell responses. In one report, no significant differences were observed in *Malat1*^{-/-} mice (Yao et al. 2018). It is difficult to interpret negative data generated from whole-body Malat1 deficiency given the multitude of cell types in which Malat1 may act. A second recent report, using RNAi to suppress Malat1 expression specifically in antigen-specific CD8⁺ T cells, detected enhanced t-Tem differentiation (Kanbar et al. 2022). This observation, which contrasts with our findings using *Malat1*^{scr/scr} mice, was suggested to occur via an epigenetic mechanism involving Malat1 interaction with Ezh2. This mechanism and the ceRNA function that we describe here are not mutually exclusive, and it is possible to observe divergent phenotypes from the different interventions used to probe Malat1 function in T cells.

Our *Malat1*^{scr/scr} mouse combined with the cell transfer system clearly demonstrates a cytotoxic T cell intrinsic requirement for Malat1 to inhibit miR-15/16 to enhance activation and protect memory cell persistence. This is consistent with our previous work on the miR-15/16 family, and fitting with the increased expression of Malat1 in memory precursors (Gagnon et al. 08/2019; Kakaradov et al. 2017). The present study builds upon these findings and provides

detailed insight into the gene regulatory programs which may drive these phenotypes. Cytotoxic T cells lacking CD28 generate similar numbers of viral specific cells at the height of infection, but fail to maintain equivalent numbers during the memory phase (Borowski et al. 2007). Further, a major outcome of CD28 ligation is the production of IL-2, an essential T cell growth factor, and this IL-2 production is required in a cell intrinsic manner for generation of CD127⁺ memory cells (Kahan et al. 2022). Here we demonstrate that not only does the Malat1-miR-15/16 circuit regulate CD28 co-stimulation, IL-2 production, and Bcl2 expression, but also the concordant outcome of maintaining CD43⁺ CD27⁺ memory cells. miR-15/16 targets a large number of genes, so it is unlikely that the effect on Bcl2 or CD28 alone is entirely responsible for the observed changes in CD43⁺ CD27⁺ t-TEM and CD43⁺ CD27⁺ memory cells. Our results are consistent with memory cells requiring a heightened level of pro-survival cues to survive the contraction bottleneck after the peak of infection. In this manner elevated Malat1 levels can act as an enhancer of pro-survival and activating cues to prevent excessive cell death in this sensitive memory population.

The importance of cytotoxic T cells is evident in the context of the global COVID-19 pandemic and the advent of CAR-T cell therapies reaching the clinic. Knowledge of the networks that regulate these cells and the critical nodes within these networks have the potential to augment technologies and therapies from vaccines to anti-tumor immunotherapy. Transcription factors and miRNAs have been extensively studied in this fashion as critical nodes in the regulation of gene transcription and translation. In the study presented here, we show Malat1 acts upstream of one such node, the miR-15/16 family. From this one interaction, Malat1 has the potential to combinatorially and synergistically regulate gene networks essential to cytotoxic T cells. This concept is easily extended when Malat1's ability to regulate multiple other miRNA families is considered. If Malat1's sequence specific function is further defined, then editing or expression of specific Malat1 sequences could be used to tune multiple miRNA families in concert while leaving other functions of this enigmatic transcript un-touched.

Materials and Methods

Mice

WT C57/BL6 mice were bred in our facility. miR-15/16^{Δ/Δ} and miR-15/16^{fl/fl} mice were derived as described in Gagnon et al 2019. *Malat1*^{scr/scr} mice were generated from WT C57/BL6 mouse zygotes electroportated with CRISPR-Cas9 RNPs and HDR template (guide and template sequences below) as described previously (Chen et al., 2016). B6.SJL-Ptprca Pepcb/BoyJ (CD45.1) strain #002014 were purchased from the Jackson Laboratory. WT P14 mice carrying the TCR transgene specific to the LCMV GP33 peptide were obtained from the Waterfield lab and were backcrossed to C57/BL6 to maintain the line. *Malat1*^{scr/scr} mice were bred to the P14 line to generate *Malat1*^{scr/scr} P14 mice. Male and female age and sex matched mice were used between 5 to 12 weeks of age. All mice were housed and bred in specific pathogen-free conditions in the Animal Barrier Facility at the University of California, San Francisco. Animal experiments were approved by the Institutional Animal Care and Use Committee of the University of California, San Francisco.

AGO2 HITS-CLIP

CD8+ T cells were isolated as below and stimulated for 3 days with αCD3 and αCD28 antibodies and grown with kool aid complete media. Subsequently the cells were rested and expanded in kool aid complete media for 2 days supplemented with 100 U/mL recombinant Human IL-2 (R&D Systems Cat# 202-IL-010/CF). Subsequently, 1*10⁶ cells were used to prepare NGS libraries as described in (Gagnon et al., 2019) & (Loeb et al., 2012). Samples were sequenced on HI-Seq 2500 (Illumina). 11 nucleotide adaptors were trimmed from each read and resultant sequences were aligned to the mm10 genome using bowtie2 (Langmead and Salzberg, 2012). To assure lack of miR-15/16 binding in *Malat1*^{scr/scr} mice was not do to errors in alignment, reads from *Malat1*^{scr/scr} cells were aligned to a mm10 genome that contained a single modification changing Malat1 from the WT allele to the *Malat1*^{scr} allele. To determine maximum binding depth across the genome and to manipulate aligned files the samtools package was

used (Li et al., 2009). To assess Ago2 binding, aligned HITS-CLIP reads were integrated across the follow genomic annotations: lncRNA genes from mouse Noncode v6 (<http://www.noncode.org/download.php>); miRNA target binding sites from TargetScan V7.2 (https://www.targetscan.org/cgi-bin/targetscan/data_download.mmu80.cgi); mm10 introns, exons, 3'UTRs, and coding genes from UCSC genome table browser (<http://genome.ucsc.edu/cgi-bin/hgGateway?db=mm10>). To assess differences in target binding at specific 3' UTR sites between WT and *Malat1^{scr/scr}* cells, reads within each 3' UTR were normalized to the total reads contained in the given 3' UTR for each genotype. To identify regions of significant Ago2 binding above background, so-called "peaks", we used the Piranha algorithm (<https://github.com/smithlabcode/piranha>) on our HITS-CLIP. To remove sites from analysis where confounding features were present, such as miRNA expression sites or rRNA repeats, bedtools intersect was used to remove these features from annotation files (Quinlan, 2014). Human AHC data from publicly available datasets were trimmed and aligned to the Hg38 genome as previously described (Karginov and Hannon, 2013; Li et al., 2018).

Cell Transfer and Infections

Spleens were harvested from WT or *Malat1^{scr/scr}* P14 CD45.2 mice into PBS and passed through 70 μ m strainers to generate a single cell suspension. Samples were then stained for live/dead (apc-cy7), Thy1.2 (BV605), CD8 α (apc), and TCRV α 2 (pe). Whole splenocytes were then transferred retro-orbitally (r.o.) into WT BoyJ (CD45.1) 7 week old male recipients such that each recipient received 20,000 Thy1.2⁺ CD8 α ⁺ TCRV α 2⁺ cells in 200 μ L PBS. To initiate LCMV infections, mice were injected intraperitoneally (i.p.) with 2×10^5 plaque forming units (p.f.u.) LCMV armstrong in 200 μ L plain RPMI. LCMV virus was produced in house as described in (Shehata et al., 2018). To initiate *Listeria Monocytogenes* infection, mice were injected r.o. with 2×10^5 colony forming units (c.f.u.) *Listeria Monocytogenes-GP33* in 100 μ L PBS. *Listeria Monocytogenes-GP33* was prepared in house as described in (Allen et al., 2020). Blood was collected via submandibular bleeds with goldenrod 4 mm lancets collected into sample tubes

coated with K2 EDTA (BD Ref# 365974) and 60 μ L of blood was lysed with 500 μ L of ACK lysis buffer. To assay spleens and livers, mice were sacrificed and organs harvested. To assay intracellular cytokine production, splenocytes were plated into 96-well u-bottom plates in complete kool-AID media and stimulated for 6 hours with a final concentration of 0.2 mg/ml GP33-41 (KAVYNFATM) in the presence of Brefeldin A.

Flow Cytometry

Spleens and livers were harvested into 2% FBS PBS with and passed through 70 μ m strainers to generate a single cell suspension. Samples were then spun at 450 r.c.f. for 5 minutes and livers were resuspended in 20% Percoll. Percoll suspensions were spun at 741 r.c.f for 20 minutes at 25°C and the supernatants discarded. Cell pellets for both spleens and livers were resuspended in 1 mL ACK lysis buffer and incubated at 4°C for 5 minutes. Lysis was stopped with 5 mL 2% FBS PBS and samples again spun at 450 r.c.f. for 5 minutes. Samples were resuspended in 2% FCS PBS and aliquoted into v-bottom 96 well plates. Live dead staining was then performed using the fixable viability dye at 1:2000 in PBS. Subsequently, cells were blocked with mouse Fc block 1:100 in 2% FCS PBS and stained for surface proteins with directly conjugated antibodies diluted 1:100 in 2% FCS PBS. Stains were incubated for 20 minutes at 4°C protected from light. For surface stains alone, LCMV samples were fixed with 4% PFA for 5 minutes at 4°C. For intracellular stains, samples were fixed and permeabilized according to the Transcription Factor Fixation Kit (Invitrogen Cat#00-5521-00). Intracellular antibodies were diluted in 1:100 in permeabilization buffer and incubated at 4°C for 30 minutes. All samples were spun at 821 r.c.f. for 5 minutes prior to being resuspended in 2% FCS PBS with 1:10 AccuCount beads (spherotech Cat #ACBP-100-10) for analysis on either the BD LSR II or the BD LSRFortessa flow cytometry analyzer.

Cell Isolation and In Vitro Functional Assays

CD8⁺ T cells were isolated from spleens using negative selection from the EasySep Mouse CD8⁺ T Cell Isolation Kit (cat# 19853). Cells were counted using trypan blue staining and the nexelcom cellometer spectrum. Cultures were started via stimulation with plate bound α CD3 (1 μ g/mL, clone 2C11) and α CD28 (1 μ g/mL, clone 37.51); plates coated overnight in PBS with Ca⁺⁺ & Mg⁺⁺ at 4°C. Cells were plated in Kool AID complete media (DMEM high glucose media supplemented with 10% FCS, pyruvate, nonessential amino acids, MEM vitamins, L-arginine, L-asparagine, L-glutamine, folic acid, beta mercaptoethanol, penicillin, and streptomycin) and spun at 450 r.c.f. for 5 minutes at 25°C to begin stimulation. For functional assays cells were harvested 2 or 4 hours after stimulation for flow cytometry, or 24 hours after stimulation for mRNA-seq. For supernatant cytokine expression, plates were spun at 450 r.c.f. for 5 minutes at 4°C 16 hours after stimulation and cell free culture medium was collected and frozen at -80°C. TNF α (Cat #), IFN γ (Cat #), and IL-2 (Cat #) were analyzed by ELISA.

miRNA qPCR

Spleens were harvested and single cell suspensions generated by passing through 70 μ m strainers. CD8⁺ T cells were isolated as above, and 2*10⁶ cells were pelleted at 450 r.c.f. for 5 minutes at 4°C. Cell pellet was resuspended in 700 μ L Trizol reagent (Ambion cat #15596018) and kept at -80°C. RNA was isolated using the Direct-zol-96 RNA Kit (zymogen Cat #R2054). This RNA was used as input to the Mir-XTM miRNA qRT-PCR TB Green[®] Kit (Takara cat# 638316) to generate miRNA cDNA. Specific primers to miR-15a, miR-15b, and miR-16 were used to quantify those miRNA species on the QPCR MACHINE (eppendorf realplex²). ribosomalRNA 5.8s was used as a housekeeping control for each sample. Each sample was run in duplicate. To quantify miRNA expression technical duplicates were averaged and then normalized to rRNA 5.8s by subtracting the rRNA 5.8s Ct value from miRNA Ct value (Δ Ct). Expression values reported are generated by 2^{- Δ Ct}.

mRNA Sequencing

1*10⁶ CD8+ T cells were harvested 24 hours after α CD3 \pm α CD28 stimulation as described above. Cells were pelleted at 450 r.c.f. for 5 minutes at 4°C. Cell pellet was resuspended in 700 uL Trizol reagent (ambion ref #15596018) and kept at -80°C. RNA was isolated using the Direct-zol-96 RNA Kit (zymogen Cat #R2054). The integrity of total RNA was checked on Fragment Analyzer (Agilent, Cat. No. DNF-472), only RNA with RQN number of above 7 was used for library construction. The starting quantity of 100ng of total RNA was used according to vendor instructions with Universal plus mRNA with Nu Quant (TECAN, Cat. No. 0520), final library PCR amplification was 17 cycles. After library completion, individual libraries were pooled equally by volume, and quantified on Fragment Analyzer (Agilent, Cat. No. DNF-474). Quantified library pool was diluted to 1nM and further diluted as per protocol and sequenced on Illumina MiniSeq (Illumina, Cat. No. FC-420-1001) to check for quality of reads. Finally, individual libraries were normalized according to MiniSeq output reads, specifically by % protein coding genes and were sequenced on one lane of NovaSeq6000 S4 PE100 (Illumina, Cat. No. 20028313). Reads were aligned to the mouse genome GRCm38 and quantified using the STAR aligner software version 2.7.2b. Read normalization and differential expression analysis was performed in the R computing environment version 3.6.1 using the software DESeq2 version 1.26. For RNA sequencing analysis, FDR-corrected p-values were used to evaluate significant differences between experimental groups using a significance threshold of 0.05. Lowly expressed genes that had fewer than 2 reads per million on average across all samples were removed from the analysis. Empirical cumulative density plots were made using the ggplot package for R. Heatmaps and hierarchical clustering was performed via the gplots package for R. Gene ontology analysis was performed using the statistical overrepresentation test for Panther pathways (Mi et al., 2019).

Statistical and Analytical Software

All flow cytometry data were analyzed using FlowJo (version 10). Statistical analyses and plotting was performed using Graphpad Prism (Version 9.2.0) and R (version 4.2.1).

Data Availability and Software

Ago2 HITS-CLIP data uploaded to NCBI GEO accession #GSE216565.

mRNA sequencing data uploaded to NCBI GEO accession #GSE216113.

Code used to analyze HITS-CLIP data summed over annotations and peaks in WT cells can be found at github.com/AnselLab/WT_HITS_CLIP_Analyses.

Code used to analyze relative binding densities of HITS-CLIP reads can be found at github.com/AnselLab/Malat1_miR1516_AGO2_HITS_CLIP.

Code used to analyze mRNAseq data for both miR-15/16 target expression and CD28 responsive genes can be found at github.com/AnselLab/Malat1_miR1516_CD3CD28_RNAseq.

Figures

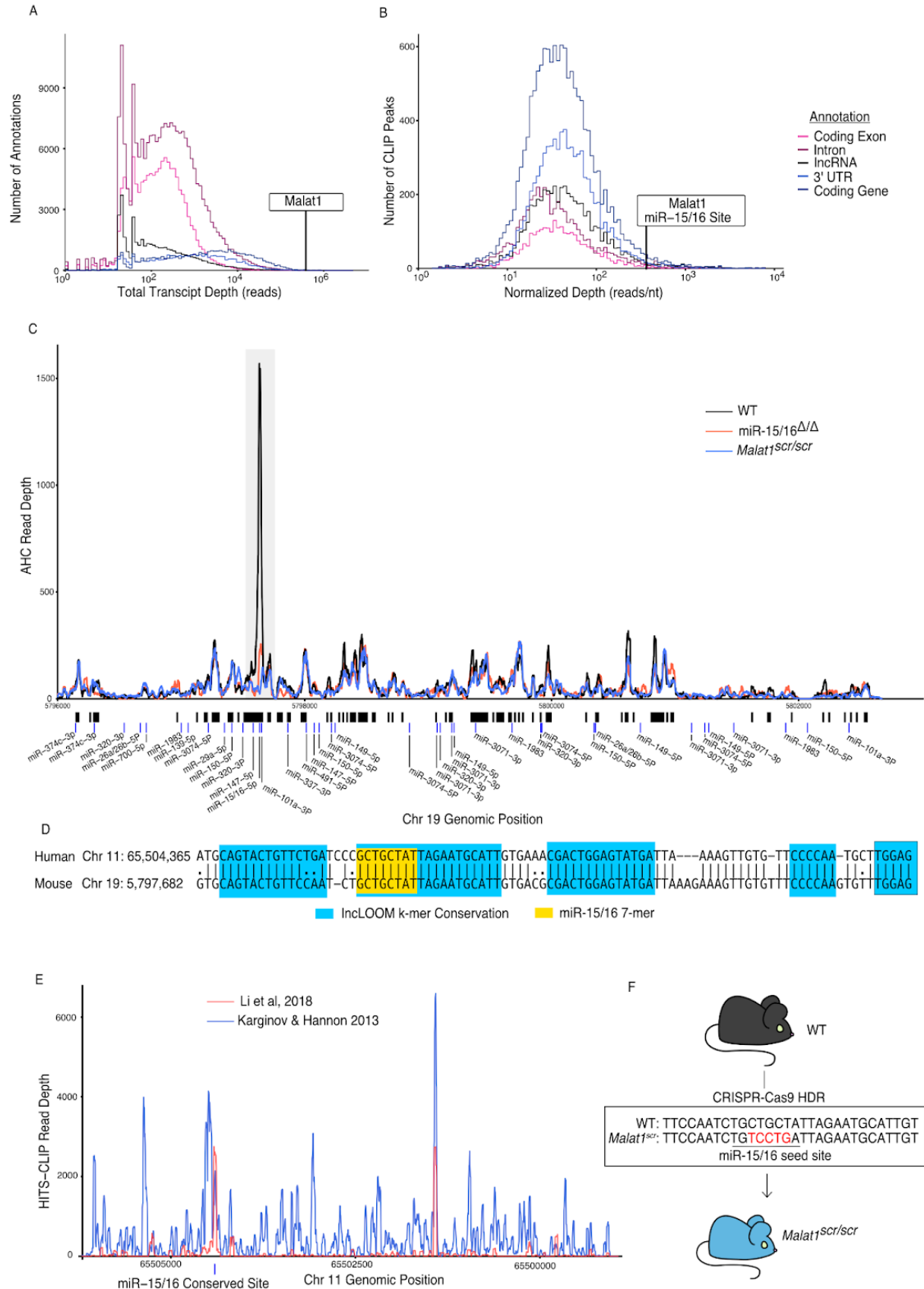


Figure 2.1. Malat1 is highly bound by miR-15/16

CD8+ T cells were isolated from spleens, grown *in vitro* for 5 days, then Ago2 transcriptomic occupancy was assayed via Ago2 HITS-CLIP.

(A-B) Transcriptome wide analysis of Ago2 HITS-CLIP libraries prepared from WT cells (combined libraries n =2).

(A) Summed reads across entire annotations. Line indicates total reads across the Malat1 transcript. Malat1 was #8 most highly bound lncRNA annotation, which was in the top 0.0091% of all lncRNA annotations analyzed with >0 HITS-CLIP reads.

(B) Ago2 HITS-CLIP peaks were identified and reads were summed within those called peaks that intersected with the given annotation. Peaks were of variable length so summed reads were normalized by peak length. Line indicates HITS-CLIP reads per nucleotide in the called peak containing the miR-15/16 binding site in Malat1. This peak was the #121 most bound HITS-CLIP peak in lncRNA peaks analyzed, which was in the top 2.3% of all evaluated peaks in lncRNAs.

(C) Ago2 HITS-CLIP binding to the mouse Malat1 locus reads from combined libraries shown (n = 2 for each genotype). Grey bar indicates the peak containing the miR-15/16 binding site. Black bars indicate regions identified as peaks by piranha. Blue bars indicate predicted binding sites of miRNAs expressed in our data set from the miRTarget custom sequence prediction algorithm. Grey bar indicates miR-15/16 binding peak.

(D) Local alignment of the human and mouse Malat1 sequences near the miR-15/16 conserved binding site. Highlighting indicates the depth of evolutionary conservation of k-mers as predicted by the IncLOOM algorithm (Ross et al., 2021).

(E) Ago2 HITS-CLIP binding to the human MALAT1 locus from publicly available data sets (Karginov and Hannon, 2013; Li et al., 2018). Blue vertical bar indicates the conserved miR-15/16 binding site.

(F) Schematic representing the creation of the *Malat1^{scr}* allele. Bases in red indicate the 5 nucleotides whose sequence was scrambled by CRISPR-Cas9 HDR to prevent miR-15/16 binding.

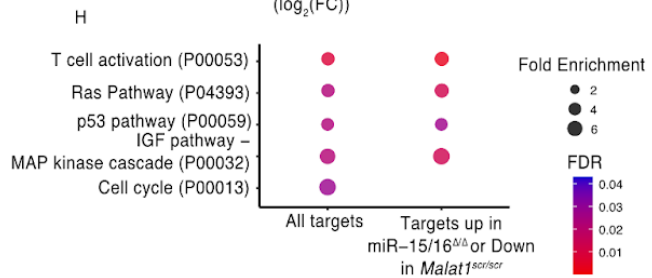
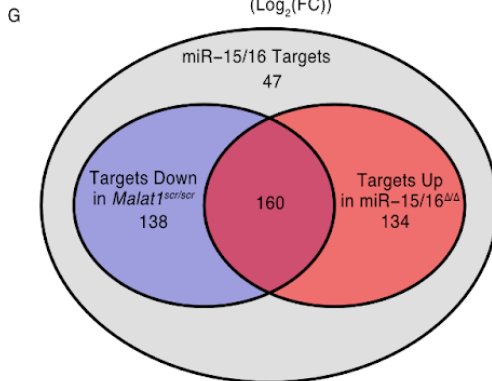
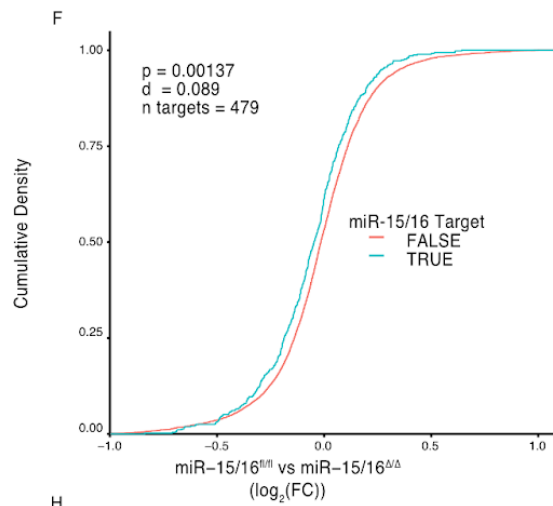
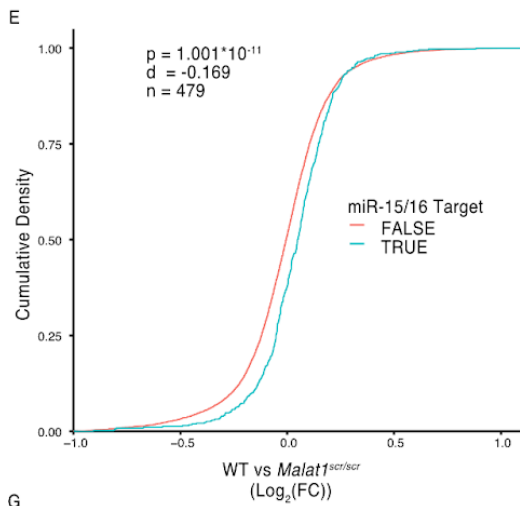
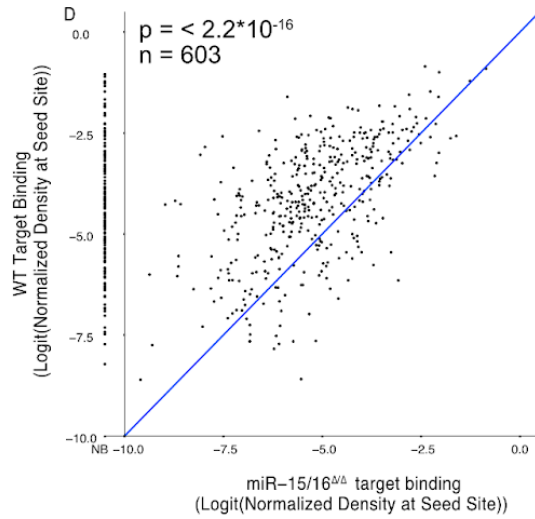
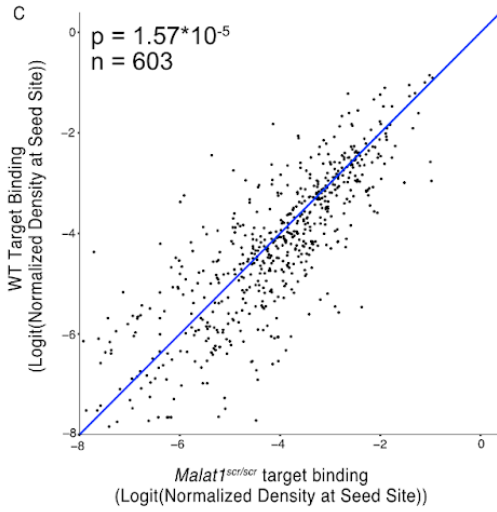
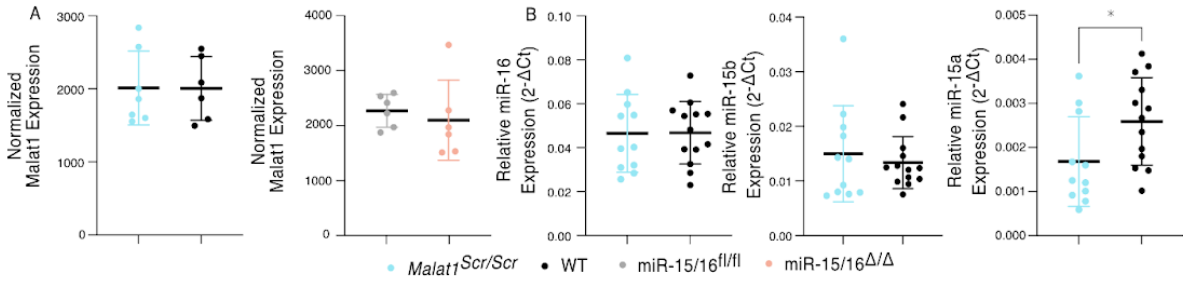


Figure 2.2. Malat1 Inhibits miR-15/16 binding and suppressive activity

(A) Malat1 expression measure by RNA-seq from CD8⁺ T cells isolated from spleens and stimulated with α CD3 and α CD28 for 24 hours (WT n = 6, *Malat1*^{scr/scr} n = 7, miR-15/16^{fl/fl} n = 6, miR-15/16 ^{Δ/Δ} n = 6; 1 experiment)

(B) miR-16, miR-15b, and miR-15a expression measured by miRNA qPCR from CD8⁺ T cells freshly isolated from spleens. Expression was determined relative to 5.8s ribosomal RNA expression. Unpaired t-test performed to determine significance.

(C-D) TargetScan predicted miR-15/16 binding sites that contained at least one HITS-CLIP read in both WT and *Malat1*^{scr/scr} CD8⁺ T cells were compared for depth of Ago2 HITS-CLIP reads.

First, reads at the predicted seed site were normalized by total Ago2 HITS-CLIP reads in a given 3' UTR. To best visualize all sites, logit transforms of these values are plotted. Paired t-test performed to determine significance. Blue line indicates the identity line. Data for each genotype are from combined libraries of n = 2 biological replicates.

(C) Comparison of WT and *Malat1*^{scr/scr} cells

(D) Comparison of WT and miR-15/16 ^{Δ/Δ} . Values to the left of the y-axis labeled with NB indicate there was no bind detected at that site in the miR-15/16 ^{Δ/Δ} cells.

(E-F) Cumulative density plots to determine changes in expression of miR-15/16 targets.

Targets determined by TargetScan predicted miR-15/16 mRNA targets that had at least one 3' UTR site with reads in both WT and *Malat1*^{scr/scr} CD8⁺ T cells. Kolmogorov-Smirnov test used to determine significant differences in the distributions of target and non-target genes.

(E) comparison of the Log₂(FC) between WT and *Malat1*^{scr/scr} samples stimulated with α CD3 and α CD28 for 24 hours

(F) comparison of the Log₂(FC) between miR-15/16^{fl/fl} and miR-15/16 ^{Δ/Δ} samples stimulated with α CD3 and α CD28 for 24 hours.

(G) Venn diagram of miR-15/16 target expression regulated in concordance with the Malat1-miR-15/16 circuit. The blue circle indicates genes with WT vs *Malat1*^{scr/scr} log₂(FC) > 0 and the red circle indicates genes with miR-15/16^{fl/fl} vs miR-15/16 ^{Δ/Δ} log₂(FC) < 0. The purple overlap indicates genes that meet both conditions and the grey indicates genes that do not meet either condition.

(H) Gene ontology analysis of the bound target set used above as well as genes regulated in accordance with the Malat1-miR-15/16 circuit with the same conditions as in F. Enrichment determined within the Panther Pathway annotations.

(* , p<0.05)

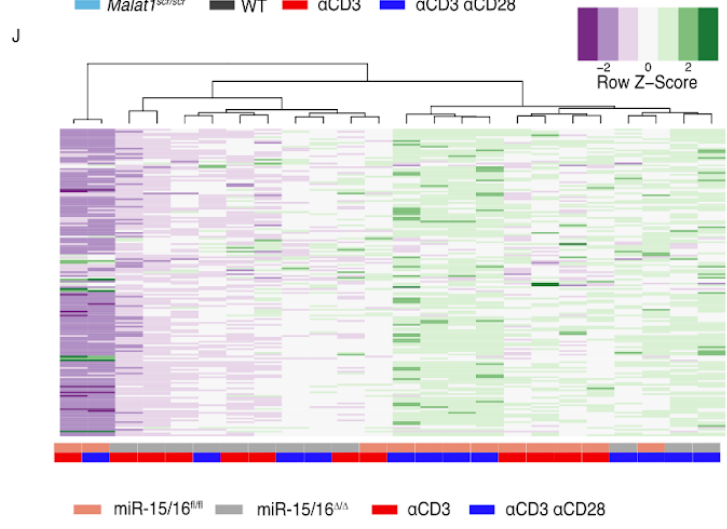
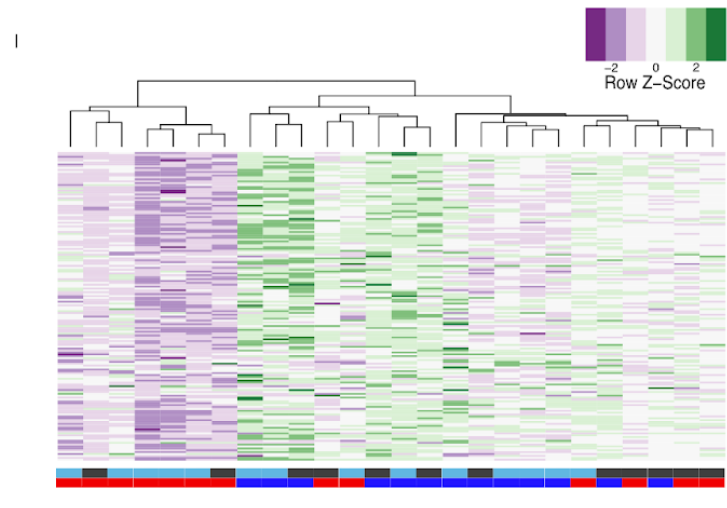
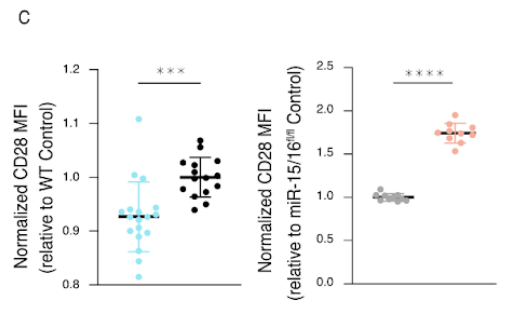
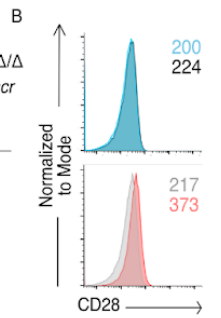
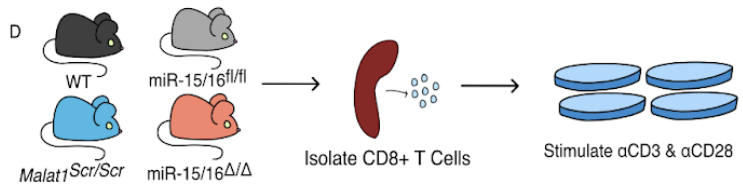
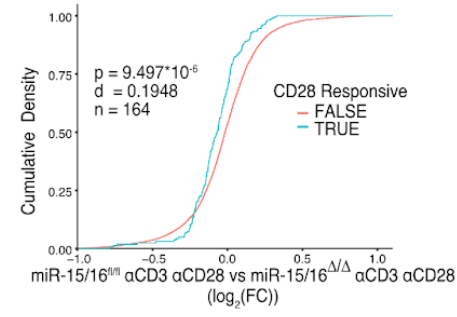
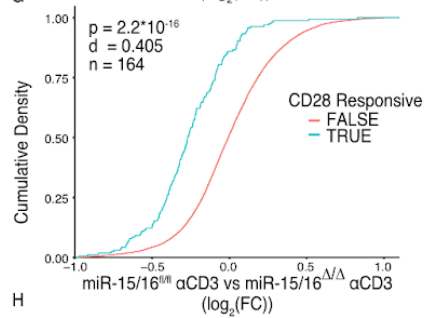
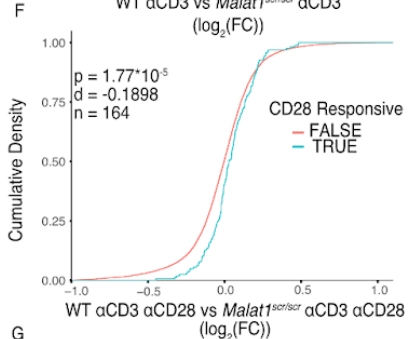
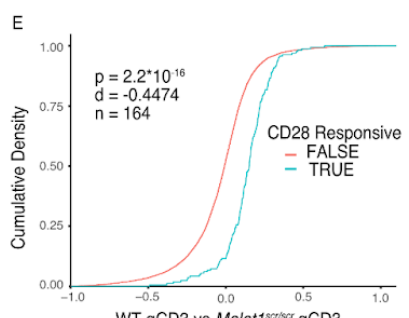
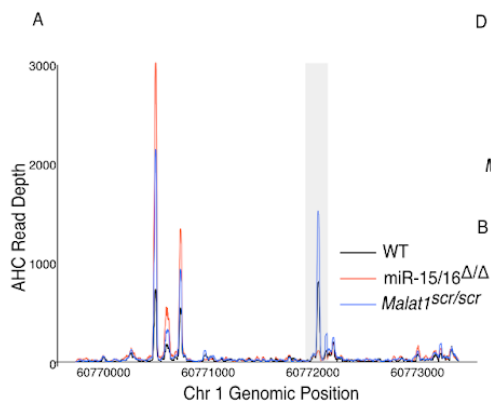


Figure 2.3. The Malat1-miR-15/16 Circuit Increase CD28 Expression and Co-stimulation induced Gene Expression

- (A) Ago2 HITS-CLIP binding at the Cd28 locus. Sequencing libraries generated from CD8⁺ T cells isolated from spleens and cultured for 5 days (combined libraries from n = 2 for each genotype). Grey bar indicates the peak containing the TargetScan predicted miR-15/16 binding site.
- (B) Schematic illustrating the assay scheme to assay acute gene expression downstream of CD28 co-stimulation
- (C) Representative flow cytometry plots of CD28 expression on naive (CD62L⁺ CD44⁻) CD8⁺ T cells from spleens of unchallenged mice. Mean fluorescence intensity for the sample reported in the upper right of the plot.
- (D) Quantification of CD28 mean fluorescence intensity normalized to the relevant control. (*Malat1*^{scr/scr} compared to WT from 3 independent experiments; miR-15/16^{fl/fl} compared to miR-15/16^{Δ/Δ} from 2 independent experiments)
- (E-H) Cumulative density plots comparing expression of CD28 responsive gene set defined as genes from (Martínez-Llordella et al., 2013) with αCD3αCD28 vs αCD3 log₂(FC) > 1.5 and adjusted p value < 0.001. Kolmogorov-Smirnov test used to determine significant differences in the distributions of target and non-target genes. αCD3 used at 1 μg/mL, and αCD28 used at 1 μg/mL.
- (E) Comparison of CD28 responsive genes in WT vs *Malat1*^{scr/scr} cells stimulated with αCD3 alone
- (F) Comparison of CD28 responsive genes in WT vs *Malat1*^{scr/scr} cells stimulated with αCD3 and αCD28
- (G) Comparison of CD28 responsive genes in miR-15/16^{fl/fl} vs miR-15/16^{Δ/Δ} cells stimulated with αCD3 alone
- (H) Comparison of CD28 responsive genes in miR-15/16^{fl/fl} vs miR-15/16^{Δ/Δ} cells stimulated with αCD3 and αCD28
- (I-J) Heatmaps of CD28 responsive gene set expression by genotype and stimulation condition. Dendrograms represent unbiased hierarchical clustering of the samples.
- (I) *Malat1*^{scr/scr} and WT samples compared with αCD3 ± αCD28
- (J) miR-15/16^{fl/fl} vs miR-15/16^{Δ/Δ} samples compared with αCD3 ± αCD28
- (* , p<0.05; **, p<0.01;***,p<0.001; ****, p<0.0001)

Figure 2.4. The Malat1-MiR-15/16 circuit increases functional outcomes of CD28 co-stimulation

(A-C) CD8⁺ T cells were isolated from spleens and stimulated with α CD3 and α CD28 antibodies, results displayed are gated on activated cells (CD69⁺ Nur77⁺)

(A) Representative histograms of CD69 and Nur77 expression 4 hours after stimulation

(B) Quantification of CD69 mean fluorescence intensity 2 and 4 hours after stimulation. Both time points reflect statistically significant changes ($p < 0.01$) by ordinary one-way ANOVA; statistics displayed on graph represent results of post-hoc multiple comparisons of *Malat1*^{scr/scr} to WT and miR-15/16^{ΔΔ} to WT. Data from 2 independent experiments, each normalized to WT average value.

(C) Quantification of Nur77 mean fluorescence intensity 2 and 4 hours after stimulation. No significant changes determined by ordinary one-way ANOVA. Data from 2 independent experiments, each normalized to WT average value.

(D-F) Quantification of cytokine secretion into the supernatant by CD8⁺ T cells isolated from spleens, stimulated α CD3 \pm α CD28, and cultured 16 hours. Cell free supernatant protein concentration measured by ELISA. Data from a single experiment

(D) Quantification of IL-2 secretion. By 2-way ANOVA, in both experiments there was a significant ($p < 0.0001$) increase in IL-2 with the addition of α CD28 stimulation. But the only significant ($p = 0.0001$) genotypic effect was increased IL-2 secretion in miR-15/16^{ΔΔ} vs miR-15/16^{mn}. Comparisons shown on plot are the results of post-hoc multiple comparison tests.

(E) Quantification of TNF α secretion. By 2-way ANOVA, in both experiments there was a significant ($p < 0.0001$) increase in IL-2 with the addition of α CD28 stimulation. But the only significant ($p = 0.003$) genotypic effect was increased IL-2 secretion in miR-15/16^{ΔΔ} vs miR-15/16^{mn}. Comparisons shown on plot are the results of post-hoc multiple comparison tests.

(F) Quantification of IFN γ secretion. By 2-way ANOVA, in both experiments there was a significant ($p < 0.0001$) increase in IL-2 with the addition of α CD28 stimulation. But no genotypic effect was observed.

(* , $p < 0.05$; **, $p < 0.01$; ***, $p < 0.001$; ****, $p < 0.0001$)

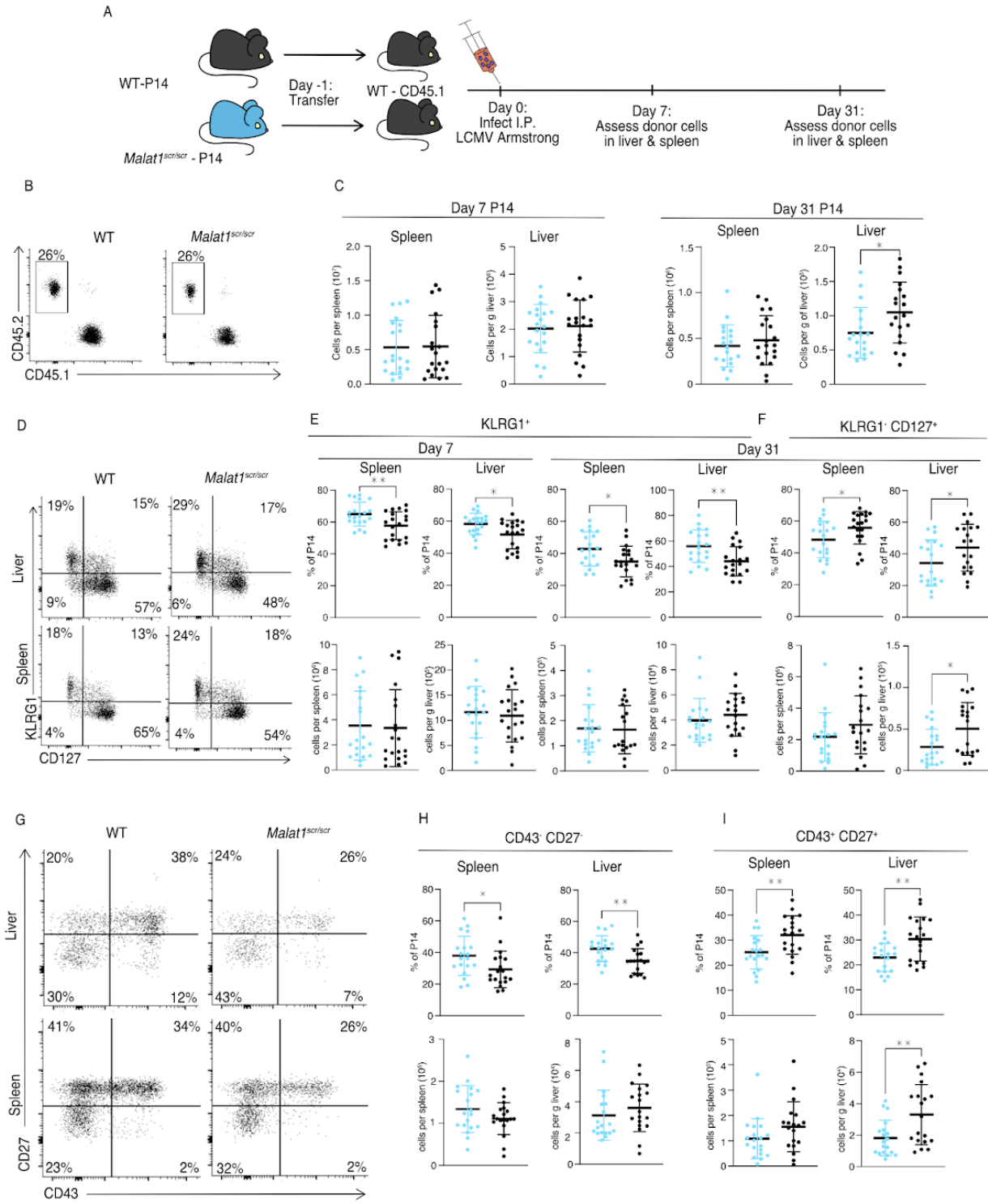


Figure 2.5. Malat1 enhances memory T cell persistence following LCMV infection

Malat1^{scr/scr} and WT cells containing the GP33 specific TCR transgene (P14) on the CD45.2 background were transferred separately into congenic CD45.1 WT hosts. One day later the recipient mice were infected with 5*10⁵ p.f.u. i.p. lcmv armstrong. LCMV specific responses were assayed by monitoring the transferred cells by flow cytometry in the blood, spleen, and liver over time (data from two independent experiments per time point)

(A) Schematic of experimental design

(B) Representative flow plots to identify and quantify transferred cells

(C) Quantification of transferred P14 cell numbers at day 7 and day 31

(D) Representative flow plots of KLRG1 and CD127 expression on P14 cells at day 31 post infection

(E) Quantification of P14 KLRG1⁺ cells by percent of P14 and total numbers in spleen and liver at day 7 and day 31 post infection

(F) Quantification of P14 KLRG1⁺ CD127⁺ by percent of P14 and total numbers in spleen and liver at day 31 post infection

(G) Representative flow plots of CD43 and CD27 expression on P14 cells at day 31 post infection

(H) Quantification of P14 CD43⁺ CD27⁺ t-Tem cells by percent of P14 and total numbers in spleen and liver at day 31 post infection

(I) Quantification of P14 CD43⁺ CD27⁺ memory cells by percent of P14 and total numbers in spleen and liver at day 31 post infection

Statistics displayed determined by unpaired t-test between *Malat1*^{scr/scr} and WT transferred cells (*, p<0.05; **, p<0.01)

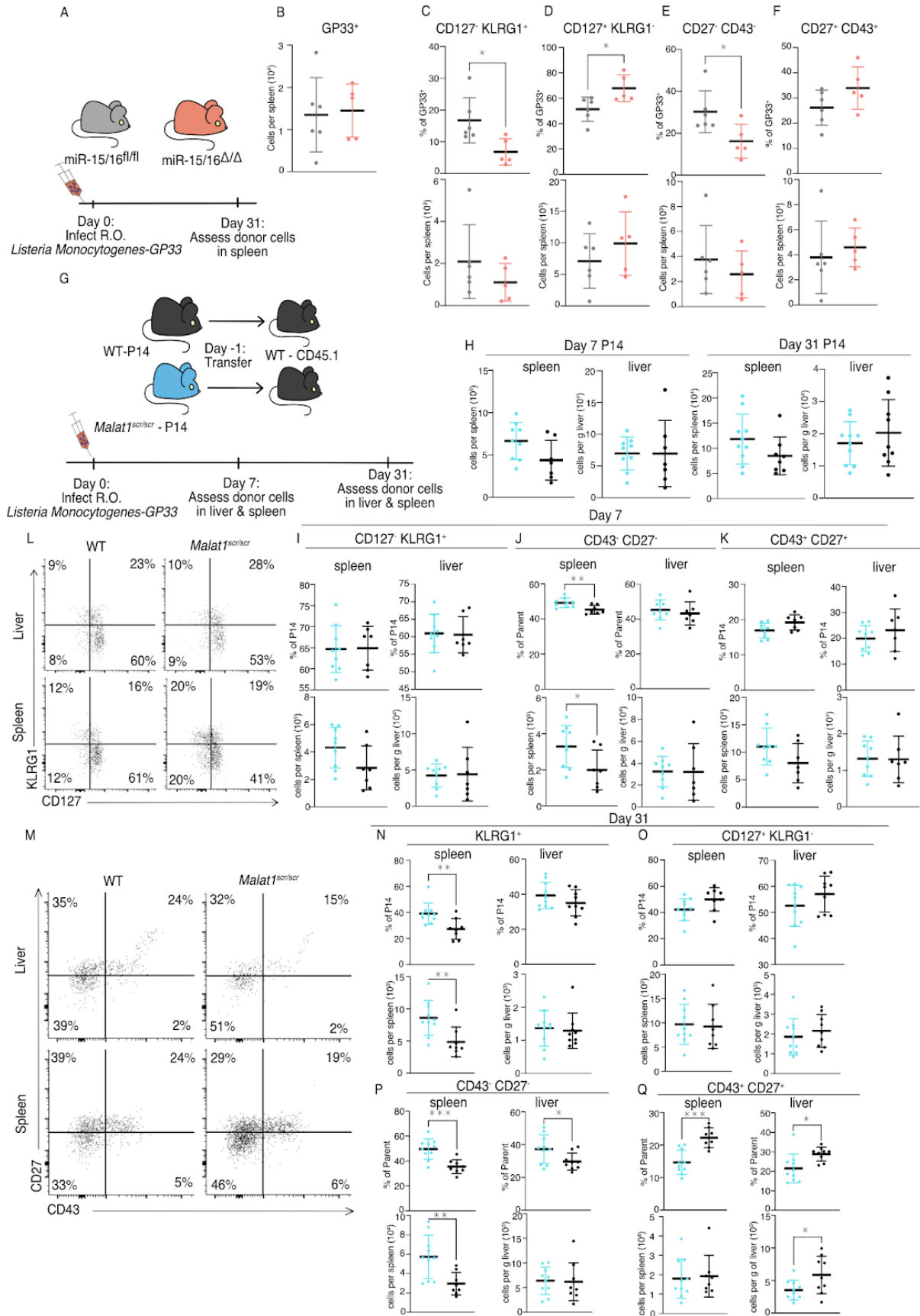


Figure 2.6. Malat1 and miR-15/16 alter memory T cell differentiation following *Listeria Monocytogenes* infection

miR-15/16^{fl/fl} and miR-15/16^{ΔΔ} with a polyclonal TCR repertoire were directly infected with 2*10⁴ colony forming units (c.f.u.) r.o. *Listeria monocytogenes-gp33* (LM-GP33). Genotypes on the plots are indicated by dot color corresponding to the schematics in A and G. LM-GP33 specific responses were then assayed in the spleen 31 days post infection (miR-15/16^{ΔΔ} n = 5 and miR-15/16^{fl/fl} n = 6 from a single experiment).

(A) schematic of experimental design

(B) Quantification of tetramer specific CD8 T cells in the spleen

(C-F) Quantification of tetramer specific subpopulations by percent of GP33+ and numbers for (C) CD127⁻ KLRG1⁺, (D) CD127⁺ KLRG1⁺, (E) CD27⁻ CD43⁺, and (F) CD27⁺ CD43⁺ populations *Malat1*^{scr/scr} and WT cells containing the GP33 specific TCR transgene (P14) on the CD45.2 background were transferred separately into congenic CD45.1 WT hosts. One day later the recipient mice were infected with 2*10⁴ c.f.u. r.o. LM-GP33. LM-GP33 specific responses were assayed by monitoring the transferred cells by flow cytometry in the spleen and liver at discrete time points (data from a single experiment per time point).

(G) Schematic of experimental design

(H) Quantification of transferred P14 cell numbers at day 7 and day 31

(I-K) Quantification of P14 (I) CD127⁻ KLRG1⁺, (J) CD43⁻ CD27⁺, and (K) CD43⁺ CD27⁻ cells by percent of P14 and total numbers in spleen and liver at day 7

(L) Representative flow plots of KLRG1 and CD127 expression on P14 cells at day 31 post infection

(M) Representative flow plots of CD43 and CD27 expression on P14 cells at day 31 post infection

(N-Q) Quantification of P14 (N) KLRG1⁻, (O) CD127⁺ KLRG1⁺, (P) CD43⁻ CD27⁺, and (Q) CD43⁺ CD27⁻ cells by percent of P14 and total numbers in spleen and liver at day 31 post infection
Statistics displayed determined by unpaired t-test between *Malat1*^{scr/scr} and WT transferred cells (*, p<0.05; **, p<0.01; ***, p<0.001)

● *Malat1^{Scr/Scr}* ● WT

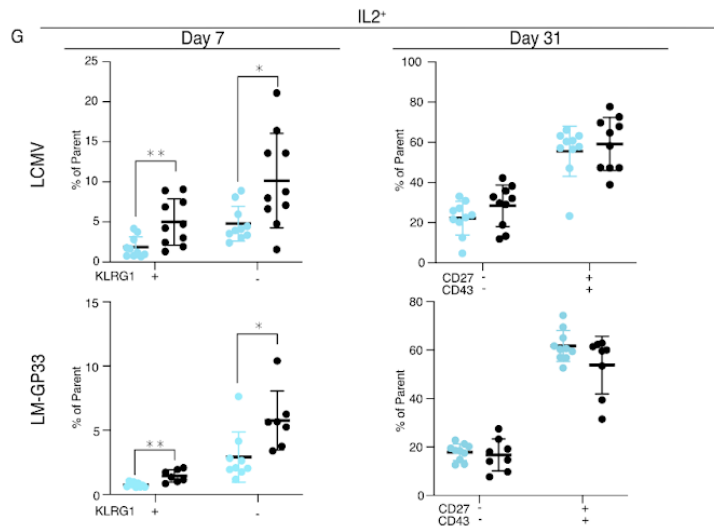
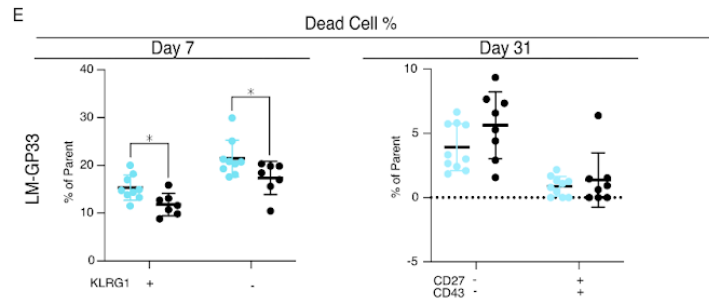
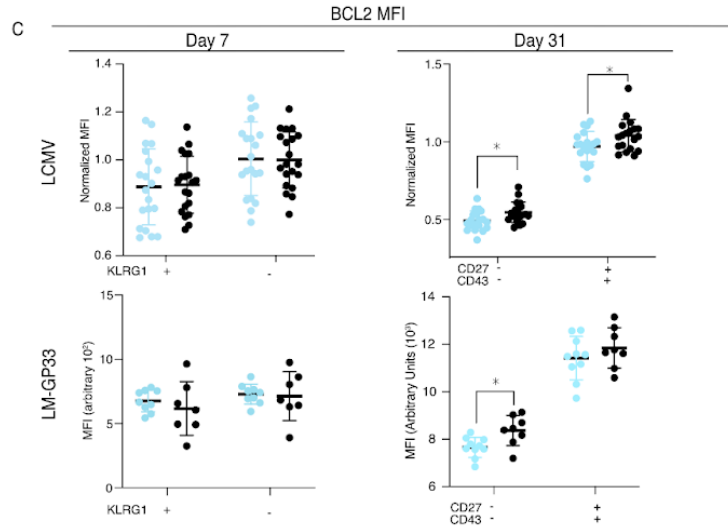
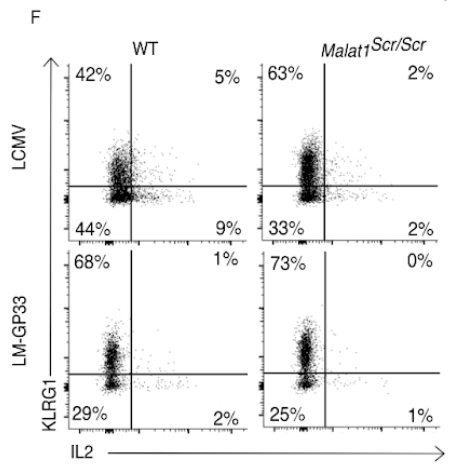
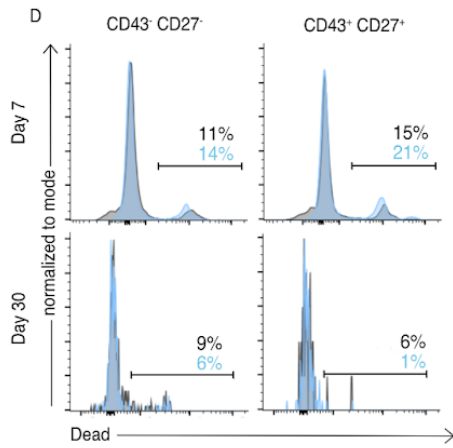
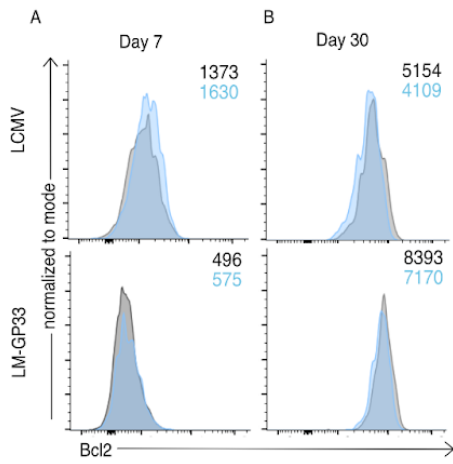


Figure 2.7. Malat1 Enhances Pro-survival Cues Downstream of T cell activation

Malat1^{scr/scr} and WT cells containing the GP33 specific TCR transgene (P14) on the CD45.2 background were transferred separately into congenic CD45.1 WT hosts. One day later the recipient mice were infected with 2×10^5 p.f.u. i.p. Lcmv armstrong or 2×10^5 c.f.u. r.o. LM-GP33. Antigen specific responses were assayed by monitoring the transferred cells by flow cytometry in the spleen.

(A-C) Bcl2 expression in transferred P14 cells in the spleen 7 and 31 days post infection for both LCMV and LM-GP33. Data from two independent experiments per LCMV time point and a single experiment per LM-GP33 time point.

(A) Representative flow cytometry plots of P14 KLRG1⁺ CD127⁻ cell Bcl2 expression 7 days post infection. Numbers shown are mean fluorescence intensity.

(B) Representative flow cytometry plots of P14 CD43⁺ CD27⁻ cell Bcl2 expression 31 days post infection. Numbers shown are mean fluorescence intensity.

(C) Quantification of Bcl2 expression producing cells by mean fluorescence intensity within the indicated P14 subpopulation defined by KLRG1 or CD27 and CD43.

(D-E) Analysis of dead cells within splenic P14 CD43 and CD27 subpopulations at days 7 and 31 post LM-GP33 infection, data from a single experiment per time point.

(D) Representative flow cytometry plots of P14 subsets defined by CD43 and CD27. Numbers shown represent percent of dead cells per the parent subpopulation

(E) Quantification of dead cells as a percentage of parent P14 subpopulation

(F-G) Analysis of IL-2 producing P14 subsets in the spleen via IL-2 capture assay at days 7 and 31 post infection for both LCMV and LM-GP33, data from a single experiment per infection per time point.

(F) Representative flow cytometry plots of all P14 cells stained for KLRG1 and captured IL-2 from both infections at day 7. Numbers represent percent of cells in that quadrant of all P14 transferred cells.

(G) Quantification of IL-2 producing cells by percent of parent within the indicated P14 subpopulation defined by KLRG1 or CD27 and CD43.

Statistics displayed determined by unpaired t-test between *Malat1^{scr/scr}* and WT transferred cells, where multiple tests were performed the Holm–Šidák method was used to correct for multiple comparisons (*, $p < 0.05$; **, $p < 0.01$)

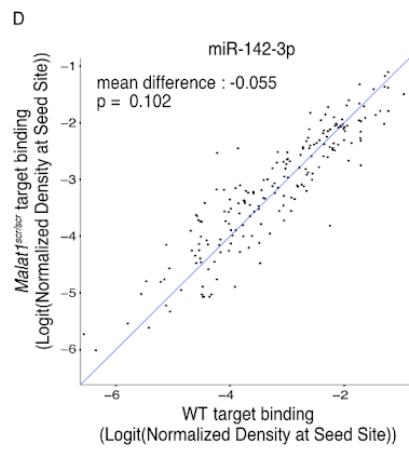
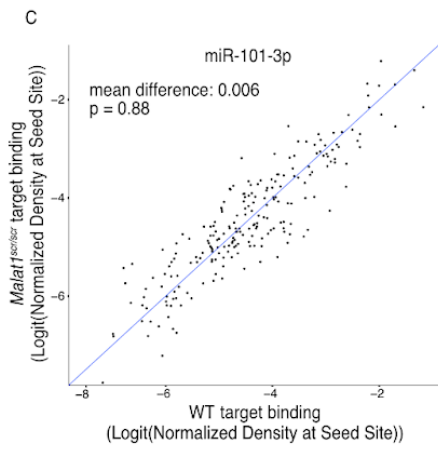
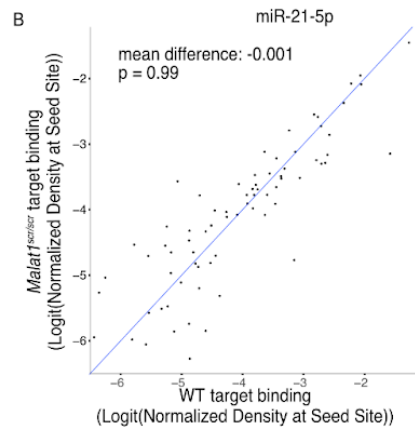
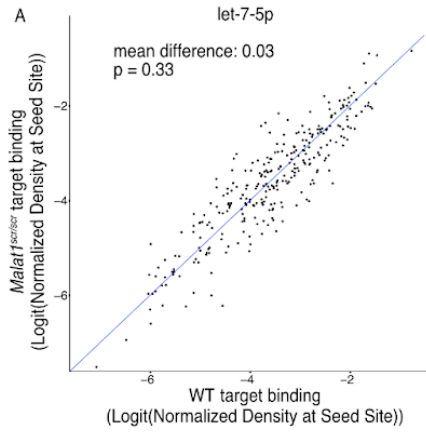
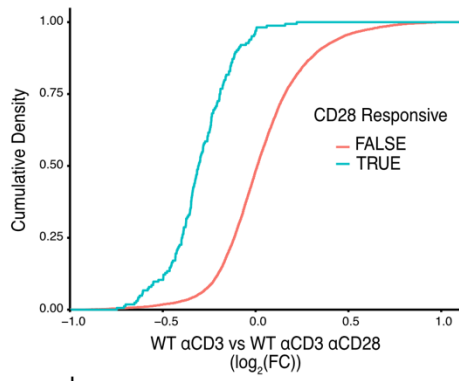


Figure 2.S1. *Malat1^{scr}* allele does not disrupt other miRNA families

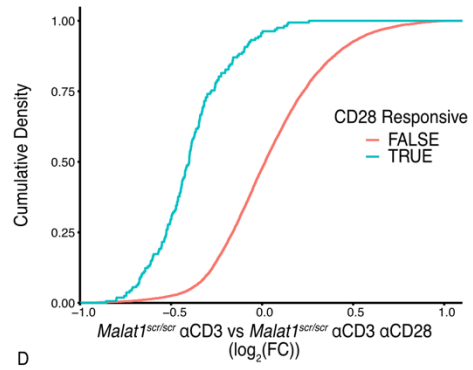
TargetScan predicted binding sites for highly expressed microRNA families in T cells that contained at least one HITS-CLIP read in both WT and *Malat1^{scr/scr}* CD8⁺ T cells were compared for depth of Ago2 HITS-CLIP reads. First, reads at the predicted seed site were normalized by total Ago2 HITS-CLIP reads in a given 3' UTR. To best visualize all sites, logit transforms of these values are plotted. Paired t-test performed to determine significance. Blue line indicates the identity line. Data for each genotype are from combined libraries of n = 2 biological replicates.

- (A) Predicted sites for let-7-5p
- (B) Predicted sites for miR-21-5p
- (C) Predicted sites for miR-101-3p
- (D) Predicted sites for miR-142-3p

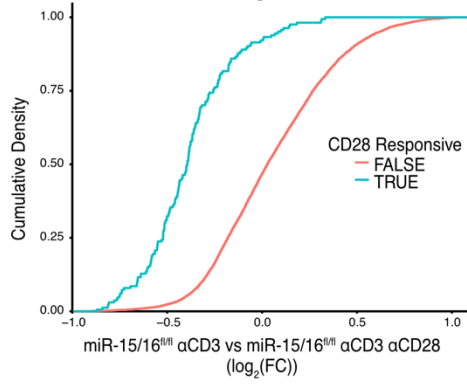
A



B



C



D

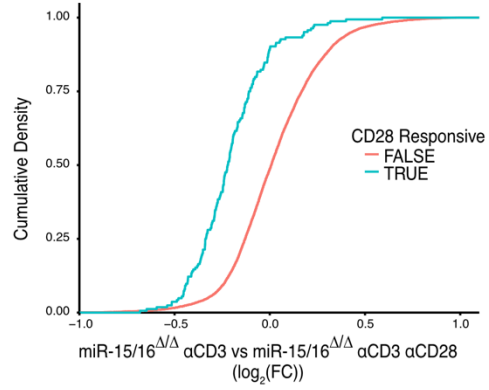
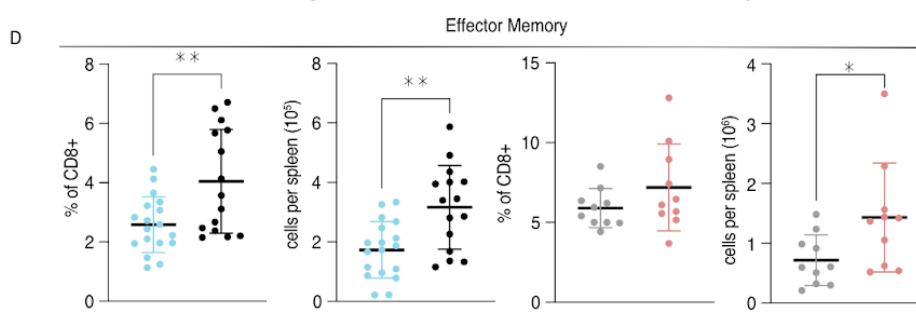
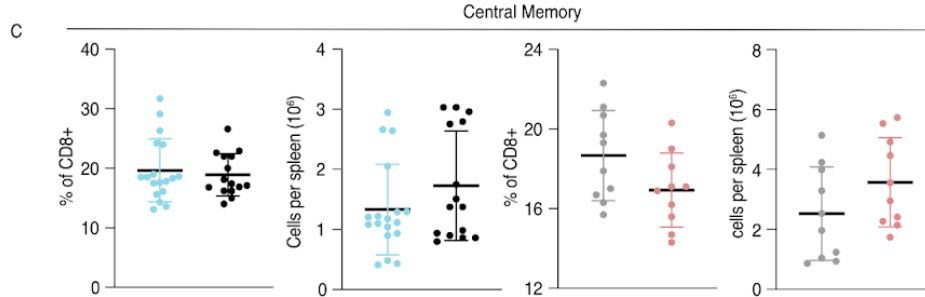
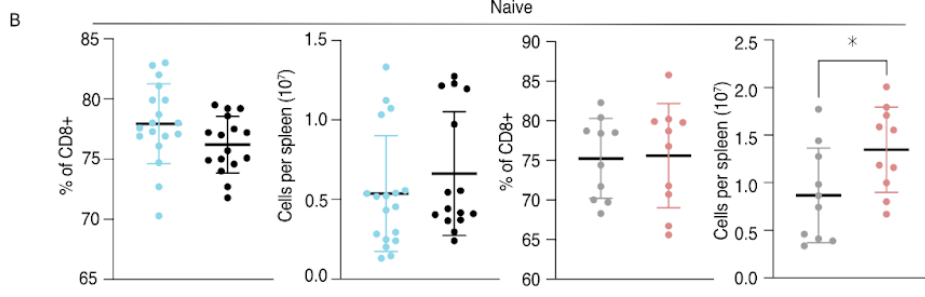
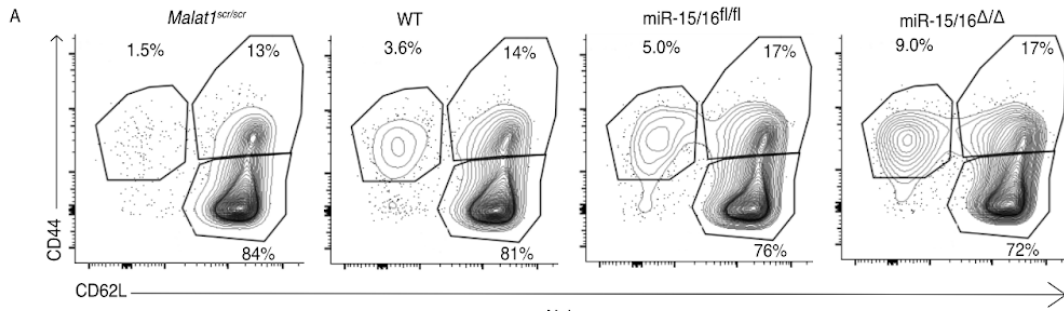


Figure 2.S2. CD28 responsive genes are induced by α CD28 stimulation in all genotypes tested

Cumulative density plots comparing expression of CD28 responsive gene set defined as genes from (Martínez-Llordella et al., 2013) with α CD3 α CD28 vs α CD3 $\log_2(\text{FC}) > 1.5$ and adjusted p value < 0.001 . Kolmogorov-Smirnov test used to determine significant differences in the distributions of target and non-target genes. α CD3 used at 1 $\mu\text{g}/\text{mL}$, and α CD28 used at 1 $\mu\text{g}/\text{mL}$. Data are from a single experiment with $n=6$ for each genotype and stimulation condition combination.

- (A) Comparison of CD28 responsive genes in WT cells
- (B) Comparison of CD28 responsive genes in *Malat1*^{scr/scr} cells
- (C) Comparison of CD28 responsive genes in miR-15/16^{fln} cells
- (D) Comparison of CD28 responsive genes in miR-15/16 ^{Δ/Δ} cells



● *Malat1^{scr/scr}* ● WT ● *miR-15/16^{fl/fl}* ● *miR-15/16Δ/Δ*

Figure 2.S3. Malat1 Regulates Memory Formation in Unchallenged Poly Clonal Animals

Cells were isolated from the spleens of young, age-matched, naive mice and analyzed by flow cytometry for CD44 and CD62L to delineate naive, effector memory, and central memory cells. Results shown are gated on CD8⁺ CD5⁻ lymphocytes. Data for *Malat1*^{scr/scr} and WT cells are from 3 independent experiments. Data for miR-15/16^{fl/fl} and miR-15/16^{ΔΔ} cells are from 2 independent experiments. Statistics displayed determined by unpaired t-test between *Malat1*^{scr/scr} and WT cells or between miR-15/16^{fl/fl} and miR-15/16^{ΔΔ} cells (*, p<0.05; **, p<0.01)

(A) Representative flow cytometry plots of CD44 and CD62L for each genotype assayed.

Percentages shown are of CD8⁺ population.

(B) Quantification of naive cells (CD62L⁺ CD44⁻)

(C) Quantification of central memory cells (CD62L⁺ CD44⁺)

(D) Quantification of effector memory cells (CD62L⁻ CD44⁺)

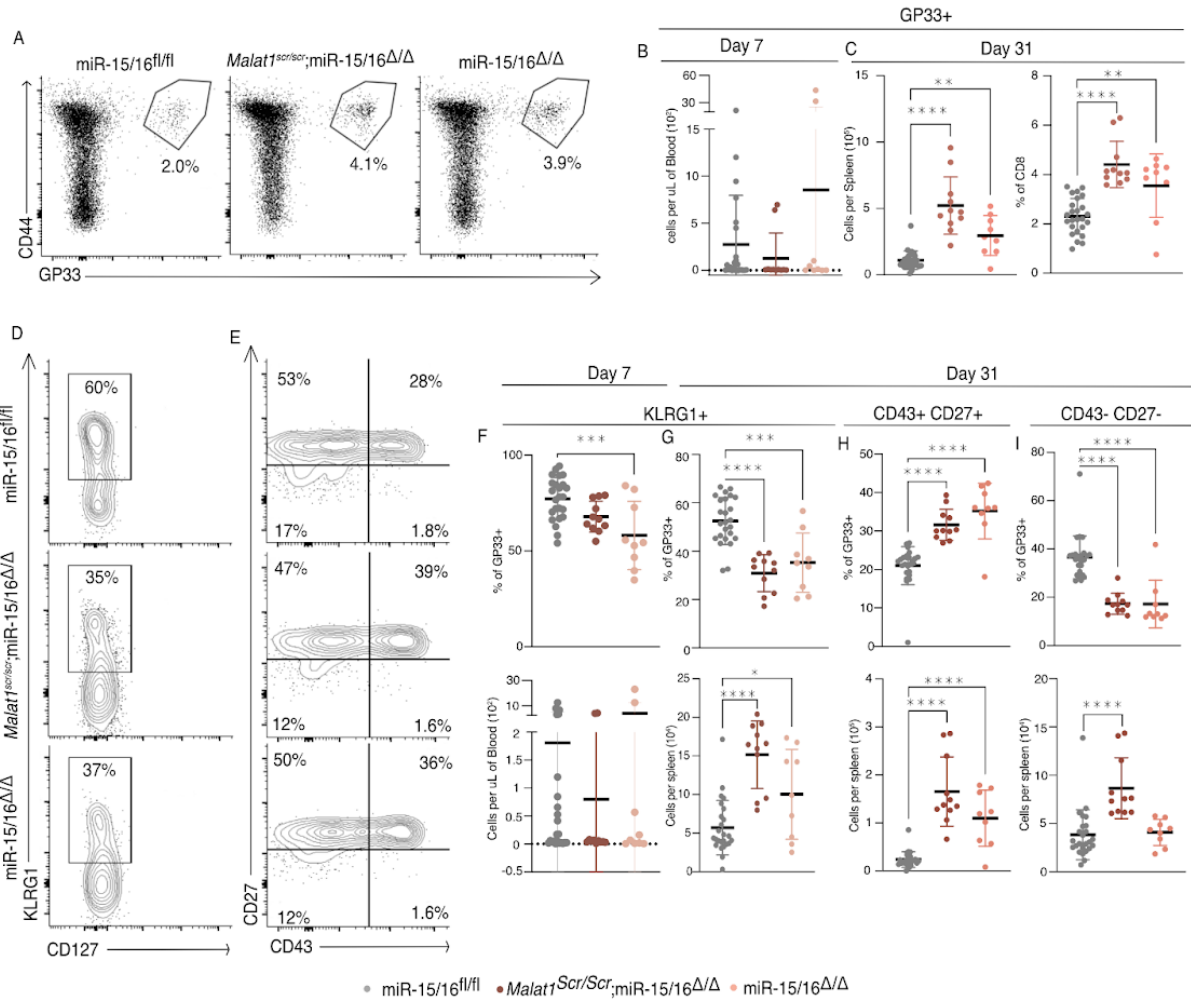


Figure 2.S4. Malat1 is epistatic to miR-15/16 in the regulation memory cell expansion following LCMV infection

Polyclonal mice of the miR-15/16^{fl/fl}, miR-15/16^{Δ/Δ}, and *Malat1*^{scr/scr};miR-15/16^{Δ/Δ} genotypes were directly infected i.p. with 5*10⁵ p.f.u. i.p. lcmv armstrong. Antigen specific responses were tracked in the blood and spleen using the GP33 tetramer at day 7 and day 31 post infection.

(A) Representative flow cytometry plots illustrating the gating on antigen specific cells using CD44 and GP33

(B) Quantification of GP33+ cells in the blood at day 7

(C) Quantification of GP33+ cells in the spleen at day 31 by absolute numbers and percent of the CD8+ T cell population

(D) Representative flow cytometry plots of KLRG1 and CD127 expression at day 31 in the antigen specific cell population

(E) Representative flow cytometry plots of CD27 and CD43 expression at day 31 in the antigen specific cell population

(F) Quantification of KLRG1⁻ antigen specific cells in the blood at day 7 by relative percentage and absolute numbers

(G) Quantification of KLRG1⁺ antigen specific cells in the spleen at day 31 by relative percentage and absolute numbers

(H) Quantification of CD43⁺ CD27⁺ memory cells in the spleen at day 31 by relative percentage and absolute numbers

(I) Quantification of CD43⁻ CD27⁻ t-Tem cells in the spleen at day 31 by relative percentage and absolute numbers

Tables

Table 2.1. lncRNAs with the most AHC reads

Noncode Gene ID	Total Reads	Chromosome	Alias	Note
NONMMUG0183 30.3	4766634	17	ENSMUST000 00198477.1	Contains rRNA repeat
NONMMUG0443 54.2	2291785	M	mt-Rnr2	Overlaps mt-ND1
NONMMUG0443 53.2	1208170	M	mt-Rnr1	
NONMMUG0763 21.1	1012732	6		Overlaps and best aligns to NONMMUG034479 .2
NONMMUG0344 78.3	1012015	6		Overlaps and best aligns to NONMMUG034479 .2
NONMMUG0344 79.2	1011610	6		Contains rRNA repeat
NONMMUG0079 38.3	785970	11		Intronic of Gm36876, contains rRNA repeat(Weirick et al., 2016)
NONMMUG0206 71.2	383447	19	Malat1	
NONMMUG0157 81.2	336664	16		Intronic of Zc3h7a, contains rRNA repeat
NONMMUG0443 21.2	317822	9		Contained in Lars2 3' UTR, contains rRNA repeat

Table 2.2. lncRNAs with the most AHC reads that do not align to rRNA repeat elements

Noncode Gene ID	Total Reads	Chromosome	Alias	Note
NONMMUG018330.3	688875	17	ENSMUST00000198477.1	Partially anti-sense to XR_877120.2, binding extends beyond rRNA repeat
NONMMUG020671.2	383447	19	Malat1	
NONMMUG094408.1	296723	6		Contains B4A/B3 SINE, binding restricted to SINE
NONMMUG005751.2	291393	11		Intronic of Dock2, contains multiple RLTR44-int repeat elements, binding restricted to RLTRs
NONMMUG094727.1	289326	6		Contains B4A/B3 SINE, binding is restricted to repeats
NONMMUG014644.3	241005	15	Pvt1	Many repeats, but binding is not restricted to any definite subset
NONMMUG096664.1	229834	15	PVt1	Splice variant of NONMMUG014644.3
NONMMUG024327.3	222686	2	Oip5os1, Cyrano	Well described in (Han et al., 2020)
NONMMUG026716.2	207631	3		Overlapping Mbnl1
NONMMUG094659.1	196269	6		Overlapping Foxp1

Table 2.3. T Cell Activation Genes Affected by Malat1-miR-15/16 Circuit

T Cell Activation Genes Affected by Malat1-miR-15/16 Circuit
Sos2
Mapk8
Cd28
Nfatc3
Mapk9
Pik3r1
Braf
Vav2
Cdc42

Table 2.4. Key Reagent Table

Reagent	Source	Detail	Catalog #
IL-2 ELISA	Invitrogen		5018280
TNF α ELISA	Invitrogen		BMS607-3
IFN γ ELISA	R&D Systems		MIF00
IL-2 Secretion Assay APC	Miltenyi Biotec		130-090-987
Malat1 CRISPR Guide 1	Dharmacon	Sequence - GCATTCTAATAGCAGCAGAT	
Malat1 HDRT Ultramer	IDT	Sequence - ACAGACCACACAGAATGCAGGTGTCT TGACTTCAGGTCATGTCTGTTCTTTGG CAAGTAATATGTGCAGTACTGTTCCAA TCTGTCCTGATTAGAATGCATTGTGAC GCGACTGGAGTATGATTAAGAAAGT TGTGTTTCCCAAGTGTGGAGTAGT GGTTGTTGGAGGAAAAGCCATGAGTA ACAGGCTGAGTGTT	
anti-CD127 PE	invitrogen	Clone-A7R34	12-1271-83
anti-CD127 FITC	invitrogen	Clone-A7R34	11-1271-82
anti-CD45.2 BV785	BioLegend	Clone-104	109839
anti-CD45.1 Alexa Fluor 700	BioLegend	Clone-A20	110724

Reagent	Source	Detail	Catalog #
anti-CD90.2 BV605	BD Biosciences	Clone-30-H12	740334
anti-CD90.2 eFluor 450	eBiosciences	Clone-53-2.1	48-0902-80
anti-CD44 PE-Cy7	eBiosciences	Clone-IM7	25-0441-82
anti-CD27 APC	eBiosciences	Clone-LG.7F9	17-0271-82
anti-CD27 FITC	eBiosciences	Clone-LG.7F9	11-0271-82
anti-Bim PE	Cell Signaling	Clone-C34C5	12186S
anti-CD43 Percp- Cy5.5	BioLegend	Clone-1B11	121224
anti-CD45.2 PE-Cy7	BD Biosciences	Clone-104	560696
anti-CD45.1 BV785	BioLegend	Clone-A20	110743
anti-Bcl2 Alexa Fluor 647	BioLegend	Clone-BCL/10C4	633510
anti-Bim Alexa Fluor 700	Cell Signaling	Clone-C34C5	28997S
GP33 Tetramer PE	NIH Tetramer Core	Peptide: KAVYNFATM	57624

Reagent	Source	Detail	Catalog #
anti-KLRG1 BV711	BD Bioscience	Clone-2F1	564014
Fixable Viability Dye eFluor 780	eBioscience		65-0865-14
anti- CD8α BV805	BD Bioscience	Clone-53-6.7	612898
anti- CD28 FITC	BioLegend	Clone-E18	122008
anti- CD69 APC	Invitrogen	Clone-H1.2F3	17-0691-82
anti- Nur77 PE	Invitrogen	Clone-12.14	12-5965-80
anti- CD62L BV605	BD Biosciences	Clone-MEL-14	563252

Chapter 3 - High Dimensional Profiling Resolves Alveolar Inflammation in Allergen Challenged Allergic Asthmatics

Abstract

Asthma is a chronic inflammatory disease affecting over 300 million people worldwide. This disease has multiple clinical presentations with multiple underlying etiologies. A major endotype of asthma is characterized by high type 2 responses to allergens. In this study we conducted segmental bronchoscopies following allergen exposure in allergic asthmatics to dissect airway responses to allergen. Using high dimension cytometry by time of flight (cytof) we identify with high resolution the immune landscape before and after allergen challenge and the heterogeneity present between subjects. This heterogeneity generally falls along a type 1/ type 2 axis. In the type 2 high individuals we find allergen reactive, systemically present Th2 cells by using TCR sequences to barcode clones between assays. Further, in the myeloid compartment we identify a chemokine axis highlighted by CCL17 and CCL22 that drives T cell infiltration beyond the clearly defined Th2 cells. This type of study provides critical confirmation and resolution of observations made in murine systems and will provide insight into the efficacy and mechanisms of current and future therapeutics for this critical disease.

Introduction

Asthma is a chronic disease of the airways affecting 334 million people with 250,000 deaths worldwide (GBD Chronic Respiratory Disease Collaborators 2020). Asthma is characterized by chronic inflammation in the airways leading to coughing, chest tightness, and airway obstruction (Padem and Saltoun 2019). In addition to episodic bronchospasm and heightened inflammation, other hallmark features of asthma include excess mucus production and airway remodeling leading to chronic obstruction and the loss of lung function (Tang et al.

2022). To combat these issues patients are maintained on inhaled steroids and treated with systemic steroids during acute exacerbations (Lin et al. 2018). The therapeutic landscape for these patients has broadened in recent years with the advent of biologics directly targeting cytokines and receptors essential to asthma pathology such as TSLP, IL-5, and IL-4 and IL-13 via their shared receptor IL-4RA(Wenzel et al. 2016; Gauvreau et al. 2014; Menzies-Gow et al. 2003). However, these therapies are expensive, require frequent injections, and work best in only a subset of patients with asthma (Moran and Pavord 2020).

The success of these therapies highlights that type 2 inflammation is a hallmark and critical component of asthma. However, there is significant heterogeneity present in this patient population (Fitzpatrick et al. 2011; Haldar et al. 2008; Moore et al. 2010). Type 1 and type 17 high subgroups of patients have elevated IFN γ or IL-17 expression in the airways (Raundhal et al. 2015; Chakir et al. 2003; Bullone et al. 2019; Ricciardolo et al. 2017). This results in these patients also exhibiting increased neutrophils in the airways (Ricciardolo et al. 2017; Bullone et al. 2019). In contrast to these subjects, there is a large portion that exhibit high levels of type 2 inflammation. The heterogeneity present in these subjects extends to several biological levels. In the lung epithelium, type 2 high individuals have been defined by gene expression changes such as the increased expression of POSTN, CLCA1, and serpinB2 which are specifically IL-13 responsive genes (Bhakta et al. 2013). These subjects also have altered cellular differentiation states in the immune system. As asthma is marked by increased serum IgE level, B cells must differentiate into IgE producing plasma cells, which is driven by IL-4 and IL-13 exposure from Th2 cells (Hammad and Lambrecht 2021). This further extends to the prevalence of cell types with type 2 high individuals exhibiting increased presence of eosinophils in the blood and sputum (Dunican et al. 2018; Castro et al. 2018).

While many studies have been conducted in mice and humans, understanding how all of these facets manifest in clinical settings in resolution achieved by modern experimental techniques has only been recently achieved (Gavala et al. 2013; Till et al. 1998; Bodey et al. 1999; Alladina et al. 2023). In particular it is important to further understand how allergen exposure in particular induces allergic responses in the local lung environment. To address this gap we performed a clinical study of allergen exposure in allergic asthmatics. In this study we then utilized high dimensional techniques to create atlases of the local lung environment after allergen exposure. Using directional bronchoscopy we could investigate the allergic response in a paired fashion within a single subject. This revealed that type 2 helper T cells are specifically allergen responsive and elevated in subjects with other characteristics of type 2 inflammation including alveolar eosinophilia and allergen specific blood IgE. Further, this study establishes the inflammatory axes present between infiltrating monocyte derived populations, the chemokine environment they establish, and the resultant ingress of T cell and other lymphocyte populations.

Results

High Dimensional Cytometry Defines Type 1 - Type 2 Axis in Airway Remodeling Upon Challenge

The local tissue inflammation of asthma necessitates a deep understanding of how the lung epithelium and alveolar space responds to the presence of allergens. Further, asthma has been characterized as a disease with heterogeneous manifestations in the human population (Fitzpatrick et al. 2011; Haldar et al. 2008; Moore et al. 2010). We sought to deeply probe how human asthmatics respond to allergen by conducting a study of segmental allergen challenge. The study was conducted over the course of three clinical visits, schematized in [Figure 3.1.A]. Subjects were enrolled with stable or well controlled asthma, not on inhaled corticosteroids.

Enrolled asthmatic subjects were between the ages of 18 to 50, had a baseline FEV1 > 75% of predicted, a methacholine PC20 < 8 mg/mL, and skin reactivity to either house dust mite *Dermatophagoides pteronyssinus* (HDM) or cat dander. Subjects that were either not allergic or not asthmatic, but met other study criteria were also enrolled as a control group. In the first clinical visit (V1), to assess allergen specific responses subjects first underwent skin prick testing to determine allergic reactivity to HDM or cat dander (cat). Also, in V1 quantitative skin prick testing was done to determine threshold allergen concentration to elicit an allergic response in the subject. In the second visit, the following experimental baseline samples were collected: bulk RNA from peripheral blood, pulmonary function spirometry, and via endoscopy epithelial brushing and bronchoalveolar lavage (BAL). Subsequent to sample collection directional bronchoscopy was used to administer the appropriate allergen into one segment of the lung while PBS diluent was administered into a contralateral segment. Visit 3 followed either 1 day or 7 days after visit 2 and the sample clinical samples were collected yielding paired allergen challenged (AC) and diluent challenged (DIL) samples from the same subject.

First examining the returned BAL fluid, allergen challenge induced significant cellular infiltration into the alveolar space [Figure 3.1 b]. The cellular composition, examined by cytopsin slides, was significantly changed by visit 3 allergen challenge for both the day 1 and day 7 time points [Figure 3.1 c & d]. In both time points, this change was dominated by an increase in eosinophils which resulted in a proportional decrease in macrophages, which were the dominant population at baseline [Figure 3.1 c&d]. While eosinophil infiltration was the clearest allergen responsive change, there was significant heterogeneity observed between subjects with some experiencing neutrophil and/or lymphocyte infiltration [Figure 3.1 c&d]. There was no clear relationship between eosinophilic and neutrophilic inflammation in the baseline and diluent samples [Figure 3.1 e]. However, allergen challenge resulted in a clear negative correlation between the proportion of eosinophilic and neutrophilic inflammation [Figure 3.1 e].

The cytopsin slides indicated a significant remodeling of the alveolar cellular space, so we sought to deeply characterize all potential immune populations. To do so, we employed high dimensional cytometry by time of flight (cytof) due to its ability to deploy high dimensional panels at scale (Nassar, Wisnewski, and Raddassi 2016). We developed a panel of 34 markers to distinguish 13 distinct cell types in the lung [Table S3.2]. Using this analysis we could accurately delineate these cell types in the BAL samples from all visits of the study and the significant remodeling of the alveolar cellular space that was observed by the cytopsin slides was replicated [Figure 3.2 a & b]. To capture the diverse changes to the cellular landscape we used the quantifications from the cytopsin slides in addition to those from cytof to perform principal component analysis (PCA) [Figure 2 3.c]. PCA revealed that the V3 diluent samples contained a similar cellular composition as evidenced by their close relationship on the plot [Figure 3.2 c]. The V3 allergen challenged samples, however, appeared to diverge away from the V3 diluent samples in two distinct directions [Figure 3.2 c]. We then repeated this analysis using only the allergen challenged samples, and we observed that the samples largely skewed along principle component 1, which represented 21.6 % of the variance in the samples [Figure 3.2d]. We then examined how the measured variables contributed to the first to principal components [Figure 2e]. This revealed that the dichotomy between neutrophils and eosinophils observed in the cytopsin slides extended to other cell types indicating modules of type 1 and type 2 inflammation induced by the allergen challenge [Figure 3.2e]. Along the negative values of PC1 we find the non-allergic samples which are high in neutrophils, monocytes, and macrophages [Figure 3.2 d&e]. Along the positive values of PC1 we find several of the day 7 samples which are high in eosinophils but also type 2 associated cells such as basophils and ILC2s [Figure 3.2 d&e]. Allergen specific IgE is a classic biomarker for elevated type 2 inflammation and plays a key role in the activation of dendritic cells, basophils, and mast cells (Siracusa et al. 2013; Platzer, Stout, and Fiebiger 2015; Choi et al. 2005; Tanaka and Furuta 2021). To further assess the steady state level of allergen specific type 2 inflammation we measured the amount of IgE

specific antibodies in the blood at baseline at visit 2. In the HDM reactive patients, few contained cat dander specific IgE, but all contained detectable HDM specific IgE [Figure 3.2 f&g]. When examining all the subjects, the concentration of IgE appeared to correlate with the value of PC1 derived from the cytof and cytospin data [Figure 3.2 g]. However, the inclusion of all samples including those of different time points and allergen reactivities, can confound this interpretation. To better visualize this correlation, we examined the relationship between PC1 and HDM specific IgE in only the HDM reactive subjects at the day 1 time point [Figure 3.2 h]. This analysis more clearly demonstrated that those subjects with high IgE levels tended to have high PC1 values as well, demonstrating that the type 2 high inflammation present in the local lung environment was reflective of a high level of systemic type 2 inflammation prior to allergen challenge [Figure 3.2 h].

IL-13 responsive genes are induced in the epithelium by allergen challenge

While remodeling the alveolar cellular environment is a key response to allergen, the alveolar and lung epithelium constitute a key barrier surface and one of the first to respond to allergen exposure (Duchesne, Okoye, and Lacy 2022; Siddiqui et al. 2021; Invernizzi, Lloyd, and Molyneaux 2020). To assess the status of the epithelium in these subjects, we collected epithelial brushings of the epithelium from V2 BL, V3 DIL, and V3 AC lung segments and performed bulk RNA sequencing. To assess the effect of allergen challenge we performed differential gene expression (DEG) analysis between the allergen challenged samples and compared this to gene sets derived from cytokine treatment of air-liquid-interface cultures of epithelial cells [figure 3.3 a-c] (Koh et al. 2023). Gene set enrichment from both allergic asthmatics and allergic non-asthmatics indicated that an IL-13 responsive gene signature was induced by allergen challenge compared to baseline [Figure 3.3 a&b]. Interestingly, only in the allergic non-asthmatics allergen challenge also induced a gene signature associated with IL-17 responsive genes [Figure 3.3c].

Given that the IL-17 gene set was only responsive in the allergic non-asthmatics we

sought to more broadly characterize if allergic asthmatics and allergic non-asthmatics exhibited similar gene expression patterns upon allergen challenge. We then examined genes that were differentially expressed (by a raw p value cut off of $p < 0.05$) between allergen challenge and baseline in each population [Figure 3.3d]. There were few DEGs shared between the populations (only 19 out of the total 1026), and this trend continued when DEGs were considered not only between allergen challenge and baseline but also allergen challenge and diluent [Figure 3.3d&e]. If we considered the DEGs which were present in both populations there were no clear modules present in DEGs that were either upregulated or downregulated in each population [Figure 3.3f]. However, we did note that *IL13RA1* was specifically up in only the allergic asthmatic group and *IL17RA* was specifically only up in the allergic non-asthmatic group [Figure 3.3d].

This apparent difference in cytokine response led us to investigate what role individual heterogeneity played in the expression of specific type 2 associated genes in the lung epithelium. Previous work has established that *periostin*, *CLCA1*, and *serpinB2* can be used as a three gene mean to establish type 2 high individuals (Bhakta et al. 2013). We then calculated this measure from our RNAseq data [Figure 3.3 e-g]. While allergen challenge did not increase this measure above baseline or diluent, we found that this measure was highest among the individuals with the highest PC1 score [Figure 3.3 e-g]. This provides further support for the consistent elevated type 2 inflammation present in those individuals irrespective of allergen challenge. We then hypothesized that this elevated type 2 status would drive persistent gene expression changes in these individuals. We then subsetted the individuals into type 2 high and type 2 low status ($PC1 > 0$ or $PC1 < 0$) and performed DEG analysis. At baseline, GO terms representing DEGs elevated in the type 2 high group reflect multiple pathways relating to protein targeting and trafficking, which is likely reflective of increased secretory cell composition of the epithelium [Figure 3.3h]. In the allergen challenged samples, the most enriched GO terms contained some similar terms (SRP-dependent cotranslational protein targeting to membrane),

but largely consisted of terms related to leukocyte activation and degranulation [Figure 3.3i]. The enrichment of these terms likely reflects the infiltration of eosinophils, neutrophils, T cells, and other leukocytes and these populations being collected with the brushings.

Allergen Challenge Induces Systemically Present Allergen Reactive Th2 Clone Alveolar Infiltration

Allergen challenge clearly induced stereotypical signs of type 2 inflammation in the alveolar space which were elevated in individuals with indications of persistent systemic type 2 inflammation. Thelper cells are an essential component of inducing and amplifying type 2 inflammation; however, in our cytof data we were not able to clearly resolve T cell subsets based upon chemokine receptor expression, as done previously (Strazza and Mor 2017; Lloyd and Hessel 2010). To further resolve the Thelper cell compartment we performed single cell mRNA sequencing (scRNAseq) and single cell TCR sequencing (scTCRseq) on a subset of samples from HDM challenged individuals. To do so, we developed a sorting strategy to enrich CD4⁺ T cells from frozen samples which were then analyzed in a multiplexed fashion [Figure 3.S1]. Utilizing this strategy we could clearly resolve multiple CD4⁺ T cell subsets including Th1 cells marked by *CXCR3*, *TNF*, and *IFNG* expression; undifferentiated and naive cells marked by *CCR7*, *SELL*, and *IL7R* expression; regulatory T cells (Treg) marked by *FOXP3*, *TNFRF18*, and *IL2RA* expression; cytotoxic -like cells marked by *GZMB* expression; interferon responsive cells marked by expression of multiple interferon responsive genes such as *IFI6*; cycling cells marked by *MKI67* expression; and Th2 cells marked by *GATA3*, *IL5*, *IL13*, and *IL4* expression [Figure 3.4 a-c]. Given that we could resolve the cellular phenotypes to this resolution, we then determined the fraction of each sample represented by each cluster [Figure 3.4 d&e]. We observe that allergen challenge generally skewed the T cell landscape from one predominantly composed of Th1 cells to one predominantly composed of undifferentiated/naive cells [Figure

3.4 e]. While the changes did not reach statistical significance, the Th2 cluster was nearly exclusively found in the allergen challenged samples [Figure 3.4 d&e]. Given the large prevalence of Th1 type cells in the diluent samples and undifferentiated/naive cells in the allergen challenged samples we calculated the single cell gene enrichment score for the gene set defining human tissue resident T cells [Figure 3.4 f] (Kumar et al. 2017). The Th1 cluster had the highest average value for this score with the undifferentiated/naive cluster having the lowest and the Th2 cluster having a score significantly lower than the Th1 cluster [Figure 3.4g]. This score stratification likely reflects that the undifferentiated/naive cells and Th2 cells are more recent entrants into the lung microenvironment as opposed to the Th1 cells which are present and activated in a non-allergen specific manner.

In addition to gene expression analysis, we also performed scTCRseq to evaluate the clonal response within the CD4⁺ T cell compartment. In this analysis we define a TCR clone as a unique TCR α and TCR β pair, and an expanded clone as a TCR clone that was present in more than one cell. When we plot the distribution of TCR clones across the scRNAseq space we found that expanded clones were present in both allergen challenge as well as diluent at both the day 1 and day 7 time points [Figure 3.5 a&b]. We find a strongest presence of expanded clones in the Th1, Th2, and Treg clusters [Figure 3.5 a&b]. Further, the fraction of each cluster and the number of cells belonging to a particular expanded clone were increased in the day 7 samples compared to the day 1 samples in the Th1, Th2, and Treg clusters [Figure 3.5 b&c]. These clonal characteristics strongly indicated evidence of TCR activation and clonal expansion in the Th1, Th2, and Treg clusters while a lack of these characteristics in undifferentiated/naive cluster was in accordance with the gene expression signatures observed.

To test if these cells were indeed antigen reactive we employed an activation induced marker assay (Bacher et al. 2016; Bacher and Scheffold 2013). We re-stimulated these samples with HDM extract or PBS vehicle for 8 hours *ex vivo* which we then stained with a panel of TotalSeqC antibodies and then performed scRNAseq and scTCRseq after enriching for CD4⁺ T

cells by flow cytometry [Figure 3.5 d]. The clusters identified by scRNAseq after this stimulation now had a distinctly different organization as compared to the samples directly assayed [Figure 3.5 e]. After stimulation, the data were primarily organized around activation status rather than cytokine expression profile [Figure 3.5 e]. Specifically within the clusters with high CD69 expression the cluster which we call "activated 1" contained the highest expression of CD40 ligand gene and protein expression as well as *NR4A1* gene expression consistent with this cluster containing the most TCR specific activation [Figure 3.5 e & f]. We also differentiate *FoxP3* expressing cells into multiple clusters with the cluster deemed "Treg 2" containing the highest *IL2RA* gene expression and CD137 protein expression indicating this cluster is most likely antigen reactive Tregs [Figure 3.5 e & f]. Further the clusters deemed activated in both the Tconventional and Treg sets had increased prevalence in the stimulated samples and the expression of activation induced genes increased as well indicating the specific activation induced by the HDM stimulation [Figure 3.5 f & g]. We then leveraged scTCRseq to trace clones found in both the directly assayed data set and the stimulated data set. In the directly assayed data set, TCR clones were generally cluster restricted [data not shown]. We then defined a direct assay phenotype for each TCR clone as the direct assay cluster which contained the most cells from that particular clone. We then annotated the stimulated data set clones by the direct assay phenotype of that clone [Figure 3.5 h]. In this mapping, we find that the directly assayed Th1 clones occupy all of the non-Treg clusters with the strongest representation in the activated clusters in the activated data set [Figure 3.5 h]. Those Th1 clones in the activated clusters had the highest expression of *IFNG*, *TNF*, *IL12*, and *NR4A1* [Figure 3.5 i]. The directly assayed Th2 clones were similarly disparately distributed, but only a minority of cells were contained within the activated cluster and in particular the activated 1 cluster [Figure 3.5 j]. Those Th2 clones that were contained in the activated 1 cluster expressed the highest expression of all three major Th2 cytokines *IL-5*, *IL-4*, and *IL-13* as well as *NR4A1* expression [Figure 3.5 k]. The directly assayed undifferentiated/naive clones were primarily found in the

unactivated clusters in the stimulated assay and those few cells found in the activated clusters did not have strong cytokine or NR4A1 expression, supporting their unreactive, undifferentiated state [Figure 3.5l]. The directly assayed Treg clones predominantly were found in the *FOXP3* expressing clusters in the stimulation assay and dominantly in the Treg2 cluster that exhibited CD137, *NR4A1*, *IL10*, and *EBI3* expression [Figure 3.5h&m]. These data indicate the stability of the Treg phenotype and that many of the Treg clones were indeed antigen specific.

Surprisingly, while Th2 cells represented the most allergen specific population in the directly assayed samples, clones from both the Th1, Th2 and Treg directly assayed clusters indicated gene expression patterns consistent with TCR activated and antigen specific reactivity. We then sought to determine if these clones exhibited systemic indications of activation. We performed bulk TCR sequencing from RNA isolated from peripheral blood and found that many of the TCRs found in both the directly assayed samples and the *ex vivo* stimulated samples were found in the blood both before and after *in vivo* allergen challenge [Figure 3.5 n-p]. We found two day 7 samples, with high type 2 inflammation by PC1, where TCRs associated with Th2 cells were enriched in the blood during visit V3 compared to V2 [Figure 3.5q]. Interestingly, the most enriched TCRs were the Th2 clones with an activated phenotype in the *ex vivo* stimulation assay [Figure 3.5q]. While certain individual clonotypes displayed enrichment post challenge we do not observe this trend consistently in clones that are either unactivated or belong to the Th1 or Treg clusters in the directly assayed data set [Figure 3.5q-s]. We observe a very similar pattern in the blood frequencies of the corresponding TCR β for these same TCR clones [data not shown]. These results indicate that allergen reactive Th2 cells are difficult to find in the airways of human asthmatics, but are most likely to be found at day 7 post allergen exposure in individuals with high levels of type 2 inflammation. Further, as these TCRs are present in the blood prior to allergen exposure indicates that these allergen reactive clones are systematically present and their expansion is not limited to the local lung environment of allergen exposure.

Allergen induces chemokine expressing monocyte derived populations that help to recruit T cells

When we assayed a subset of samples in which we enriched CD4+ T cells, we also assayed other cells in the sample separately by scRNAseq. However, the large number of granulocytes, particularly eosinophils and neutrophils, presented a technical challenge in generating quality scRNAseq data. To address this issue, at the same time as we used flow cytometry to sort and enrich CD4+ T cells we used the same sorting strategy to enrich for all leukocyte populations that were not CD4+ T cells, neutrophils, and eosinophils [Figure 3.S1]. In the subsequently enriched cells, we identify 9 cell type clusters, by unbiased nearest neighbor clustering, including cells in both the myeloid and lymphoid compartments of the immune system [Figure 3.6 a-c]. We identify 4 primary myeloid clusters, with 3 representing a spectrum of macrophages and 1 representing dendritic cells [Figure 3.6a-c]. The dendritic cells appear to be infiltrating via a monocyte precursor due to the expression of *CD1A*, *FCER1A*, and *CXCR4* [Figure 3.6 a-c] (Collin and Bigley 2018). The macrophage clusters identified across all clusters expressed *MARCO* and *MRC1*, but unbiased analysis indicated that *CXCR4*, *FABP4*, *CD14*, *VCAN*, *CCL2*, and *CCL13* were expressed in patterns unique to each cluster [Figure 6a-c]. Of particular interest, the cluster high for chemokine expression demonstrated some hallmarks of M2, or alternatively activated, macrophages which have been speculated to be important in allergic disease [Figure 3.6 a-c] (Saradna et al. 2018). Further, this cluster also appears to be monocyte derived due to the high expression of *CD14* [Figure 3.6 b&c]. The other two major macrophage clusters were defined by high *FABP4*, *MARCO*, and *MRC1* suggesting these may be the tissue resident alveolar macrophages [Figure 6 b & c] (Liang et al. 2019). The final macrophage clusters identified are interferon responsive with high expression of *SIGLEC1*, a gene shown to be induced by viral infection of macrophages [Figure 3.6 b&c](Herzog et al. 2022). The final myeloid cluster present closely associated with other macrophage clusters,

contained very few cells, and was marked by *CYP2S1* and *ITGA3* expression [Figure 3.6 b&c]. In the first analysis of all cells, we are able to delineate a clear B-cell cluster (marked by *MS4A1* and *JCHAIN* expression) and a mixed cytotoxic lymphocyte cluster by the combined expression of *CD8A*, *TRDC*, and *NKG7* [Figure 3.6 b&c]. To better resolve this final cluster, we isolated those cells and performed sub-clustering and marker gene analysis [Figure 3.6d-f]. This resulted in 5 clusters identified in which 3 contained CD8+ T cells (one seemed to contain contaminating macrophages) and were primarily delineated by the expression level of *IL32* [Figure 3.6 d-f]. The other two remaining clusters contained NK cells and gamma delta T cells which could not be fully resolved and the final cluster did not contain any striking marker gene expression except that it generally contained much lower read density than the other clusters [Figure 3.6 d-f].

We then sought to determine how allergen challenge changed this landscape. In contrast to the T cell compartment, day 1 samples did not yield any clear statistically significant changes and the only statistically significant change in the day 7 samples was an increase in the combined mixed lymphocyte population [Figure 3.7 a&b]. As cell population changes were not evident, we next evaluated if gene expression programs were influenced by allergen challenge. Strikingly, unbiased evaluation of DEGs indicated that chemokine gene programs were strongly induced in several of the major clusters [Figure 3.7 c&d]. Notably, in the monocyte derived M2-like macrophages and the monocyte derived dendritic cells *CCL3* (Log₂FC 71.5 & 146.8 respectively), *CCL17* (Log₂FC INF & INF respectively), *CCL22* (Log₂FC 121,7 & 110 respectively), and *CCR1* (Log₂FC 14.8 & 35.8 respectively) were induced by allergen challenge [Figure 3.7 c&d]. Further, *CCR5* and *CCR6* were induced on the monocyte derived dendritic cell population [Figure 3.7 c& d]. In a similar pro-inflammatory fashion, *CCL5* was induced by allergen challenge in the mixed lymphocyte population [Figure 3.7 c&d]. In opposition to these allergen induced changes, in the tissue resident alveolar macrophage population *CCL18* was reduced by allergen challenge [Figure 3.7 c&d]. As these chemokines have been shown to have important chemotactic properties for Th2 cells, we then sought to see if similar programs were

induced by allergen challenge in the CD4+ T cell compartment [Figure 3.7 e](Pilette et al. 2004). In contrast to the induction of chemokine receptors in macrophage populations we did not observe any change in *CCR4* or *CCR5* induced by allergen [Figure 3.7 e]. Further, the distribution of these receptors was generally broad [Figure 3.7 e]. In line with previous work, expression of PTGDR2 and lack of *CCR6* best identified Th2 cells' chemokine receptor profile [Figure 3.7e & Figure 3.4 b&c] (Hirai et al. 2001). Interestingly, Tregs exclusively expressed *CCR8* and the expression of this receptor was higher in the diluent samples, connecting Tregs strongly to *CCL8* expression by the tissue resident alveolar macrophages [Figure 3.7 c-e]. *CCL17* (TARC) and *CCL22* have been shown to be important mediators of type 2 inflammation in asthma by recruiting *CCR4*+ Th2 cells (Pilette et al. 2004). We compared the presence of the mo-DC and monocyte derived macrophage populations expressing *CCL17* and *CCL22* with the Th1 and Th2 populations from the allergen challenged samples [Figure 3.7 f]. Surprisingly, both of these populations correlated negatively with Th2 cells, and both of them correlated positively with Th1 cells [Figure 3.7 f]. This result suggests that macrophage and monocyte derived populations in the lung are important to define the chemokine signature shortly after allergen exposure. However, chemokines like *CCL5*, *CCL17*, and *CCL22* may not have Th2 specific effects in the lung due to wide expression of the receptors *CCR5* and *CCR4* on various T cell subsets.

Discussion

Understanding the local lung response to allergen is critical as the most detrimental aspects of asthma are localized in nature such as mucus plugging (Tang et al. 2022). In this study we demonstrate that allergen induces significant changes of the lung microenvironment primarily through ingress of inflammatory populations that display significant heterogeneity between subjects. Essential to this is understanding the inflammatory circuits that drive the

recruitment of particular populations. Through unbiased DEG analysis we show that expression of *CCL3*, *CCL17*, and *CCL22* are allergen induced genes within monocyte derived macrophage and dendritic cell populations. These cytokines have been shown to induce Th2 cell chemotaxis due to the expression of *CCR4* on Th2 cells (Pilette et al. 2004). However, our data indicate that these chemokines act broadly on the T cell compartment as *CCR5* and *CCR4* expression is promiscuous among alveolar present T cells. Our data also highlight other interesting aspects of chemokine receptors in the T cell compartment. Notably, *CCR6* is sparsely expressed and in no particular cluster of CD4+ T cells, outside of low expression on the Th2 cells. This is consistent with poor *IL17A* or *IL17F* expression in the data set, and low involvement of these pathways in allergic forms of asthma (Melgert et al. 2007). In the Treg compartment, *CCR8* stands out as a specifically expressed chemokine receptor that connects closely to the *CCL18* produced by tissue resident macrophages. Thus, this represents human confirmation of the immunoregulatory role of this circuit observed in mouse models of asthma (Jheng et al. 2023).

Further, it is a substantial advance that we clearly show Th2 infiltration into the alveolar space and that scRNAseq defines these cells in part by the canonical transcription factor *GATA3* and cytokines *IL-5*, *IL-4*, and *IL-13*. Our data indicate that these cells contain expanded clones which increase at the day 7 time point compared to day 1. Further, the utilization of the AIM assay demonstrates that these Th2 cell clones in at least some cases are antigen reactive and present in the blood before allergen challenge. These reactive clones also expand in the blood repertoire post challenge. This suggests a model in which type 2 high individuals have systematically present Th2 cells, which are primed by dendritic cells in draining lymph nodes to expand systemically. These Th2 cells are then recruited to the lung alveolar environment by sensing chemokine cues and others such as prostaglandins given their specific expression of *PTGDR2*. This has interesting implications for the relationship between presence of Th2 cells in the peripheral blood and the local inflammatory environment in the lung after allergen exposure.

Past work has established that AIM assays can be used to identify Th2 cells in the peripheral blood of asthmatics, and our data support the idea that those individuals would have increased type 2 inflammation in the alveolar space as well (Bacher et al. 2016).

Our data have interesting implications for what the function would be of these Th2 cells in the alveolar space. Even in type 2 high individuals our data show that while eosinophils are early entrants upon allergen challenge, monocyte derived populations and T cells expressing type 1 cytokines also mark a significant infiltrating population in the airways. The Th2 cells then are more dominant at later time points following allergen exposure. A potential model then becomes that these Th2 cells are there to support longer term tissue remodeling and support for eosinophil survival and chemotaxis via providing IL-5 directly within the airways. As long term airway remodeling is a critical part of asthma, our data highlight chemokine pathways that may aid in preventing acute airway inflammation but also the longer time frame that type 2 cytokines may be acting. This suggests that local blockade of type 2 cytokines may be important to prevention of disease progression.

On the whole, this study represents an important combination of many high dimensional techniques used together to generate an atlas of the human asthmatic response to allergen from epithelial cell gene expression, broad cellular landscape changes, and specific changes within potent inflammatory cells. We can use these data to define a type 1 / type 2 axis across subjects and correlate more detailed measures with broad airway changes. In the type 2 individuals in particular we observe Th2 cells, which through using TCR sequences as barcodes we show are systemically present and at least some are allergen reactive. We further highlight key modules of chemokine activity that are allergen induced. This type of study provides critical confirmation and resolution of observations made in murine systems and recent publications and will provide insight into the efficacy and mechanisms of current and future therapeutics for this critical disease (Alladina et al. 2023).

Materials and Methods

Human Subjects and Clinical Study

Subjects were enrolled and samples collected as part of the Allergen Challenge for Evoked Phenotypes in Asthma (ACE Study, AADCRD-UCSF-01). This is a non-double blind study that was initially started with visit 3 time point randomization. However, after discussions with the NIH/NIAID sponsor, visit randomization ceased in favor of prioritization of the 1 day time point. Subjects were enrolled primarily from the web based QuesGen system (described by IRB protocol #10-06127). The study was undertaken with the goal to provide a defined allergic stimulus that will promote the cellular and molecular events to increase the observed biological signal and allow time-course analyses. For this reason, the primary subjects were allergic to either HDM or cat dander with stable or well-controlled asthma. Non-asthmatic and non-allergic non-asthmatic controls were also enrolled, but to a lower number. The primary inclusion criteria for asthmatics were: subject must be able to understand and provide informed consent, prior physician-diagnosed asthma, 18 to 50 years of age, pre-BD baseline (V1) FEV1 > 75% of predicted, skin test reactivity as described below, and methacholine PC20 < 8 mg/mL. The inclusion criteria for controls were: subject must be able to understand and provide informed consent, age 18 to 50, pre-BD baseline (V1) FEV1 > 90% of predicted, and methacholine PC20 > 16 mg/mL. Controls were differentiated into allergic and non-allergic groups based upon skin prick testing described below. This study was supported by the NIH/NIAID grant 5U19AI077439 and registered to clinicaltrials.gov under the identifier NCT02230189.

Skin Prick Testing

Qualitative skin prick allergen reactivity testing was performed using the Multi-Test II skin test applicators. The applicator was carefully removed from the Dipwell Tray and pressed into the forearm skin of the subject with sufficient pressure to allow adequate penetration of the points.

The subject was monitored during reaction incubation, and the histamine and saline negative controls were read at 15 minutes. The allergen results were read at 20 minutes by outlining each wheal with a marking pen. A wheal diameter of 3mm in diameter was considered a positive reaction. Based on the results of the qualitative skin prick test, a quantitative skin prick test was done using the Morrow Brown Disposable Skin Testing Needles. Serial dilutions of either cat dander or HDM were chosen based on the qualitative skin test. Using the Disposable Skin Testing needle a drop of each dilution was applied to the skin and then a prick with the needle was administered in the middle of the droplet. After 20 minutes, the reaction wheal were read in the same way as before. The lowest concentration to elicit a wheal reaction great than 3 mm in diameter was considered the "Threshold concentration".

Segmental Allergen Challenge

To perform segmental allergen challenge (SAC) the V2 bronchoscopy 2 mL of either diluent or allergen were administered into distinct lobes of the lung. Diluent was administered into the right upper lobe and allergen (cat dander or HDM) was administered into the right middle lobe. A test dose was administered consisting of 1/30th the threshold allergen concentration determined from skin prick testing. If after at least two minutes, there is no evidence of mucosal inflammation a second larger dose of allergen was administered. This dose consisted of 2 mL of allergen at 1/3rd the threshold allergen concentration. V3 samples were collected from the right upper lobe and the right middle lobe via 3, 50 mL installations in each lobe.

Cytospins

The cells were counted in the BAL fluid and 10 mL of BAL fluid was normalized to a cellular concentration such that it will yield 40,000 to 50,000 cells per cytocentrifuge slide. 60 μ L of cell suspension was transferred into four shandon cytopsin funnels and centrifuged at 500 rpm for 5

minutes. Slides were stained using the Shandon Diff-quick kit. Slides were subsequently counted and evaluated by light microscopy.

mRNA Sequencing from Epithelial Brushings

Collected epithelial cell brushing remaining after cytopsin preparation and cell counts were spun at 500 rpm for 5 minutes. The supernatant was discarded and the cells were disrupted by adding 600 μ L of QIAzol. Samples were vortexed for 1 minute to ensure complete lysis of cells. Samples were stored at -80°C .

Sample Storage and Cytof

BAL fluid was counted using Turks solution and hemocytometer. Cell pellets were resuspended in CYTOF staining buffer at a concentration of 100×10^6 cells/mL. The resuspended pellets were kept on ice until subsequent staining and fixation. Samples not used for cytof were resuspended in 10% DMSO, 10% FCS, RPMI and stored at -80°C .

Bulk TCR Sequencing from Peripheral Blood

Peripheral Whole blood was collected on clinical visits 2 and 3 into PAXgene tubes to collect stabilized RNA. RNA was subsequently isolated using the Qiagen PAXgene kit and stored at -80°C . RNA quality was assessed by the agilent bioanalyzer and 14 out of 18 had RNA integrity (RIN) scores > 8 , 2 out of 18 had RIN scores > 7 , and 2 out of 18 had RIN scores ≥ 6.5 . Isolated RNA was used as input into the Takara SMARTer Human TCR ab Profiling kit for next generation sequencing library preparation. These libraries sequenced on the NovaSeq6000 SP using PE-150 reads. FASTQs generated were analyzed using the Cogent NGS Immune Profiler software provided by Takara to generate TCR α and TCR β sequences present and the fraction contained within the sample.

scRNAseq and scTCRseq from BAL

Frozen BAL aliquots were thawed at 37°C and washed with RPMI-1640, 20% FCS, 25 µg/mL DNase I. Samples were then passed through a 40 µm filter and washed 1X with 2% FCS, 1 mM EDTA PBS. The samples were then stained with Invitrogen™ eBioscience™ Fixable Viability Dye eFluor™ 780, CD4 PE-Cy7, CD45 ef450, CD3E APC, CD20 FITC, CD56 FITC, CD14 FITC, CD19 FITC, CD16 FITC, CD15 AF700, CD24 PE, and CD206 BV605. Cells were then resuspended in 2% FCS, 25 mM HEPES (pH 7.0), 1 mM EDTA PBS for sorting on the Aria Fusion S854 with biosafety cabinet and aerosole control. Samples were sorted to remove granulocytes (eosinophils and neutrophils) and separate CD4+ T cells from the remaining populations. CD4+ T cell samples from 4 distinct individuals at a time were mixed and resuspended at 1000 cells/µL. These mixed samples were then run on a single lane of a 10X chip for GEM production and cDNA libraries of the 5' V3 gene expression and TCR kit. The remaining cell populations were also resuspended at 1000 cells/µL, but samples were not multiplexed. These samples were run on their own lane of the 10X chip for GEM production and cDNA library production using the 3' gene expression kit. Samples were sequenced on illumina sequencer. FASTQ files generated were processed by 10X cell ranger software to generate gene counts and barcode assignment. For the multiplexed CD4+ cell samples a combination of FREEMUXLET and DEMUXLET software was used to unbiasedly identify which cells belong to each subject by single nucleotide polymorphisms in the axiom 1000 data set (Van der Auwera et al. 2013; Kang et al. 2018; popscl: A suite of population scale ...). Sample QC, integration, PCA, dimensionality reduction, clustering, marker gene, and DEG analysis were performed using the Seurat package V3 for R (Stuart et al. 2019).

Statistics and Analytical Software

Statistical analyses and plotting was performed using Graphpad Prism (Version 9.2.0) and R (version 4.2.1).

Figures

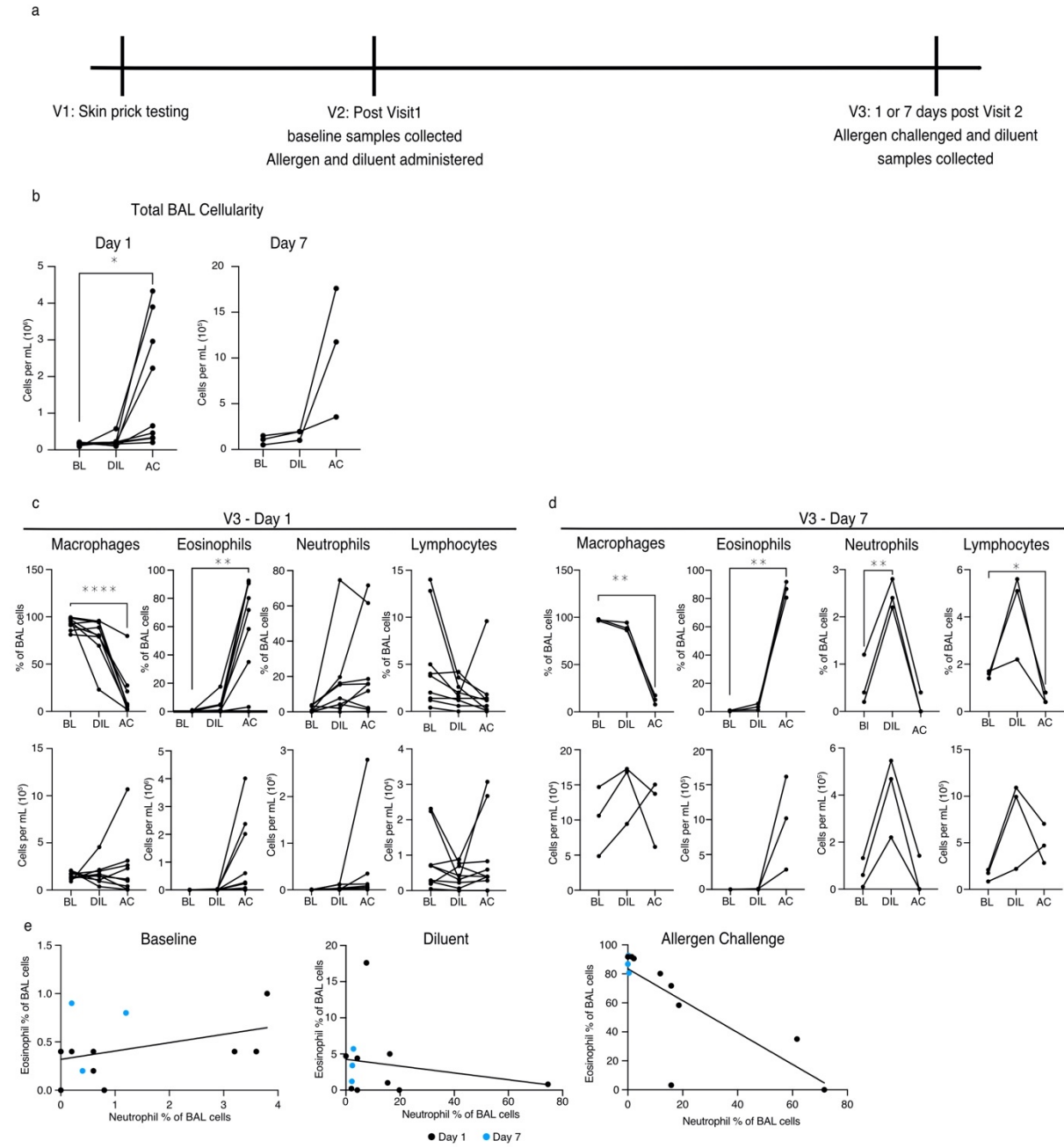


Figure 3.1. Allergen challenge induces leukocyte infiltration into the BAL

- a. Schematic of study design and clinical visits
- b. Total BAL cellularity measured by cells per mL of BAL fluid returned from bronchoscopies at all time points for subjects challenged with HDM
- c. BAL cell composition quantified by cytopsin slides from subjects challenged with HDM and part of the day 1 arm of the study as both percent of cells counted and concentration per mL of returned BAL fluid
- d. BAL cell composition quantified by cytopsin slides from subjects challenged with HDM and part of the day 1 arm of the study as both percent of cells counted and concentration per mL of returned BAL fluid
- e. Comparison of eosinophil and neutrophil composition of BAL fluid by percent of cells counted in cytopsin data at the baseline visit, the diluent sample, and the allergen challenged sample for both the day 1 and day 7 samples. Baseline: $R^2 = 0.1464$, $p = 0.2196$. Diluent: $R^2 = 0.0735$, $p = 0.5364$. Allergen challenge: $R^2 = 0.621$, $p = 0.0023$. Statistics displayed determined by Dunnett's multiple comparisons test following one-way anova between DIL versus BL and AC versus BL (*, adjusted $p < 0.05$; **, adjusted $p < 0.01$; ***, adjusted $p < 0.001$; ****, adjusted $p < 0.05$)

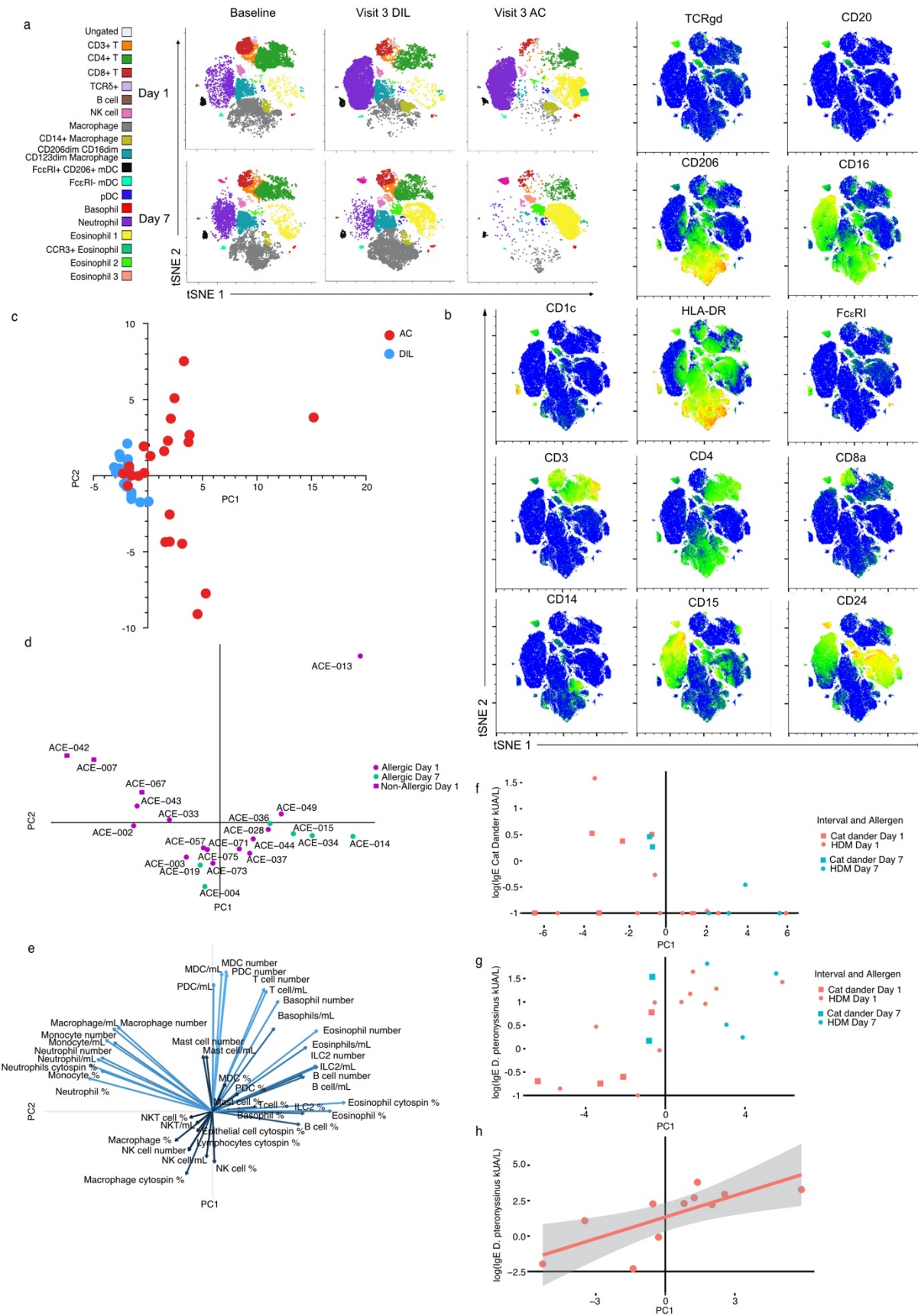


Figure 3.2. Cytof resolves Type 1 - Type 2 axis of response to allergen challenge

- a. tSNE dimensional reduction of BAL cell populations determined by cytof indicating the detection of 19 distinct cell types by unbiased clustering. Populations are separated by clinical visit and V3 time point. Each plot represents concatenation of the subjects for that condition and only the samples from allergic asthmatics challenged with HDM are shown.
- b. tSNE heatmaps indicating key marker gene expression across the dimensionally reduced plot. Data are concatenated from all subjects and time points from allergic asthmatics challenged with HDM. Cool colors indicate low expression while warm colors indicate high expression.
- c. Principal component 1 versus principal component 2 principal component analysis of all BAL populations measured by cytof bivariate gating and cytospin slides for all individuals, time points, and treatments including those challenged with either cat dander and HDM
- d. Principal component 1 versus principal component 2 from subsequent principal component analysis of all BAL populations measured by cytof bivariate gating and cytospin slides for only the V3 allergen challenged samples including those challenged with either cat dander and HDM
- e. Vectorized display of how each variable incorporated into the principal component analysis contribute the principal component 1 and principal component 2
- f. Blood concentration of baseline cat dander specific IgE versus the PC1 value from the allergen challenge only PCA for all subjects
- g. Blood concentration of baseline *Dermatophagoides pteronyssinus* specific IgE versus the PC1 value from the allergen challenge only PCA for all subjects
- h. Blood concentration of baseline *Dermatophagoides pteronyssinus* specific IgE versus the PC1 value from the allergen challenge only PCA for only HDM challenged day 1 subjects. $R^2 = 0.546$ and $p = 0.009358$.

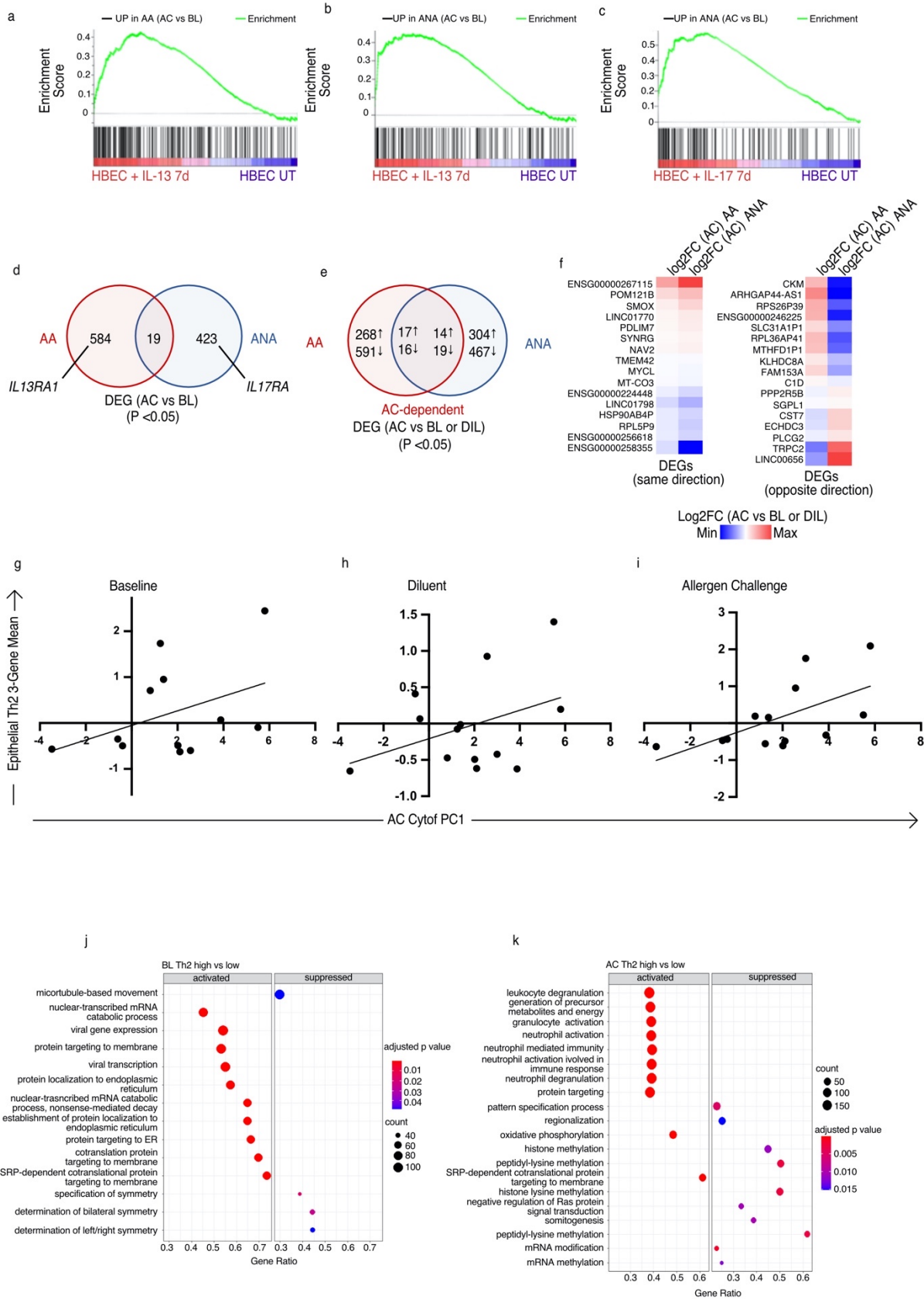


Figure 3.3. IL-13 responsive genes are induced by allergen challenge and highest in subjects with Type 2 high BAL infiltration

- a. Gene set enrichment analysis (GSEA) for IL-13 responsive gene set derived from cytokine-treated air liquid interface (ALI) epithelial cultures. Genes were ranked by fold change between allergen challenge and baseline for HDM treated allergic asthmatics. Normalized enrichment score 1.8, Normalized P value ~ 0 .
- b. GSEA for IL-13 responsive gene set derived from cytokine-treated ALI epithelial cultures. Genes were ranked by fold change between allergen challenge and baseline for HDM treated allergic non-asthmatics. Normalized enrichment score 1.83, Normalized P value ~ 0 .
- c. GSEA for IL-17 responsive gene set derived from cytokine-treated ALI epithelial cultures. Genes were ranked by fold change between allergen challenge and baseline for HDM treated allergic non-asthmatics. Normalized enrichment score 2.47, Normalized P value ~ 0 .
- d. Venn diagram describing the overlap between allergen challenge versus baseline differentially expressed genes between allergic asthmatics and allergic non-asthmatics defined by raw p value less than 0.05.
- e. Venn diagram describing the overlap between allergen challenge versus baseline and allergen challenge versus diluent differentially expressed genes between allergic asthmatics and allergic non-asthmatics defined by raw p value less than 0.05.
- f. Heatmaps describing the DEGs from allergen challenge vs baseline and allergen challenge vs diluent that were shared between allergic asthmatics and allergic non-asthmatics. The heatmap on the left illustrates the DEGs that were differentially expressed in the same direction in both allergic asthmatics and allergic non-asthmatics and the right illustrates the DEGs that were differentially expressed in opposite directions in allergic asthmatics and allergic non-asthmatics.
- g. Calculation of the epithelial IL-13 responsive gene score at baseline compared to allergen challenge BAL PC1 from figure 2d for HDM challenge subjects. $R^2 = 0.164$, $p = 0.191$.
- h. Calculation of the epithelial IL-13 responsive gene score in diluent challenged samples compared to allergen challenge BAL PC1 from figure 2d for HDM challenge subjects. $R^2 = 0.149$, $p = 0.193$.
- i. Calculation of the epithelial IL-13 responsive gene score in allergen challenged samples compared to allergen challenge BAL PC1 from figure 2d for HDM challenge subjects. $R^2 = 0.357$, $p = 0.0311$.
- j. Gene Ontology (GO) enrichment analysis for genes differentially expressed at baseline between type 2 high subjects (defined as PC1 > 0) and type 2 low subjects (Defined as PC1 < 0) for subjects challenged with HDM
- k. GO enrichment analysis for genes differentially expressed in allergen challenge samples between type 2 high subjects (defined as PC1 > 0) and type 2 low subjects (Defined as PC1 < 0) for subjects challenged with HDM

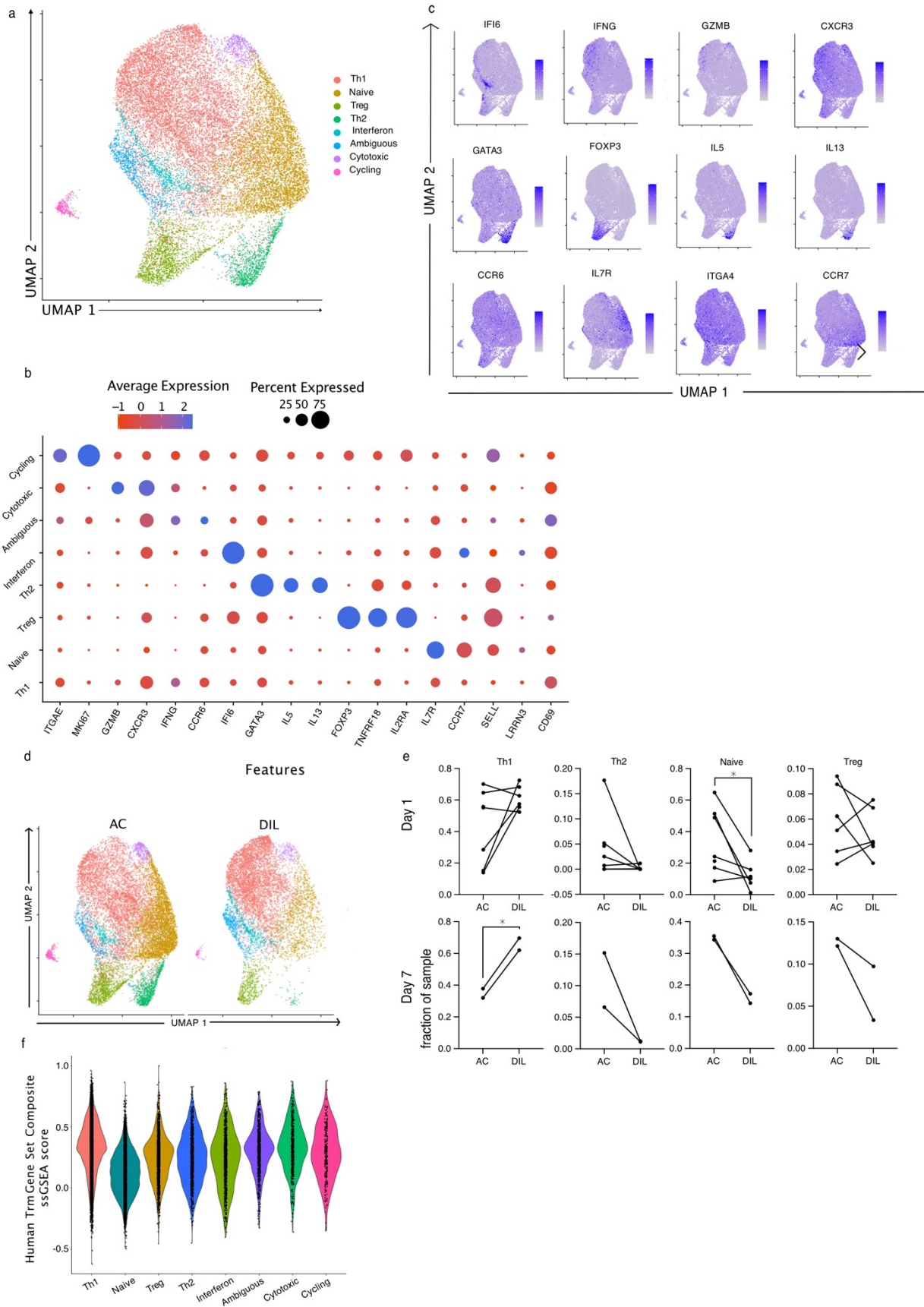


Figure 3.4. scRNAseq on enriched CD4+ T cells resolves allergen induced Th2 Cells

- a. UMAP illustrating CD4+ T cell subsets identified by unbiased clustering of scRNAseq from frozen samples enriched for CD4+ T cells via flow cytometry
- b. Dot plot illustrating marker gene expression in the clusters identified in (a) where color indicates intensity of expression and dot size represents percentage of cells within that cluster expressing a given gene
- c. Feature plots for marker gene expression in the UMAP space defined in (a) and darker blue color indicates increased intensity of given gene expression
- d. UMAP split by V3 sample treatment of either allergen challenge or diluent with each cell color coded by unbiased clustering assignment
- e. Allergen versus diluent representation of each cluster identified in (a) as a fraction of sample identified by the given cluster. Lines indicate paired samples obtained from the same subject.
- f. Single cell gene enrichment scores for a tissue residency gene program defined by [\(Kumar et al. 2017\)](#) plotted for each cluster identified in (a) for all samples assayed. Each dot represents a single cell and the violin plot illustrates the population distribution. Statistics displayed determined by paired t-test between AC and DIL samples (*, $p < 0.05$)

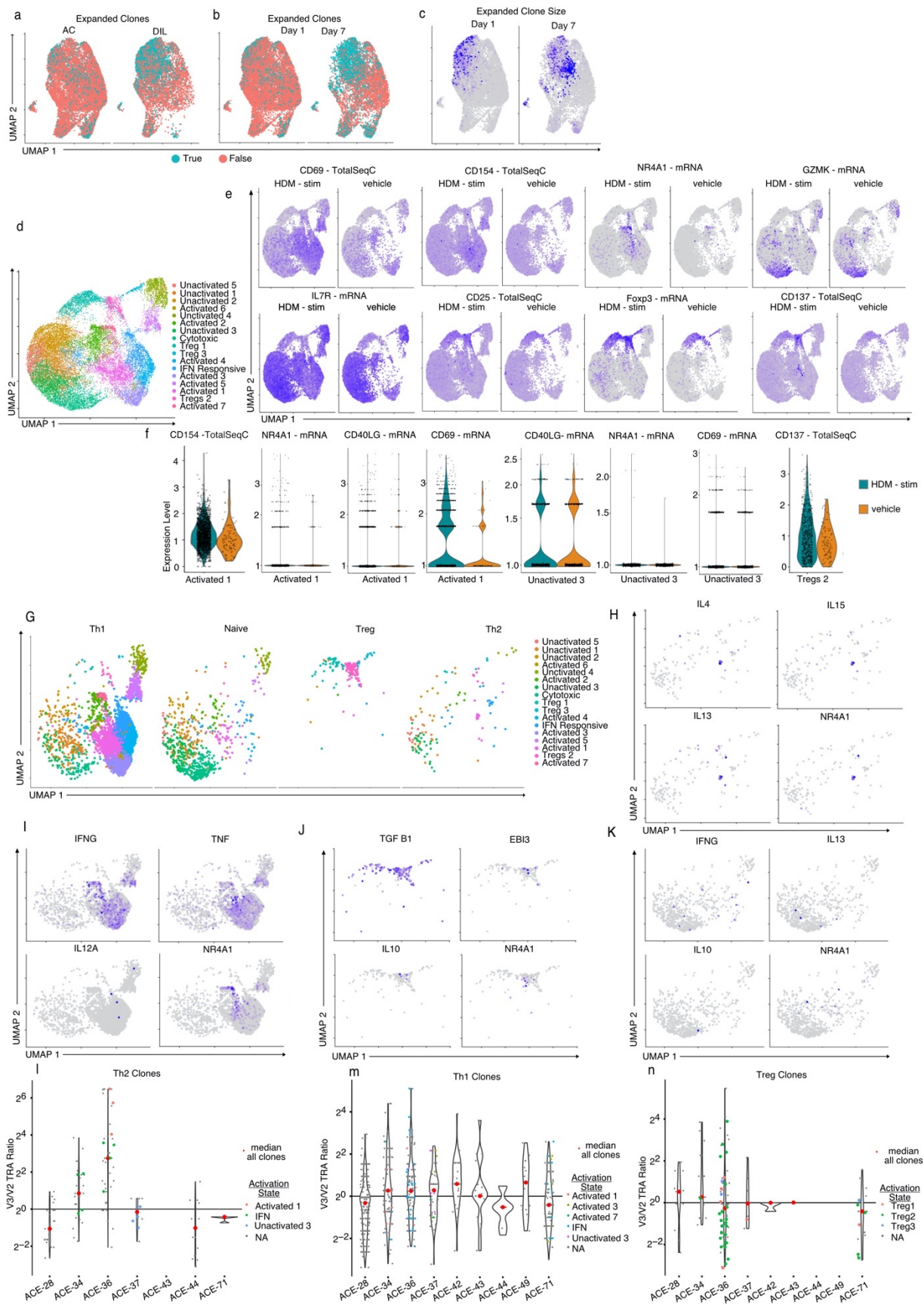


Figure 3.5. Expanded Th2 clones are allergen reactive and expand in the blood post-challenge

- a. UMAP of CD4+ T cells identified in the directly assayed data set described in Figure 4. Individual cells are color coded by their status as part of an expanded T cell clone, defined by 2 or more cells containing the exact same TCRalpha and TCRbeta pair. The plot contains all samples assayed and is split by the treatment condition of the sample.
- b. UMAP of CD4+ T cells identified in the freshly assayed data set described in Figure 4. Individual cells are color coded by their status as part of an expanded T cell clone, defined by 2 or more cells containing the exact same TCRalpha and TCRbeta pair. The plot contains all samples assayed and is split by the time point of the sample.
- c. UMAP of CD4+ T cells identified in the freshly assayed data set described in Figure 4. Individual cells are color coded by how many other cells belong to their T cell clonotype, defined by 2 or more cells containing the exact same TCRalpha and TCRbeta pair. The plot contains all samples assayed and is split by the time point of the sample.
- (d-k) Activated induced mark assay where BAL aliquots were thawed and stimulated for 8 hours with HDM extract and then sorted by flow cytometry prior to analyzing gene expression and TCR sequences by scRNAseq
- d. UMAP of CD4+ T cells from the AIM assay. Individual cells are color coded by their unbiased cluster designation.
- e. Feature plots of key marker gene/protein expression in the AIM assay split between the *ex vivo* treatment conditions. Gene expression detected via direct sequencing of the mRNA molecule is denoted with “-mRNA”. Protein expression detected via oligo tagged antibody binding to the marker of interest is denoted with “-TotalSeqC”. Darker blue indicates increased expression of that gene/protein.
- f. Gene/protein expression of key TCR activation induced genes in cluster designated “activated 1” and cluster designated “unactivated 3”. Each dot indicates the expression level of the given gene/protein for a single cell in that cluster and *ex vivo* treatment. All samples are included and split by *ex vivo* treatment. Violin plot captures the distribution for a given gene/protein in that cluster and *ex vivo* treatment group.
- g. UMAP as defined in d, but split by the phenotype of each clonotype in the directly assayed data set. TCR sequences were used to barcode the cells present in both the directly assayed aliquots and the *ex vivo* stimulated AIM assay. Clonotypes were assigned a phenotype from the cluster most represented in that clonotype from the directly assayed data set.
- h. Feature plots illustrating type 2 cytokine and activation induced gene expression in AIM clones containing TCR clonotypes defined as Th2 in the directly assayed data set
- i. Feature plots illustrating type 1 cytokine and activation induced gene expression in AIM clones containing TCR clonotypes defined as Th1 in the directly assayed data set
- j. Feature plots illustrating regulatory T cell cytokines and activation induced gene expression in AIM clones containing TCR clonotypes defined as Tregs in the directly assayed data set
- k. Feature plots illustrating type 1, type 2, and regulatory T cell cytokines and activation induced gene expression in AIM clones containing TCR clonotypes defined as undifferentiated/naive in the directly assayed data set
- (l-n) TCR sequencing was performed on bulk RNA isolated from peripheral blood at clinical visits 2 and 3. TCRalpha prevalence was determined by the percent of total TCR reads a given alpha chain occupied. V3/V2 enrichment was determined by the ratio of prevalence for a given TCRalpha at visit 3 divided by the prevalence for the same TCRalpha at visit 2.
- l. Enrichment of TCR alpha sequences associated with clonotypes identified as Th2 clones in the directly assayed data set. Select clones that were also identified in the AIM assay are color coded by the most prominent cluster from that assay.

- m. Enrichment of TCR alpha sequences associated with clonotypes identified as Th1 clones in the directly assayed data set. Select clones that were also identified in the AIM assay are color coded by the most prominent cluster from that assay.
- n. Enrichment of TCR alpha sequences associated with clonotypes identified as Treg clones in the directly assayed data set. Select clones that were also identified in the AIM assay are color coded by the most prominent cluster from that assay.

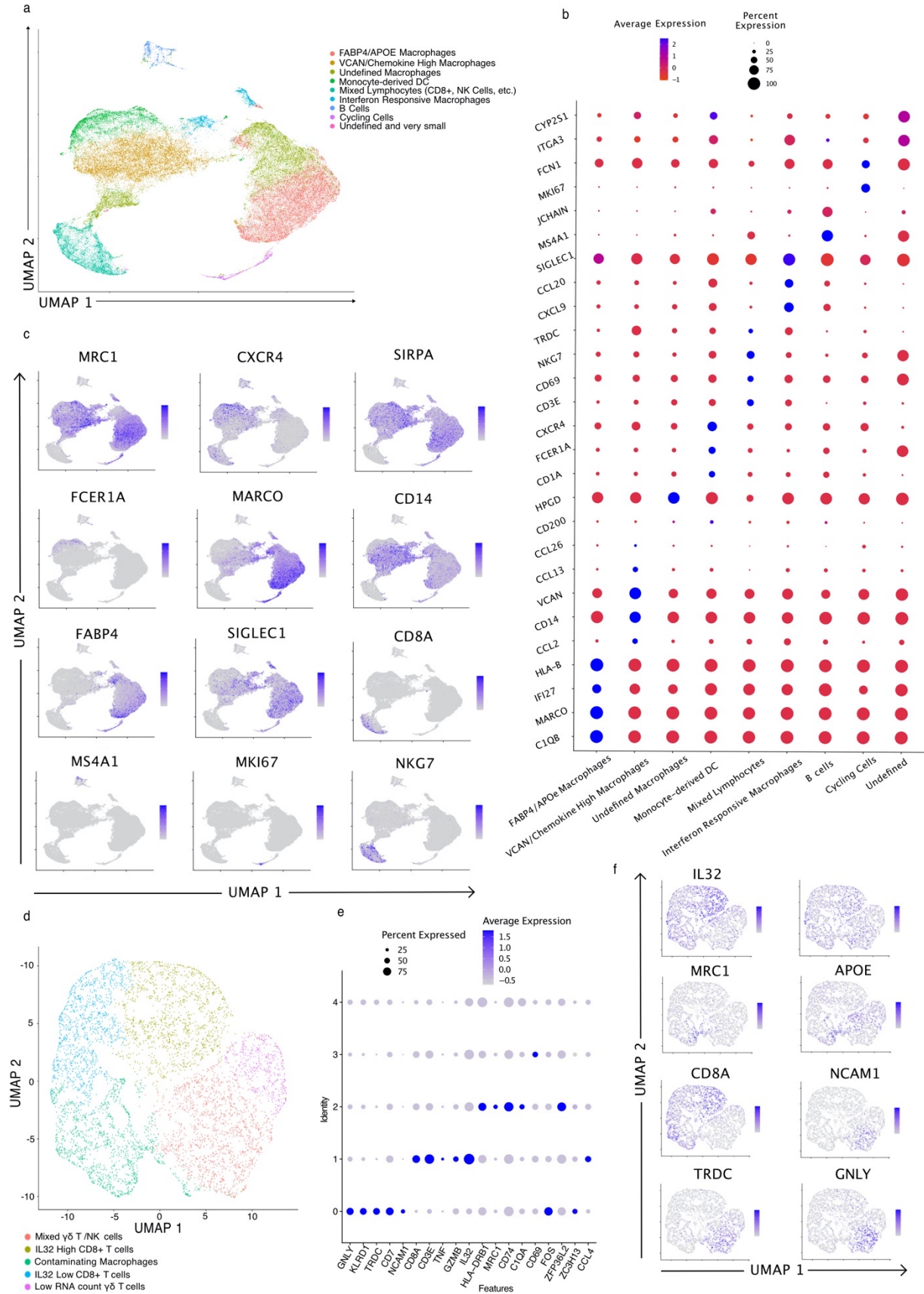


Figure 3.6. scRNA defines non-granulocyte, non-CD4+ T cell populations

Frozen BAL aliquots were thawed and sorted by flow cytometry to remove neutrophils and eosinophils. CD4+ T cells were separately assayed as shown in figure 4 & 5, the rest of the cells in the sample were assayed scRNAseq.

- a. UMAP showing dimensionally reduced visualization of scRNAseq data. Each dot represents a cell color coded by the cluster identified through unbiased nearest neighbors clustering. All samples displayed.
- b. Dot plot indicating key marker gene expression. Dot size indicates percent of cells in a given cluster expressing a given gene and color indicates the intensity of expression.
- c. Feature plots visualizing key marker gene expression displayed in UMAP space defined in (a). Increasingly dark blue color indicates increased expression of the indicated gene
- (d-f) The mixed cytotoxic lymphocyte cluster from the whole data set was subset and dimensional reduction and clustering analyses were performed to further resolve the populations.
 - d. UMAP showing dimensional reduced visualization of sub-clustered cytotoxic lymphocytes. Each dot represents a cell color coded by the new higher resolution unbiased nearest neighbors clustering. All samples are displayed.
 - e. Dot plot indicating key marker gene expression. Dot size indicates percent of cells in a given cluster expressing a given gene and color indicates the intensity of expression.
 - f. Feature plots visualizing key marker gene expression displayed in UMAP space defined in (d). Increasingly dark blue color indicates increased expression of the indicated gene

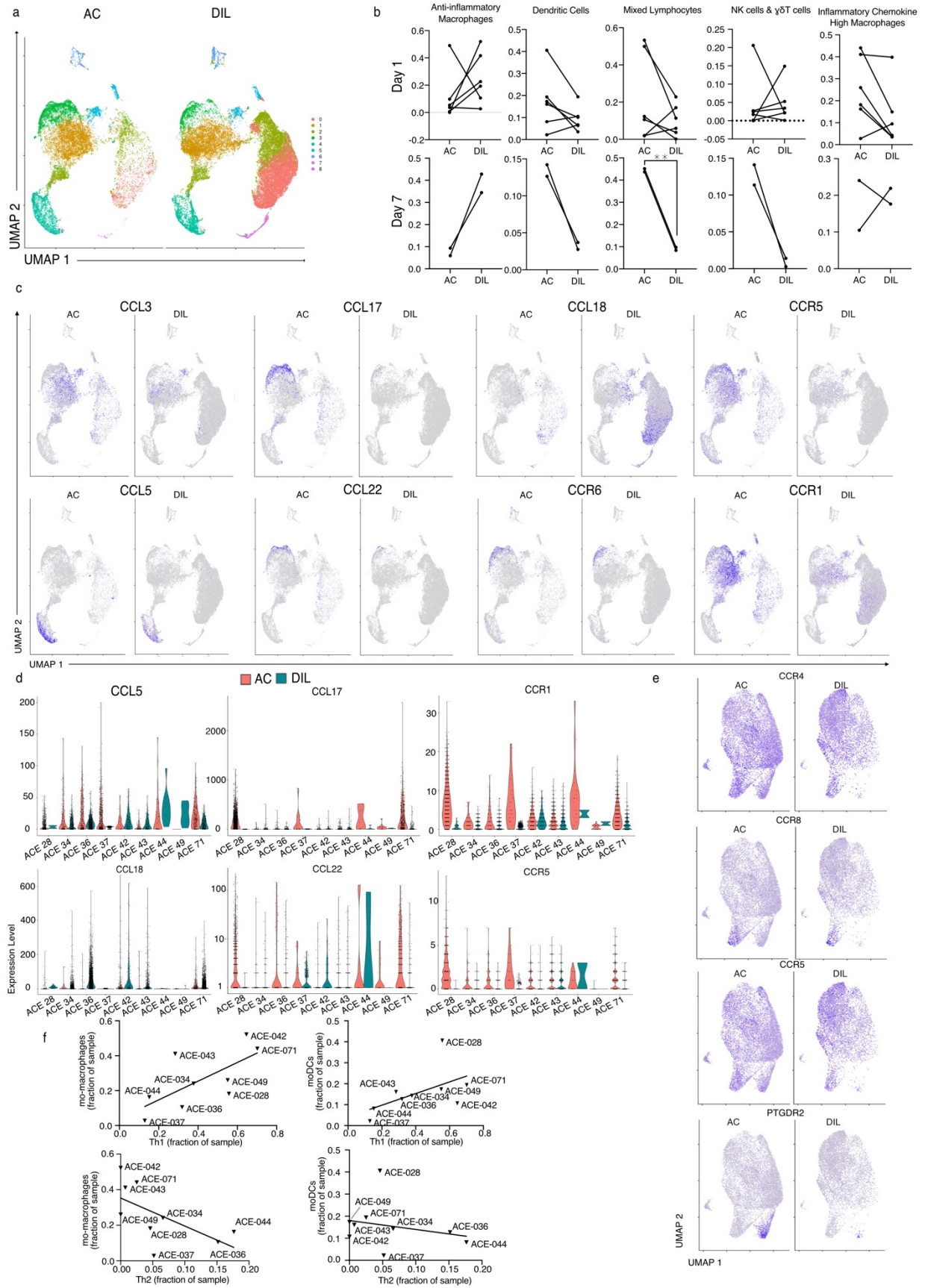


Figure 3.7. Allergen induces T cell recruiting chemokine expression in monocyte derived populations

Single cell analysis defined in figure 6 is analyzed for differences in cellular composition and gene expression and is connected to gene expression and cellular composition in the CD4+ T cell data set defined in figure 4.

- a. UMAP dimensionally reduced plot from figure 6a split by V3 sample treatment.
- b. Allergen versus diluent representation of each cluster identified in (a) as a fraction of sample identified by the given cluster. Lines indicate paired samples obtained from the same subject.
- c. Feature plots split by allergen challenge and diluent of key chemokine and chemokine receptor genes identified as differentially expressed by Wilcoxon Rank Sum test.
- d. Gene expression of differentially expressed key chemokine and chemokine receptor genes broken down by subject and sample treatment. CCL5 is subset on the mixed cytotoxic lymphocyte cluster. CCL17 and CCL22 are subset on the mo-DC cluster. CCR1 and CCR5 is subset on the monocyte derived macrophage cluster. CCL18 is subset on the tissue-resident alveolar macrophage cluster. Each dot represents a single cell and the violin plot illustrates the population distribution.
- e. Feature plots indicating the expression of chemotactic receptors on the directly analyzed data set from figure 4, split by sample treatment and color intensity by gene expression.
- f. Correlation between monocyte derived populations and Th1 and Th2 subsets define in the directly analyzed data set from figure 4. Plotted relationship line represents linear regression of the two variables. Th1 vs mo-macrophages: $R^2 = 0.465$, $p = 0.129$. Th1 vs mo-DCs: $R^2 = 0.298$, $p = 0.0957$. Th2 vs mo-macrophages: $R^2 = 0.381$, $p = 0.0767$. Th2 vs mo-DCs: $R^2 = 0.059$, $p = 0.526$.

Statistics displayed determined by paired t-test between AC and DIL samples (**, $p < 0.01$)

A

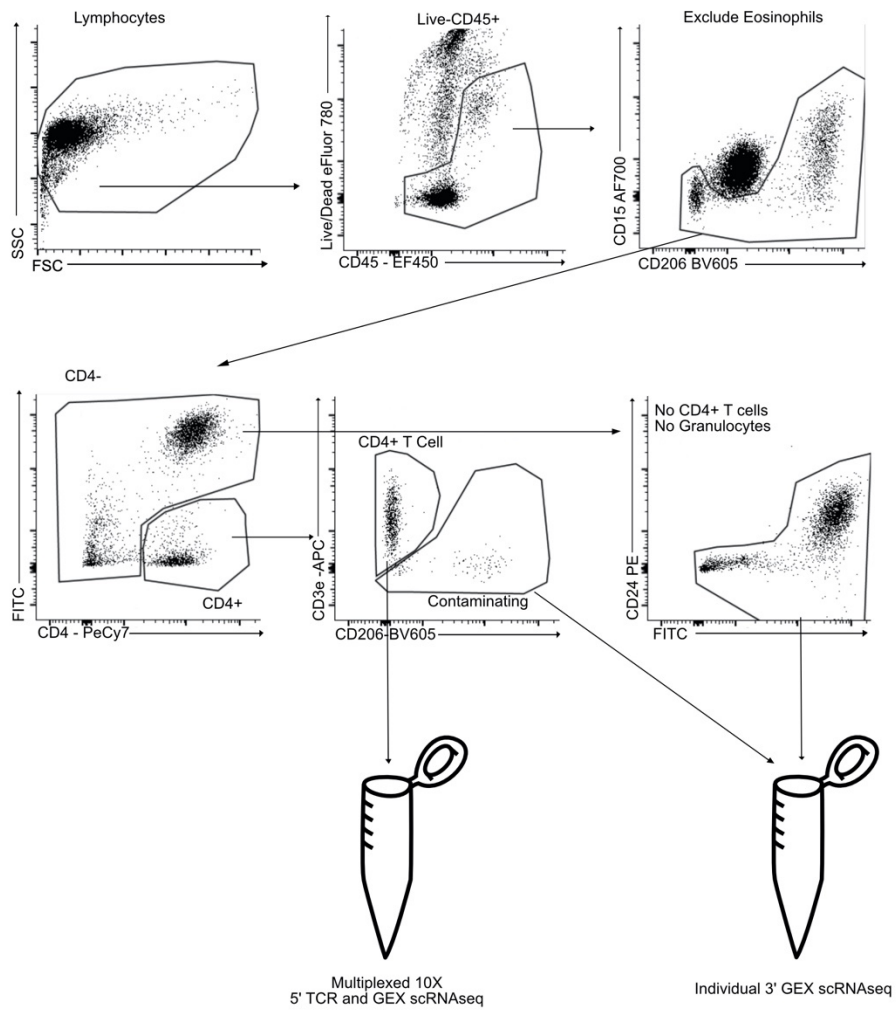


Figure S3.1. Sorting strategy for CD4+ enrichment and granulocyte depletion prior to scRNAseq

- a. Sorting strategy schematic in which lymphocytes were sorted to include live CD45+ cells. Then CD15+ CD206 low cells were excluded as they included Neutrophils and Eosinophils. This population was then split into 2 populations dependent on CD4 expression and staining with a host of lineage markers in the FITC channel. The CD4+ positive FITC- cells were then sorted based upon CD3e and CD206 expression to obtain a pure CD4+ T cell population. All other cells besides the CD4+ FITC- cells were then checked that no CD24+ CD206- eosinophils were present. This population as well as any CD206+ contaminants from the CD4+ FITC- gate were then sorted together.

Tables

Table 3.1. 10X scRNAseq Samples Assayed

ID	V3 Time Point	Diagnosis	Allergen	AC/DIL
ACE-28	1 day	AA	HDM	AC only
ACE-34	7 day	AA	HDM	both
ACE-36	7 day	AA	HDM	both
ACE-37	1 day	AA	HDM	both
ACE-42	1 day	NANA	Cat dander	both
ACE-43	1 day	AA	HDM	both
ACE-44	1 day	AA	HDM	both
ACE-49	1 day	AA	HDM	both
ACE-71	1 day	AA	HDm	both

Table 3.2. SNPs Used for Sample Identification

Total SNPs Evaluated	Unique SNPs	Shared SNPs
36637	3194	33443

Table 3.3. Assigning cells from homogenous data sets to individuals defined via unbiased demultiplexing of heterogeneous samples

Homogeneous 3' Data Set Tested	Assigned Individual from Unbiased Demultiplexing of CD4+ T Cell Data			
	Individual 1	Individual 2	Individual 3	Individual 4
ACE-34	0	643	2	0
ACE-36	0	0	825	0
ACE-37	1	6	0	1054
ACE-71	3512	0	0	5

Table 3.4. Cross Referencing assignments of cells from two independent heterogeneous samples containing the same individuals

Sample Set 2 Individual	Assigned Individual from Unbiased Demultiplexing of CD4+ T Cell Data			
	Individual 1	Individual 2	Individual 3	Individual 4
Individual 1	2917	0	0	0
Individual 2	0	2627	0	0
Individual 3	1	0	2516	0
Individual 4	0	0	0	678

Table S.3.1 Key Reagents Used

Reagent	Source	Detail	Catalog #
CD4 - PE-Cy7	Biologend	Clone OKT4	317413
CD45 - ef450	Invitrogen	2D1	48-9459-42
CD24 PE	BD Biosciences	ML5	560991
CD206 BV605	BD Biosciences	19.2	740417
CD3 APC	Biologend	UCHT1	300412
CD15 AF700	Biologend	HI98	301919
CD20 FITC	Biologend	2H7	302303
CD19 FITC	Biologend	HIB19	302206
CD16 FITC	Biologend	3G8	302005
CD14 FITC	Biologend	HCD14	325603
CD56 FITC	Biologend	MEM-188	304603

Table S3.2 Antibodies used for cytof staining and analysis

Channel-Metal	Marker ID	Clone	Source
154Sm	CD45	HI30	Fluidigm
158Gd*	CD45RA	HI100	BioLegend
165Ho	CD45RO	UCHL1	Fluidigm
142Nd	CD19	HIB19	Fluidigm
147Sm	CD20	2H7	Fluidigm
144Nd	CD38	HIT2	Fluidigm
167Er	CD27	O323	Fluidigm
170Er	CD3	UCHT1	Fluidigm
145Nd	CD4	RPA-T4	Fluidigm
146Nd	CD8a	RPA-T8	Fluidigm
152Sm	TCR $\gamma\delta$	11F2	Fluidigm
156Gd	CD183	G025H7	Fluidigm
141Pr	CD196	G034E3	Fluidigm
172Yb*	CD194	L291H4	BioLegend
173Yb*	CD69	FN50	BioLegend
149Sm	CD25	2A3	Fluidigm
176Yb	CD127	A019D5	Fluidigm
163Dy	CD294	BM16	Fluidigm
169Tm*	ST2	B4E6	MdBio
153Eu	CD7	CD7-6B7	Fluidigm
150Nd*	CD56	HCD56	BioLegend
148Nd	CD16	3G8	Fluidigm
164Dy	CD15	W6D3	Fluidigm
166Er	CD24	ML5	Fluidigm

Channel-Metal	Marker ID	Clone	Source
162Dy*	CD193	5E8	BioLegend
175Lu*	CD206	15-2	BioLegend
160Gd	CD14	M5E2	Fluidigm
171Yb*	CD1c	L161	BioLegend
159Tb	CD11c	Bu15	Fluidigm
174Yb	HLD-DR	L243	Fluidigm
151Eu	CD123	6H6	Fluidigm
168Er*	FcεRI	AER-37	BioLegend
143Nd	CD117	104D2	Fluidigm
198Pt	Cisplatin	NA	Fluidigm

Chapter 4: Conclusion

These studies together span the scales of immunology from the regulation of gene expression to cellular modules of inflammation to human inflammatory disease. While the specific topics may be divergent there are key themes that underlie both the biology investigated in each chapter and network centric approaches taken. Central to these studies are the roles that T cells play in the immune system. T cells possess effector functions that play direct roles in inflammatory processes such as the killing of virally infected cells (Bachmann et al. 1999). Beyond this, T cells act as a central inflammatory node interfacing with many distinct cell types to coordinate a network of immune responses.

T cells' first role in coordinating immune responses is antigen recognition and activation through the TCR (Murali-Krishna et al. 1998). However, for this activation to be full and complete T cells require secondary and tertiary signals. CD28 has been well established as a secondary co-stimulatory signal and IL-2, in paracrine and autocrine fashions, is important for supporting and sustaining T cell responses (Martínez-Llordella et al. 2013; Vandenberghe et al. 1993; Toumi et al. 2022; Whyte et al. 2022; Pipkin et al. 2010). In chapter 2 of the work presented here, it is demonstrated how the non-coding RNA circuit composed of Malat1 and miR-15/16 regulated these signals. In particular, this circuit regulates CD28 directly and together with a network of other genes in that pathway induces a gene expression pattern that augments the costimulatory signal. Further, this circuit augments IL-2 production amplifying the activating effect.

After this activation and recognition phase T cells can coordinate the immune response primarily through cytokine secretion (Bachmann et al. 1999). In this way, T cells interface between innate immune pattern based activation mechanisms and an amplified full immune response. For instance, CD4⁺ T cells in the presence of allergens such as house dust mite, can differentiate into Type 2 T helper cells (Th2) defined by the production of IL-4, IL-5, and IL-13

(Hammad and Lambrecht 2021; Boonpiyathad et al. 2019). Through these cytokines, Th2 cells can direct B cells to class switch to IgE producing plasma cells, recruit and activate eosinophils, and change epithelial cell states towards the production of mucus secretion (Siddiqui et al. 2021; Hammad and Lambrecht 2021; Boonpiyathad et al. 2019). Chapter 3, presented here, deeply explores the Th2 response within human asthmatics. We find that Th2 cells are present in human asthmatics with an elevated type 2 high inflammatory tone defined by elevated presence of eosinophils, basophils, and ILC2s in the bronchoalveolar space after allergen challenge. Further, these subjects have elevated IL-13 responsive gene expression in the epithelium before and after challenge and high HDM specific IgE in the blood. This illustrates that this a coherent module of type 2 inflammation present systemically before challenge and revealed and amplified at the local site of allergen exposure. We connect these programs not only to the presence of Th2 cells but the antigen specific activation of these cells. TCR sequencing shows that the subset of Th2 cells activated by allergen are present in the blood before challenge and expand after challenge. While this is not an interventional study, and causal lines cannot be drawn, this illustrates how a network can be constructed between the systemic blood compartment and a multifaceted response in the local lung environment of allergen exposure.

These studies together illustrate the broad and potent role that T cells play in coordinating the immune response to a wide variety of insults from allergens to bacteria to viruses. Further, these results support the notion that proper regulation of T cells is of great importance to organismal health and that this regulation occurs through layered mechanisms. Not only are gene programs regulated at the transcriptional level but we show this regulation extends to 5 nucleotides in the lncRNA Malat1 that contribute to miR-15/16 target regulation. In the future these studies could contribute to precise engineering of cell therapies or better clinical trial and therapeutic design for asthma.

References

- Abudayyeh, Omar O., Jonathan S. Gootenberg, Patrick Essletzbichler, Shuo Han, Julia Joung, Joseph J. Belanto, Vanessa Verdine, et al. 2017. "RNA Targeting with CRISPR-Cas13." *Nature* 550 (7675): 280–84.
- Alladina, Jehan, Neal P. Smith, Tristan Kooistra, Kamil Slowikowski, Isabela J. Kernin, Jacques Deguine, Henry L. Keen, et al. 2023. "A Human Model of Asthma Exacerbation Reveals Transcriptional Programs and Cell Circuits Specific to Allergic Asthma." *Science Immunology* 8 (83): eabq6352.
- Allen, Breanna M., Kamir J. Hiam, Cassandra E. Burnett, Anthony Venida, Rachel DeBarge, Iliana Tenvooren, Diana M. Marquez, Nam Woo Cho, Yaron Carmi, and Matthew H. Spitzer. 2020. "Systemic Dysfunction and Plasticity of the Immune Macroevironment in Cancer Models." *Nature Medicine* 26 (7): 1125–34.
- Arun, Gayatri, Disha Aggarwal, and David L. Spector. 2020. "MALAT1 Long Non-Coding RNA: Functional Implications." *Non-Coding RNA* 6 (2).
<https://doi.org/10.3390/ncrna6020022>.
- Ashouri, Judith F., and Arthur Weiss. 2017. "Endogenous Nur77 Is a Specific Indicator of Antigen Receptor Signaling in Human T and B Cells." *Journal of Immunology* 198 (2): 657–68.
- Ashwal-Fluss, Reut, Markus Meyer, Nagarjuna Reddy Pamudurti, Andranik Ivanov, Osnat Bartok, Mor Hanan, Naveh Evantal, Sebastian Memczak, Nikolaus Rajewsky, and

- Sebastian Kadener. 2014. “circRNA Biogenesis Competes with Pre-mRNA Splicing.” *Molecular Cell* 56 (1): 55–66.
- Bacher, Petra, Frederik Heinrich, Ulrik Stervbo, Mikalai Nienen, Marco Vahldieck, Christina Iwert, Katrin Vogt, et al. 2016. “Regulatory T Cell Specificity Directs Tolerance versus Allergy against Aeroantigens in Humans.” *Cell* 167 (4): 1067–78.e16.
- Bacher, Petra, and Alexander Scheffold. 2013. “Flow-Cytometric Analysis of Rare Antigen-Specific T Cells.” *Cytometry. Part A: The Journal of the International Society for Analytical Cytology* 83 (8): 692–701.
- Bachmann, M. F., M. Barner, A. Viola, and M. Kopf. 1999. “Distinct Kinetics of Cytokine Production and Cytolysis in Effector and Memory T Cells after Viral Infection.” *European Journal of Immunology* 29 (1): 291–99.
- Badovinac, Vladimir P., Brandon B. Porter, and John T. Harty. 2002. “Programmed Contraction of CD8(+) T Cells after Infection.” *Nature Immunology* 3 (7): 619–26.
- Baltz, Alexander G., Mathias Munschauer, Björn Schwanhäusser, Alexandra Vasile, Yasuhiro Murakawa, Markus Schueler, Noah Youngs, et al. 2012. “The mRNA-Bound Proteome and Its Global Occupancy Profile on Protein-Coding Transcripts.” *Molecular Cell* 46 (5): 674–90.
- Bao, Xichen, Xiangpeng Guo, Menghui Yin, Muqddas Tariq, Yiwei Lai, Shahzina Kanwal, Jiajian Zhou, et al. 2018. “Capturing the Interactome of Newly Transcribed RNA.” *Nature Methods* 15 (3): 213–20.

Bartel, David P. 2018. "Metazoan MicroRNAs." *Cell* 173 (1): 20–51.

Behrens, Gesine, Stephanie L. Edelmann, Timsse Raj, Nina Kronbeck, Thomas Monecke, Elena Davydova, Elaine H. Wong, et al. 2021. "Disrupting Roquin-1 Interaction with Regnase-1 Induces Autoimmunity and Enhances Antitumor Responses." *Nature Immunology* 22 (12): 1563–76.

Benhalevy, Daniel, Dimitrios G. Anastasakis, and Markus Hafner. 2018. "Proximity-CLIP Provides a Snapshot of Protein-Occupied RNA Elements in Subcellular Compartments." *Nature Methods* 15 (12): 1074–82.

Bhakta, Nirav R., Owen D. Solberg, Christine P. Nguyen, Cindy N. Nguyen, Joseph R. Arron, John V. Fahy, and Prescott G. Woodruff. 2013. "A qPCR-Based Metric of Th2 Airway Inflammation in Asthma." *Clinical and Translational Allergy* 3 (1): 24.

Bin Zhang; Gayatri Arun; YuntaonbspS. Mao; Zsolt Lazar; Gene Hung; Gourab Bhattacharjee; Xiaokun Xiao; CarmennbspJ. Booth; Jie Wu; Chaolin Zhang; DavidnbspL. Spector, Gayatri Arun, Yuntao S. Mao, Zsolt Lazar, Gene Hung, Gourab Bhattacharjee, Xiaokun Xiao, et al. 2012. "The lncRNA Malat1 Is Dispensable for Mouse Development but Its Transcription Plays a Cis-Regulatory Role in the Adult." *CellReports* 2 (1): 111–23.

Blake, Davia, and Kristen W. Lynch. 2021. "The Three as: Alternative Splicing, Alternative Polyadenylation and Their Impact on Apoptosis in Immune Function." *Immunological Reviews* 304 (1): 30–50.

- Blake, Davia, Caleb M. Radens, Max B. Ferretti, Matthew R. Gazzara, and Kristen W. Lynch. 2022. "Alternative Splicing of Apoptosis Genes Promotes Human T Cell Survival." *eLife* 11 (October). <https://doi.org/10.7554/eLife.80953>.
- Blattman, Joseph N., Jason M. Grayson, E. John Wherry, Susan M. Kaech, Kendall A. Smith, and Rafi Ahmed. 2003. "Therapeutic Use of IL-2 to Enhance Antiviral T-Cell Responses in Vivo." *Nature Medicine* 9 (5): 540–47.
- Bodey, K. J., A. E. Semper, A. E. Redington, J. Madden, L. M. Teran, S. T. Holgate, and A. J. Frew. 1999. "Cytokine Profiles of BAL T Cells and T-Cell Clones Obtained from Human Asthmatic Airways after Local Allergen Challenge." *Allergy* 54 (10): 1083–93.
- Boonpiyathad, Tadech, Zeynep Celebi Sözener, Pattraporn Satitsuksanoa, and Cezmi A. Akdis. 2019. "Immunologic Mechanisms in Asthma." *Seminars in Immunology* 46 (December): 101333.
- Borowski, Annie B., Alina C. Boesteanu, Yvonne M. Mueller, Caterina Carafides, David J. Topham, John D. Altman, Stephen R. Jennings, and Peter D. Katsikis. 2007. "Memory CD8+ T Cells Require CD28 Costimulation." *Journal of Immunology* 179 (10): 6494–6503.
- Bu, Dechao, Haitao Luo, Fei Jiao, Shuangfang Fang, Chengfu Tan, Zhiyong Liu, and Yi Zhao. 2015. "Evolutionary Annotation of Conserved Long Non-Coding RNAs in Major Mammalian Species." *Science China. Life Sciences* 58 (8): 787–98.
- Bullone, Michela, Vitina Carriero, Francesca Bertolini, Anna Folino, Alessandro Mannelli, Antonino Di Stefano, Isabella Gnemmi, Roberto Torchio, and Fabio L. M. Ricciardolo.

2019. “Elevated Serum IgE, Oral Corticosteroid Dependence and IL-17/22 Expression in Highly Neutrophilic Asthma.” *The European Respiratory Journal: Official Journal of the European Society for Clinical Respiratory Physiology* 54 (5).

<https://doi.org/10.1183/13993003.00068-2019>.

Carbonell Sala, Sílvia, Barbara Uszczyńska-Ratajczak, Julien Lagarde, Rory Johnson, and Roderic Guigó. 2021. “Annotation of Full-Length Long Noncoding RNAs with Capture Long-Read Sequencing (CLS).” *Methods in Molecular Biology* 2254: 133–59.

Carpenter, Susan. 2022. *Long Noncoding RNA*. Springer International Publishing.

Casolaro, Vincenzo, Xi Fang, Brian Tancowny, Jinshui Fan, Fan Wu, Subramanya Srikantan, S. Yukiko Asaki, et al. 2008. “Posttranscriptional Regulation of IL-13 in T Cells: Role of the RNA-Binding Protein HuR.” *The Journal of Allergy and Clinical Immunology* 121 (4): 853–59.e4.

Castello, Alfredo, Bernd Fischer, Katrin Eichelbaum, Rastislav Horos, Benedikt M.

Beckmann, Claudia Strein, Norman E. Davey, et al. 2012. “Insights into RNA Biology from an Atlas of Mammalian mRNA-Binding Proteins.” *Cell* 149 (6): 1393–1406.

Castro, Mario, Jonathan Corren, Ian D. Pavord, Jorge Maspero, Sally Wenzel, Klaus F. Rabe, William W. Busse, et al. 2018. “Dupilumab Efficacy and Safety in Moderate-to-Severe Uncontrolled Asthma.” *The New England Journal of Medicine* 378 (26): 2486–96.

Chakir, Jamila, Joanne Shannon, Sophie Molet, Motonori Fukakusa, Jack Elias, Michel Laviolette, Louis-Philippe Boulet, and Qutayba Hamid. 2003. “Airway Remodeling-Associated Mediators in Moderate to Severe Asthma: Effect of Steroids on TGF-Beta,

IL-11, IL-17, and Type I and Type III Collagen Expression.” *The Journal of Allergy and Clinical Immunology* 111 (6): 1293–98.

Chatrikhi, Rakesh, Michael J. Mallory, Matthew R. Gazzara, Laura M. Agosto, Wandi S. Zhu, Adam J. Litterman, K. Mark Ansel, and Kristen W. Lynch. 2019. “RNA Binding Protein CELF2 Regulates Signal-Induced Alternative Polyadenylation by Competing with Enhancers of the Polyadenylation Machinery.” *Cell Reports* 28 (11): 2795–2806.e3.

Chen, C. Y., and A. B. Shyu. 1994. “Selective Degradation of Early-Response-Gene mRNAs: Functional Analyses of Sequence Features of the AU-Rich Elements.” *Molecular and Cellular Biology* 14 (12): 8471–82.

Chen, Jing, Jason Cascio, Joseph D. Magee, Patsharaporn Techasintana, Matthew M. Gubin, Garrett M. Dahm, Robert Calaluce, Shiguang Yu, and Ulus Atasoy. 2013. “Posttranscriptional Gene Regulation of IL-17 by the RNA-Binding Protein HuR Is Required for Initiation of Experimental Autoimmune Encephalomyelitis.” *Journal of Immunology* 191 (11): 5441–50.

Chen, Lisha, Hongbing Yao, Kai Wang, and Xiangfeng Liu. 12 2017. “Long Non-Coding RNA MALAT1 Regulates ZEB1 Expression by Sponging miR-143-3p and Promotes Hepatocellular Carcinoma Progression.” *Journal of Cellular Biochemistry* 118 (12): 4836–43.

Chen, Sean, Benjamin Lee, Angus Yiu-Fai Lee, Andrew J. Modzelewski, and Lin He. 2016. “Highly Efficient Mouse Genome Editing by CRISPR Ribonucleoprotein Electroporation of Zygotes.” *The Journal of Biological Chemistry* 291 (28): 14457–67.

- Chen, Yali, Juan Liu, Xiaomin Zhang, Ha Zhu, Yujia Wang, Zhiqing Li, Yanfang Liu, et al. 2022. “lncRNA-GM Targets Foxo1 to Promote T Cell-Mediated Autoimmunity.” *Science Advances* 8 (31): eabn9181.
- Chen, Yao, Ryan Zander, Achia Khatun, David M. Schauder, and Weiguo Cui. 2018. “Transcriptional and Epigenetic Regulation of Effector and Memory CD8 T Cell Differentiation.” *Frontiers in Immunology* 9 (December): 2826.
- Choi, Inseon S., Youngil I. Koh, Jeom-Seok Koh, and Min-Gu Lee. 2005. “Sensitivity of the Skin Prick Test and Specificity of the Serum-Specific IgE Test for Airway Responsiveness to House Dust Mites in Asthma.” *The Journal of Asthma: Official Journal of the Association for the Care of Asthma* 42 (3): 197–202.
- Cimmino, Amelia, George Adrian Calin, Muller Fabbri, Marilena V. Iorio, Manuela Ferracin, Masayoshi Shimizu, Sylwia E. Wojcik, et al. 2005. “miR-15 and miR-16 Induce Apoptosis by Targeting BCL2.” *Proceedings of the National Academy of Sciences of the United States of America* 102 (39): 13944–49.
- Collin, Matthew, and Venetia Bigley. 2018. “Human Dendritic Cell Subsets: An Update.” *Immunology* 154 (1): 3–20.
- Decker, Carolyn J., and Roy Parker. 2012. “P-Bodies and Stress Granules: Possible Roles in the Control of Translation and mRNA Degradation.” *Cold Spring Harbor Perspectives in Biology* 4 (9): a012286.

- Deng, Liling, Guohua Liu, Chanjuan Zheng, Liwen Zhang, Yang Kang, and Fei Yang. 2019. "Circ-LAMP1 Promotes T-Cell Lymphoblastic Lymphoma Progression via Acting as a ceRNA for miR-615-5p to Regulate DDR2 Expression." *Gene* 701 (June): 146–51.
- Djuranovic, Sergej, Ali Nahvi, and Rachel Green. 2012. "miRNA-Mediated Gene Silencing by Translational Repression Followed by mRNA Deadenylation and Decay." *Science* 336 (6078): 237–40.
- Dorsett, Yair, Kevin M. McBride, Mila Jankovic, Anna Gazumyan, To-Ha Thai, Davide F. Robbiani, Michela Di Virgilio, et al. 2008. "MicroRNA-155 Suppresses Activation-Induced Cytidine Deaminase-Mediated Myc-Igh Translocation." *Immunity* 28 (5): 630–38.
- Duchesne, Marc, Isobel Okoye, and Paige Lacy. 2022. "Epithelial Cell Alarmin Cytokines: Frontline Mediators of the Asthma Inflammatory Response." *Frontiers in Immunology* 13 (October): 975914.
- Dunican, Eleanor M., Brett M. Elicker, David S. Gierada, Scott K. Nagle, Mark L. Schiebler, John D. Newell, Wilfred W. Raymond, et al. 2018. "Mucus Plugs in Patients with Asthma Linked to Eosinophilia and Airflow Obstruction." *The Journal of Clinical Investigation* 128 (3): 997–1009.
- Eberlein, Jens, Bennett Davenport, Tom T. Nguyen, Francisco Victorino, Tim Sparwasser, and Dirk Homann. 2012-2. "Multiple Layers of CD80/86-Dependent Costimulatory Activity Regulate Primary, Memory, and Secondary Lymphocytic Choriomeningitis Virus-Specific T Cell Immunity." *Journal of Virology* 86 (4): 1955–70.

- Eichhorn, Stephen W., Huili Guo, Sean E. McGeary, Ricard A. Rodriguez-Mias, Chanseok Shin, Daehyun Baek, Shu-Hao Hsu, Kalpana Ghoshal, Judit Villén, and David P. Bartel. 2014. “mRNA Destabilization Is the Dominant Effect of Mammalian microRNAs by the Time Substantial Repression Ensues.” *Molecular Cell* 56 (1): 104–15.
- Elguindy, Mahmoud M., and Joshua T. Mendell. 2021. “NORAD-Induced Pumilio Phase Separation Is Required for Genome Stability.” *Nature* 595 (7866): 303–8.
- Emming, Stefan, Niccolò Bianchi, Sara Polletti, Chiara Balestrieri, Cristina Leoni, Sara Montagner, Michele Chirichella, Nicolas Delaleu, Gioacchino Natoli, and Silvia Monticelli. 2020. “A Molecular Network Regulating the Proinflammatory Phenotype of Human Memory T Lymphocytes.” *Nature Immunology* 21 (4): 388–99.
- Essig, Katharina, Desheng Hu, Joao C. Guimaraes, Dominik Alterauge, Stephanie Edelmann, Timsse Raj, Jan Kranich, et al. 2017. “Roquin Suppresses the PI3K-mTOR Signaling Pathway to Inhibit T Helper Cell Differentiation and Conversion of Treg to Tfr Cells.” *Immunity* 47 (6): 1067–82.e12.
- Essig, Katharina, Nina Kronbeck, Joao C. Guimaraes, Claudia Lohs, Andreas Schlundt, Anne Hoffmann, Gesine Behrens, et al. 2018. “Roquin Targets mRNAs in a 3'-UTR-Specific Manner by Different Modes of Regulation.” *Nature Communications* 9 (1): 3810.
- Fabian, Marc R., Filipp Frank, Christopher Rouya, Nadeem Siddiqui, Wi S. Lai, Alexey Karetnikov, Perry J. Blackshear, Bhushan Nagar, and Nahum Sonenberg. 2013. “Structural Basis for the Recruitment of the Human CCR4-NOT Deadenylase Complex by Tristetraprolin.” *Nature Structural & Molecular Biology* 20 (6): 735–39.

- Fitzpatrick, Anne M., W. Gerald Teague, Deborah A. Meyers, Stephen P. Peters, Xingnan Li, Huashi Li, Sally E. Wenzel, et al. 2011. "Heterogeneity of Severe Asthma in Childhood: Confirmation by Cluster Analysis of Children in the National Institutes of Health/National Heart, Lung, and Blood Institute Severe Asthma Research Program." *The Journal of Allergy and Clinical Immunology* 127 (2): 382–89.e1–13.
- Fraser, J. D., B. A. Irving, G. R. Crabtree, and A. Weiss. 1991. "Regulation of Interleukin-2 Gene Enhancer Activity by the T Cell Accessory Molecule CD28." *Science* 251 (4991): 313–16.
- Fuse, Shinichiro, Weijun Zhang, and Edward J. Usherwood. 2008. "Control of Memory CD8+ T Cell Differentiation by CD80/CD86-CD28 Costimulation and Restoration by IL-2 during the Recall Response." *Journal of Immunology* 180 (2): 1148–57.
- Gagnon, John D., Robin Kageyama, Hesham M. Shehata, Marlys S. Fassett, Darryl J. Mar, Eric J. Wigton, Kristina Johansson, et al. 08/2019. "miR-15/16 Restrain Memory T Cell Differentiation, Cell Cycle, and Survival." *Cell Reports* 28 (8): 2169–81.e4.
- Garcia-Doval, Carmela, and Martin Jinek. 2017. "Molecular Architectures and Mechanisms of Class 2 CRISPR-Associated Nucleases." *Current Opinion in Structural Biology* 47 (December): 157–66.
- Garcia-Moreno, Manuel, Marko Noerenberg, Shuai Ni, Aino I. Järvelin, Esther González-Almela, Caroline E. Lenz, Marcel Bach-Pages, et al. 2019. "System-Wide Profiling of RNA-Binding Proteins Uncovers Key Regulators of Virus Infection." *Molecular Cell* 74 (1): 196–211.e11.

Gauvreau, Gail M., Paul M. O’Byrne, Louis-Philippe Boulet, Ying Wang, Donald Cockcroft, Jeannette Bigler, J. Mark FitzGerald, et al. 2014. “Effects of an Anti-TSLP Antibody on Allergen-Induced Asthmatic Responses.” *The New England Journal of Medicine* 370 (22): 2102–10.

Gavala, M. L., E. A. B. Kelly, S. Esnault, S. Kukreja, M. D. Evans, P. J. Bertics, G. L. Chupp, and N. N. Jarjour. 2013. “Segmental Allergen Challenge Enhances Chitinase Activity and Levels of CCL18 in Mild Atopic Asthma.” *Clinical and Experimental Allergy: Journal of the British Society for Allergy and Clinical Immunology* 43 (2): 187–97.

GBD Chronic Respiratory Disease Collaborators. 2020. “Prevalence and Attributable Health Burden of Chronic Respiratory Diseases, 1990-2017: A Systematic Analysis for the Global Burden of Disease Study 2017.” *The Lancet. Respiratory Medicine* 8 (6): 585–96.

Gibb, Ewan A., Emily A. Vucic, Katey S. S. Enfield, Greg L. Stewart, Kim M. Lonergan, Jennifer Y. Kennett, Daiana D. Becker-Santos, et al. 2011. “Human Cancer Long Non-Coding RNA Transcriptomes.” *PloS One* 6 (10): e25915.

Gruber, Andreas R., Georges Martin, Philipp Müller, Alexander Schmidt, Andreas J. Gruber, Rafal Gumienny, Nitish Mittal, et al. 2014. “Global 3’ UTR Shortening Has a Limited Effect on Protein Abundance in Proliferating T Cells.” *Nature Communications* 5 (November): 5465.

Grujic, Mirjana, Christina Bartholdy, Melissa Remy, Daniel D. Pinschewer, Jan P. Christensen, and Allan R. Thomsen. 2010. “The Role of CD80/CD86 in Generation and

Maintenance of Functional Virus-Specific CD8⁺ T Cells in Mice Infected with Lymphocytic Choriomeningitis Virus.” *Journal of Immunology* 185 (3): 1730–43.

Guo, Rong, Yonghui Su, Qi Zhang, Bingqiu Xiu, Sheng Huang, Weiru Chi, Liyi Zhang, et al. 2023. “LINC00478-Derived Novel Cytoplasmic lncRNA LacRNA Stabilizes PHB2 and Suppresses Breast Cancer Metastasis via Repressing MYC Targets.” *Journal of Translational Medicine* 21 (1): 120.

Hafner, Markus, Maria Katsantoni, Tino Köster, James Marks, Joyita Mukherjee, Dorothee Staiger, Jernej Ule, and Mihaela Zavolan. 2021. “CLIP and Complementary Methods.” *Nature Reviews Methods Primers* 1 (1): 1–23.

Hafner, Markus, Markus Landthaler, Lukas Burger, Mohsen Khorshid, Jean Hausser, Philipp Berninger, Andrea Rothballer, et al. 2010. “Transcriptome-Wide Identification of RNA-Binding Protein and microRNA Target Sites by PAR-CLIP.” *Cell* 141 (1): 129–41.

Haldar, Pranab, Ian D. Pavord, Dominic E. Shaw, Michael A. Berry, Michael Thomas, Christopher E. Brightling, Andrew J. Wardlaw, and Ruth H. Green. 2008. “Cluster Analysis and Clinical Asthma Phenotypes.” *American Journal of Respiratory and Critical Care Medicine* 178 (3): 218–24.

Hammad, Hamida, and Bart N. Lambrecht. 2021. “The Basic Immunology of Asthma.” *Cell* 184 (6): 1469–85.

Hanieh, Hamza, Kazuya Masuda, Hozaiifa Metwally, Jaya P. Chalise, Maged Mohamed, Kishan K. Nyati, Daron M. Standley, et al. 2018. “Arid5a Stabilizes OX40 mRNA in

Murine CD4⁺ T Cells by Recognizing a Stem-Loop Structure in Its 3'UTR." *European Journal of Immunology* 48 (4): 593–604.

Han, Jaeil, Collette A. LaVigne, Benjamin T. Jones, He Zhang, Frank Gillett, and Joshua T. Mendell. 2020. "A Ubiquitin Ligase Mediates Target-Directed microRNA Decay Independently of Tailing and Trimming." *Science* 370 (6523).
<https://doi.org/10.1126/science.abc9546>.

Han, Jinxiong, Jun Zhang, Li Chen, Bin Shen, Jiankui Zhou, Bian Hu, Yinan Du, Peri H. Tate, Xingxu Huang, and Wensheng Zhang. 2014. "Efficient in Vivo Deletion of a Large Imprinted lncRNA by CRISPR/Cas9." *RNA Biology* 11 (7): 829–35.

Hendel, Ayal, Rasmus O. Bak, Joseph T. Clark, Andrew B. Kennedy, Daniel E. Ryan, Subhadeep Roy, Israel Steinfeld, et al. 2015. "Chemically Modified Guide RNAs Enhance CRISPR-Cas Genome Editing in Human Primary Cells." *Nature Biotechnology* 33 (9): 985–89.

Herzog, Silva, Paraskevi C. Fragkou, Borros M. Arneth, Samr Mkhlof, and Chrysanthi Skevaki. 2022. "Myeloid CD169/Siglec1: An Immunoregulatory Biomarker in Viral Disease." *Frontiers of Medicine* 9 (September): 979373.

Hewitson, James P., Katie A. West, Kylie R. James, Gulab Fatima Rani, Nidhi Dey, Audrey Romano, Najmeeyah Brown, Sarah A. Teichmann, Paul M. Kaye, and Dimitris Lagos. 2020. "Malat1 Suppresses Immunity to Infection through Promoting Expression of Maf and IL-10 in Th Cells." *The Journal of Immunology*, April.
<https://doi.org/10.4049/jimmunol.1900940>.

Heyd, Florian, and Kristen W. Lynch. 2010. "Phosphorylation-Dependent Regulation of PSF by GSK3 Controls CD45 Alternative Splicing." *Molecular Cell* 40 (1): 126–37.

Hikono, Hirokazu, Jacob E. Kohlmeier, Shiki Takamura, Susan T. Wittmer, Alan D. Roberts, and David L. Woodland. 2007. "Activation Phenotype, rather than Central- or Effector-Memory Phenotype, Predicts the Recall Efficacy of Memory CD8+ T Cells." *The Journal of Experimental Medicine* 204 (7): 1625–36.

Hirai, H., K. Tanaka, O. Yoshie, K. Ogawa, K. Kenmotsu, Y. Takamori, M. Ichimasa, et al. 2001. "Prostaglandin D2 Selectively Induces Chemotaxis in T Helper Type 2 Cells, Eosinophils, and Basophils via Seven-Transmembrane Receptor CRTH2." *The Journal of Experimental Medicine* 193 (2): 255–61.

Hoefig, Kai P., Alexander Reim, Christian Gallus, Elaine H. Wong, Gesine Behrens, Christine Conrad, Meng Xu, et al. 2021. "Defining the RBPome of Primary T Helper Cells to Elucidate Higher-Order Roquin-Mediated mRNA Regulation." *Nature Communications* 12 (1): 5208.

Hou, Yan, Junjie Sun, Jie Huang, Fengzhi Yao, Xuelian Chen, Bin Zhu, and Dongchi Zhao. 2021. "Circular RNA circRNA_0000094 Sponges microRNA-223-3p and up-Regulate F-Box and WD Repeat Domain Containing 7 to Restrain T Cell Acute Lymphoblastic Leukemia Progression." *Human Cell* 34 (3): 977–89.

Huang, Huilin, Hengyou Weng, Wenju Sun, Xi Qin, Hailing Shi, Huizhe Wu, Boxuan Simen Zhao, et al. 2018. "Recognition of RNA N6-Methyladenosine by IGF2BP Proteins Enhances mRNA Stability and Translation." *Nature Cell Biology* 20 (3): 285–95.

- Huang, Rongbing, Mengting Han, Liying Meng, and Xing Chen. 2018. “Transcriptome-Wide Discovery of Coding and Noncoding RNA-Binding Proteins.” *Proceedings of the National Academy of Sciences of the United States of America* 115 (17): E3879–87.
- Iancu, Ortal, Daniel Allen, Orli Knop, Yonathan Zehavi, Dor Breier, Adaya Arbiv, Atar Lev, et al. 2023. “Multiplex HDR for Disease and Correction Modeling of SCID by CRISPR Genome Editing in Human HSPCs.” *Molecular Therapy. Nucleic Acids* 31 (March): 105–21.
- Invernizzi, Rachele, Clare M. Lloyd, and Philip L. Molyneaux. 2020. “Respiratory Microbiome and Epithelial Interactions Shape Immunity in the Lungs.” *Immunology* 160 (2): 171–82.
- Ito-Kureha, Taku, Cristina Leoni, Kayla Borland, Giulia Cantini, Marian Bataclan, Rebecca N. Metzger, Gregor Ammann, et al. 2022. “The Function of Wtap in N6-Adenosine Methylation of mRNAs Controls T Cell Receptor Signaling and Survival of T Cells.” *Nature Immunology* 23 (8): 1208–21.
- Janowski, Robert, Gitta A. Heinz, Andreas Schlundt, Nina Wommelsdorf, Sven Brenner, Andreas R. Gruber, Michael Blank, et al. 2016. “Roquin Recognizes a Non-Canonical Hexaloop Structure in the 3'-UTR of Ox40.” *Nature Communications* 7 (March): 11032.
- Jeltsch, Katharina M., Desheng Hu, Sven Brenner, Jessica Zöllner, Gitta A. Heinz, Daniel Nagel, Katharina U. Vogel, et al. 2014. “Cleavage of Roquin and Regnase-1 by the Paracaspase MALT1 Releases Their Cooperatively Repressed Targets to Promote T(H)17 Differentiation.” *Nature Immunology* 15 (11): 1079–89.

- Jheng, Min-Jhen, Takao Kobayashi, Koji Iijima, and Hirohito Kita. 2023. “Chemokine Receptor CCR8 and CCR8-Bearing Cells Are Involved in Regulation of Type 2 Immunity in Response to Airborne Allergens.” *The Journal of Allergy and Clinical Immunology* 151 (2): AB219.
- Ji, Ping, Sven Diederichs, Wenbing Wang, Sebastian Böing, Ralf Metzger, Paul M. Schneider, Nicola Tidow, et al. 2003. “MALAT-1, a Novel Noncoding RNA, and Thymosin beta4 Predict Metastasis and Survival in Early-Stage Non-Small Cell Lung Cancer.” *Oncogene* 22 (39): 8031–41.
- Kahan, Shannon M., Rakesh K. Bakshi, Jennifer T. Ingram, R. Curtis Hendrickson, Elliot J. Lefkowitz, David K. Crossman, Laurie E. Harrington, Casey T. Weaver, and Allan J. Zajac. 2022. “Intrinsic IL-2 Production by Effector CD8 T Cells Affects IL-2 Signaling and Promotes Fate Decisions, Stemness, and Protection.” *Science Immunology* 7 (68): eabl6322.
- Kakaradov, Boyko, Janilyn Arsenio, Christella E. Widjaja, Zhaoren He, Stefan Aigner, Patrick J. Metz, Bingfei Yu, et al. 2017. “Early Transcriptional and Epigenetic Regulation of CD8 + T Cell Differentiation Revealed by Single-Cell RNA Sequencing.” *Nature Immunology* 18 (4): 422–32.
- Kanbar, Jad N., Shengyun Ma, Eleanor S. Kim, Nadia S. Kurd, Matthew S. Tsai, Tiffani Tysl, Christella E. Widjaja, et al. 2022. “The Long Noncoding RNA Malat1 Regulates CD8+ T Cell Differentiation by Mediating Epigenetic Repression.” *The Journal of Experimental Medicine* 219 (6). <https://doi.org/10.1084/jem.20211756>.

- Kang, Hyun Min, Meena Subramaniam, Sasha Targ, Michelle Nguyen, Lenka Maliskova, Elizabeth McCarthy, Eunice Wan, et al. 2018. “Multiplexed Droplet Single-Cell RNA-Sequencing Using Natural Genetic Variation.” *Nature Biotechnology* 36 (1): 89–94.
- Karginov, Fedor V., and Gregory J. Hannon. 2013. “Remodeling of Ago2-mRNA Interactions upon Cellular Stress Reflects miRNA Complementarity and Correlates with Altered Translation Rates.” *Genes & Development* 27 (14): 1624–32.
- Karginov, Timofey A., Antoine Ménoret, and Anthony T. Vella. 2022. “Optimal CD8+ T Cell Effector Function Requires Costimulation-Induced RNA-Binding Proteins That Reprogram the Transcript Isoform Landscape.” *Nature Communications* 13 (1): 3540.
- Katsuyama, Takayuki, Hao Li, Denis Comte, George C. Tsokos, and Vaishali R. Moulton. 2019. “Splicing Factor SRSF1 Controls T Cell Hyperactivity and Systemic Autoimmunity.” *The Journal of Clinical Investigation* 129 (12): 5411–23.
- Katsuyama, Takayuki, and Vaishali R. Moulton. 2021. “Splicing Factor SRSF1 Is Indispensable for Regulatory T Cell Homeostasis and Function.” *Cell Reports* 36 (1): 109339.
- Khan, Mohd Moin, Meraj Hasan Khan, Ubaid Ullah Kalim, Sofia Khan, Sini Junntila, Niklas Paulin, Lingjia Kong, Omid Rasool, Laura L. Elo, and Riitta Lahesmaa. 2022. “Long Intergenic Noncoding RNA MIAT as a Regulator of Human Th17 Cell Differentiation.” *Frontiers in Immunology* 13 (June): 856762.

- Kim, Soo Hee, Se Hoon Kim, Woo Ick Yang, Soo Jeong Kim, and Sun Och Yoon. 2017. “Association of the Long Non-Coding RNA MALAT1 with the Polycomb Repressive Complex Pathway in T and NK Cell Lymphoma.” *Oncotarget* 8 (19): 31305–17.
- Kleaveland, Benjamin, Charlie Y. Shi, Joanna Stefano, and David P. Bartel. 2018. “A Network of Noncoding Regulatory RNAs Acts in the Mammalian Brain.” *Cell* 174 (2): 350–62.e17.
- Koh, Kyung Duk, Luke R. Bonser, Walter L. Eckalbar, Ofer Yizhar-Barnea, Jiangshan Shen, Xiaoning Zeng, Kirsten L. Hargett, et al. 2023. “Genomic Characterization and Therapeutic Utilization of IL-13-Responsive Sequences in Asthma.” *Cell Genomics* 3 (1): 100229.
- König, Julian, Kathi Zarnack, Gregor Rot, Tomaz Curk, Melis Kayikci, Blaz Zupan, Daniel J. Turner, Nicholas M. Luscombe, and Jernej Ule. 2010. “iCLIP Reveals the Function of hnRNP Particles in Splicing at Individual Nucleotide Resolution.” *Nature Structural & Molecular Biology* 17 (7): 909–15.
- Kontoyiannis, D., M. Pasparakis, T. T. Pizarro, F. Cominelli, and G. Kollias. 1999. “Impaired On/off Regulation of TNF Biosynthesis in Mice Lacking TNF AU-Rich Elements: Implications for Joint and Gut-Associated Immunopathologies.” *Immunity* 10 (3): 387–98.
- Kopp, Florian, and Joshua T. Mendell. 2018. “Functional Classification and Experimental Dissection of Long Noncoding RNAs.” *Cell* 172 (3): 393–407.

- Kumar, Brahma V., Wenji Ma, Michelle Miron, Tomer Granot, Rebecca S. Guyer, Dustin J. Carpenter, Takashi Senda, et al. 2017. "Human Tissue-Resident Memory T Cells Are Defined by Core Transcriptional and Functional Signatures in Lymphoid and Mucosal Sites." *Cell Reports* 20 (12): 2921–34.
- Kurtulus, Sema, Pulak Tripathi, Maria E. Moreno-Fernandez, Allyson Sholl, Jonathan D. Katz, H. Leighton Grimes, and David A. Hildeman. 2011. "Bcl-2 Allows Effector and Memory CD8+ T Cells to Tolerate Higher Expression of Bim." *Journal of Immunology* 186 (10): 5729–37.
- Langmead, Ben, and Steven L. Salzberg. 2012. "Fast Gapped-Read Alignment with Bowtie 2." *Nature Methods* 9 (4): 357–59.
- Lee, Hyun Hee, Nal Ae Yoon, Mai-Tram Vo, Chae Won Kim, Je Moon Woo, Hee Jeong Cha, Young Woo Cho, Byung Ju Lee, Wha Ja Cho, and Jeong Woo Park. 2012. "Tristetraprolin down-Regulates IL-17 through mRNA Destabilization." *FEBS Letters* 586 (1): 41–46.
- Lee, J. T., L. S. Davidow, and D. Warshawsky. 1999. "Tsix, a Gene Antisense to Xist at the X-Inactivation Centre." *Nature Genetics* 21 (4): 400–404.
- Leppek, Kathrin, Johanna Schott, Sonja Reitter, Fabian Poetz, Ming C. Hammond, and Georg Stoecklin. 2013. "Roquin Promotes Constitutive mRNA Decay via a Conserved Class of Stem-Loop Recognition Motifs." *Cell* 153 (4): 869–81.

- Leppik, Kathrin, and Georg Stoecklin. 2014. "An Optimized Streptavidin-Binding RNA Aptamer for Purification of Ribonucleoprotein Complexes Identifies Novel ARE-Binding Proteins." *Nucleic Acids Research* 42 (2): e13.
- Liang, Xiaoliang, Kushagra Gupta, Joselyn Rojas Quintero, Manuela Cernadas, Lester Kobzik, Helen Christou, Gerald B. Pier, Caroline A. Owen, and Sule Çataltepe. 2019. "Macrophage FABP4 Is Required for Neutrophil Recruitment and Bacterial Clearance in *Pseudomonas Aeruginosa* Pneumonia." *FASEB Journal: Official Publication of the Federation of American Societies for Experimental Biology* 33 (3): 3562–74.
- Li, Heng, Bob Handsaker, Alec Wysoker, Tim Fennell, Jue Ruan, Nils Homer, Gabor Marth, Goncalo Abecasis, Richard Durbin, and 1000 Genome Project Data Processing Subgroup. 2009. "The Sequence Alignment/Map Format and SAMtools." *Bioinformatics* 25 (16): 2078–79.
- Li, Hua-Bing, Jiyu Tong, Shu Zhu, Pedro J. Batista, Erin E. Duffy, Jun Zhao, Will Bailis, et al. 2017. "m6A mRNA Methylation Controls T Cell Homeostasis by Targeting the IL-7/STAT5/SOCS Pathways." *Nature* 548 (7667): 338–42.
- Lin, Jiangtao, Xin Zhou, Changzheng Wang, Chuntao Liu, Shaoxi Cai, and Mao Huang. 2018. "Symbicort® Maintenance and Reliever Therapy (SMART) and the Evolution of Asthma Management within the GINA Guidelines." *Expert Review of Respiratory Medicine* 12 (3): 191–202.

- Liu, Qin, Hanjiang Fu, Fang Sun, Haoming Zhang, Yi Tie, Jie Zhu, Ruiyun Xing, Zhixian Sun, and Xiaofei Zheng. 2008. “miR-16 Family Induces Cell Cycle Arrest by Regulating Multiple Cell Cycle Genes.” *Nucleic Acids Research* 36 (16): 5391–5404.
- Liu, Weijun, and Xiaowei Wang. 2019. “Prediction of Functional microRNA Targets by Integrative Modeling of microRNA Binding and Target Expression Data.” *Genome Biology* 20 (1): 18.
- Li, Yahui, Jason A. Estep, and Fedor V. Karginov. 2018. “Transcriptome-Wide Identification and Validation of Interactions between the miRNA Machinery and HuR on mRNA Targets.” *Journal of Molecular Biology* 430 (3): 285–96.
- Lloyd, Clare M., and Edith M. Hessel. 2010. “Functions of T Cells in Asthma: More than Just T(H)2 Cells.” *Nature Reviews. Immunology* 10 (12): 838–48.
- Loeb, Gabriel B., Aly A. Khan, David Canner, Joseph B. Hiatt, Jay Shendure, Robert B. Darnell, Christina S. Leslie, and Alexander Y. Rudensky. 2012. “Transcriptome-Wide miR-155 Binding Map Reveals Widespread Noncanonical microRNA Targeting.” *Molecular Cell* 48 (5): 760–70.
- Luan, Wenkang, Lubo Li, Yan Shi, Xuefeng Bu, Yun Xia, Jinlong Wang, Henry Siaw Djangmah, Xiaohui Liu, Yongping You, and Bin Xu. 2016. “Long Non-Coding RNA MALAT1 Acts as a Competing Endogenous RNA to Promote Malignant Melanoma Growth and Metastasis by Sponging miR-22.” *Oncotarget* 7 (39): 63901–12.
- Lu, Dong, Rinako Nakagawa, Sandra Lazzaro, Philipp Staudacher, Cei Abreu-Goodger, Tom Henley, Sara Boiani, et al. 2014. “The miR-155-PU.1 Axis Acts on Pax5 to Enable

Efficient Terminal B Cell Differentiation.” *The Journal of Experimental Medicine* 211 (11): 2183–98.

Maggirwar, S. B., E. W. Harhaj, and S. C. Sun. 1997. “Regulation of the Interleukin-2 CD28-Responsive Element by NF-ATp and Various NF-kappaB/Rel Transcription Factors.” *Molecular and Cellular Biology* 17 (5): 2605–14.

Mai, David, Omar Johnson, Jordan Reff, Ting-Jia Fan, John Scholler, Neil C. Sheppard, and Carl H. June. 2023. “Combined Disruption of T Cell Inflammatory Regulators Regnase-1 and Roquin-1 Enhances Antitumor Activity of Engineered Human T Cells.” *Proceedings of the National Academy of Sciences of the United States of America* 120 (12): e2218632120.

Mallory, Michael J., Samuel J. Allon, Jinsong Qiu, Matthew R. Gazzara, Iulia Tapescu, Nicole M. Martinez, Xiang-Dong Fu, and Kristen W. Lynch. 2015. “Induced Transcription and Stability of CELF2 mRNA Drives Widespread Alternative Splicing during T-Cell Signaling.” *Proceedings of the National Academy of Sciences of the United States of America* 112 (17): E2139–48.

Mandal, Pankaj K., Leonardo M. R. Ferreira, Ryan Collins, Torsten B. Meissner, Christian L. Boutwell, Max Friesen, Vladimir Vrbanac, et al. 2014. “Efficient Ablation of Genes in Human Hematopoietic Stem and Effector Cells Using CRISPR/Cas9.” *Cell Stem Cell* 15 (5): 643–52.

Martínez-Llordella, Marc, Jonathan H. Esensten, Samantha L. Bailey-Bucktrout, Robert H. Lipsky, Ann Marini, Jun Chen, Mohamed Mughal, Mark P. Mattson, Dennis D. Taub,

and Jeffrey A. Bluestone. 2013. “CD28-Inducible Transcription Factor DEC1 Is Required for Efficient Autoreactive CD4+ T Cell Response.” *The Journal of Experimental Medicine* 210 (8): 1603–19.

Martinez, Nicole M., Laura Agosto, Jinsong Qiu, Michael J. Mallory, Matthew R. Gazzara, Yoseph Barash, Xiang-Dong Fu, and Kristen W. Lynch. 2015. “Widespread JNK-Dependent Alternative Splicing Induces a Positive Feedback Loop through CELF2-Mediated Regulation of MKK7 during T-Cell Activation.” *Genes & Development* 29 (19): 2054–66.

Ma, Shengyun, Bing Zhou, Yohei Abe, Nicholas Chen, Claire Luo, Anna Zheng, Yuxin Li, et al. 2022. “LncRNA Malat1 Represses Th17 Effector Program by Maintaining a Critical Bivalent Super-Enhancer and Promotes Intestinal Inflammation.” *bioRxiv*.
<https://doi.org/10.1101/2022.03.21.485192>.

Masoumi, Farimah, Samira Ghorbani, Farideh Talebi, William G. Branton, Samira Rajaei, Christopher Power, and Farshid Noorbakhsh. 2019. “Malat1 Long Noncoding RNA Regulates Inflammation and Leukocyte Differentiation in Experimental Autoimmune Encephalomyelitis.” *Journal of Neuroimmunology* 328 (March): 50–59.

Masuda, Kazuya, Barry Ripley, Riko Nishimura, Takashi Mino, Osamu Takeuchi, Go Shioi, Hiroshi Kiyonari, and Tadamitsu Kishimoto. 2013. “Arid5a Controls IL-6 mRNA Stability, Which Contributes to Elevation of IL-6 Level in Vivo.” *Proceedings of the National Academy of Sciences of the United States of America* 110 (23): 9409–14.

- Masuda, Kazuya, Barry Ripley, Kishan Kumar Nyati, Praveen Kumar Dubey, Mohammad Mahabub-Uz Zaman, Hamza Hanieh, Mitsuru Higa, et al. 2016. "Arid5a Regulates Naive CD4+ T Cell Fate through Selective Stabilization of Stat3 mRNA." *The Journal of Experimental Medicine* 213 (4): 605–19.
- Matloubian, M., S. R. Kolhekar, T. Somasundaram, and R. Ahmed. 1993. "Molecular Determinants of Macrophage Tropism and Viral Persistence: Importance of Single Amino Acid Changes in the Polymerase and Glycoprotein of Lymphocytic Choriomeningitis Virus." *Journal of Virology* 67 (12): 7340–49.
- Ma, Weirui, and Christine Mayr. 2018. "A Membraneless Organelle Associated with the Endoplasmic Reticulum Enables 3'UTR-Mediated Protein-Protein Interactions." *Cell* 175 (6): 1492–1506.e19.
- McAuley, Grace E., Gloria Yiu, Patrick C. Chang, Gregory A. Newby, Beatriz Campo-Fernandez, Sorel T. Fitz-Gibbon, Xiaomeng Wu, et al. 2023. "Human T Cell Generation Is Restored in CD3 δ Severe Combined Immunodeficiency through Adenine Base Editing." *Cell*, March. <https://doi.org/10.1016/j.cell.2023.02.027>.
- Melgert, B. N., W. Timens, H. A. Kerstjens, M. Geerlings, M. A. Luinge, J. P. Schouten, D. S. Postma, and M. N. Hylkema. 2007. "Effects of 4 Months of Smoking in Mice with Ovalbumin-Induced Airway Inflammation." *Clinical and Experimental Allergy: Journal of the British Society for Allergy and Clinical Immunology* 37 (12): 1798–1808.
- Menzies-Gow, Andrew, Patrick Flood-Page, Roma Sehmi, John Burman, Qutayba Hamid, Douglas S. Robinson, A. Barry Kay, and Judah Denburg. 2003. "Anti-IL-5

(mepolizumab) Therapy Induces Bone Marrow Eosinophil Maturational Arrest and Decreases Eosinophil Progenitors in the Bronchial Mucosa of Atopic Asthmatics.” *The Journal of Allergy and Clinical Immunology* 111 (4): 714–19.

Mi, Huaiyu, Anushya Muruganujan, Xiaosong Huang, Dustin Ebert, Caitlin Mills, Xinyu Guo, and Paul D. Thomas. 2019. “Protocol Update for Large-Scale Genome and Gene Function Analysis with the PANTHER Classification System (v.14.0).” *Nature Protocols* 14 (3): 703–21.

Milner, J. Justin, Hongtuyet Nguyen, Kyla Omilusik, Miguel Reina-Campos, Matthew Tsai, Clara Toma, Arnaud Delpoux, et al. 2020. “Delineation of a Molecularly Distinct Terminally Differentiated Memory CD8 T Cell Population.” *Proceedings of the National Academy of Sciences of the United States of America* 117 (41): 25667–78.

Mino, Takashi, Noriki Iwai, Masayuki Endo, Kentaro Inoue, Kotaro Akaki, Fabian Hia, Takuya Uehata, et al. 2019. “Translation-Dependent Unwinding of Stem-Loops by UPF1 Licenses Regnase-1 to Degrade Inflammatory mRNAs.” *Nucleic Acids Research* 47 (16): 8838–59.

Mino, Takashi, Yasuhiro Murakawa, Akira Fukao, Alexis Vandebon, Hans-Hermann Wessels, Daisuke Ori, Takuya Uehata, et al. 2015. “Regnase-1 and Roquin Regulate a Common Element in Inflammatory mRNAs by Spatiotemporally Distinct Mechanisms.” *Cell* 161 (5): 1058–73.

Moore, Michael J., Nathalie E. Blachere, John J. Fak, Christopher Y. Park, Kirsty Sawicka, Salina Parveen, Ilana Zucker-Scharff, Bruno Moltedo, Alexander Y. Rudensky, and

Robert B. Darnell. 2018. “ZFP36 RNA-Binding Proteins Restrain T Cell Activation and Anti-Viral Immunity.” *eLife* 7 (May). <https://doi.org/10.7554/eLife.33057>.

Moore, Wendy C., Deborah A. Meyers, Sally E. Wenzel, W. Gerald Teague, Huashi Li, Xingnan Li, Ralph D’Agostino Jr, et al. 2010. “Identification of Asthma Phenotypes Using Cluster Analysis in the Severe Asthma Research Program.” *American Journal of Respiratory and Critical Care Medicine* 181 (4): 315–23.

Moran, Angela, and Ian D. Pavord. 2020. “Anti-IL-4/IL-13 for the Treatment of Asthma: The Story so Far.” *Expert Opinion on Biological Therapy* 20 (3): 283–94.

Murali-Krishna, K., J. D. Altman, M. Suresh, D. J. Sourdive, A. J. Zajac, J. D. Miller, J. Slansky, and R. Ahmed. 1998. “Counting Antigen-Specific CD8 T Cells: A Reevaluation of Bystander Activation during Viral Infection.” *Immunity* 8 (2): 177–87.

“Mus Musculus Annotation Report.” n.d. Accessed March 25, 2023.

https://www.ncbi.nlm.nih.gov/genome/annotation_euk/Mus_musculus/109/.

Nakagawa, Shinichi, Joanna Y. Ip, Go Shioi, Vidisha Tripathi, Xinying Zong, Tetsuro Hirose, and Kannanganattu V. Prasanth. 2012. “Malat1 Is Not an Essential Component of Nuclear Speckles in Mice.” *RNA* 18 (8): 1487–99.

Nassar, Ala F., Adam V. Wisnewski, and Khadir Raddassi. 2016. “Mass Cytometry Moving Forward in Support of Clinical Research: Advantages and Considerations.” *Bioanalysis* 8 (4): 255–57.

Nicolet, Benoit P., Nordin D. Zandhuis, V. Maria Lattanzio, and Monika C. Wolkers. 2021.

“Sequence Determinants as Key Regulators in Gene Expression of T Cells.”

Immunological Reviews 304 (1): 10–29.

Nie, Jiayan, and Qiu Zhao. 2020. “Lnc-ITSN1-2, Derived From RNA Sequencing, Correlates

With Increased Disease Risk, Activity and Promotes CD4⁺ T Cell Activation,

Proliferation and Th1/Th17 Cell Differentiation by Serving as a ceRNA for IL-23R via

Sponging miR-125a in Inflammatory Bowel Disease.” *Frontiers in Immunology* 11

(May): 852.

Nurk, Sergey, Sergey Koren, Arang Rhie, Mikko Rautiainen, Andrey V. Bzikadze, Alla

Mikheenko, Mitchell R. Vollger, et al. 2022. “The Complete Sequence of a Human

Genome.” *Science* 376 (6588): 44–53.

Oberdoerffer, Shalini, Luis Ferreira Moita, Daniel Neems, Rui P. Freitas, Nir Hacohen, and

Anjana Rao. 2008. “Regulation of CD45 Alternative Splicing by Heterogeneous

Ribonucleoprotein, hnRNPLL.” *Science* 321 (5889): 686–91.

Olson, Janelle A., Cameron McDonald-Hyman, Stephen C. Jameson, and Sara E. Hamilton.

2013. “Effector-like CD8⁺ T Cells in the Memory Population Mediate Potent Protective

Immunity.” *Immunity* 38 (6): 1250–60.

Ouafik, L ’houcine, Caroline Berenguer-Daize, and Yolande Berthois. 2009. “Adrenomedullin

Promotes Cell Cycle Transit and up-Regulates Cyclin D1 Protein Level in Human

Glioblastoma Cells through the Activation of c-Jun/JNK/AP-1 Signal Transduction

Pathway.” *Cellular Signalling* 21 (4): 597–608.

- Padem, Nurcicek, and Carol Saltoun. 2019. "Classification of Asthma." *Allergy and Asthma Proceedings: The Official Journal of Regional and State Allergy Societies* 40 (6): 385–88.
- Perez-Perri, Joel I., Birgit Rogell, Thomas Schwarzl, Frank Stein, Yang Zhou, Mandy Rettel, Annika Brosig, and Matthias W. Hentze. 2018. "Discovery of RNA-Binding Proteins and Characterization of Their Dynamic Responses by Enhanced RNA Interactome Capture." *Nature Communications* 9 (1): 4408.
- Petkau, Georg, Twm J. Mitchell, Krishnendu Chakraborty, Sarah E. Bell, Vanessa D Angeli, Louise Matheson, David J. Turner, et al. 2022. "The Timing of Differentiation and Potency of CD8 Effector Function Is Set by RNA Binding Proteins." *Nature Communications* 13 (1): 2274.
- Pilette, C., J. N. Francis, S. J. Till, and S. R. Durham. 2004. "CCR4 Ligands Are up-Regulated in the Airways of Atopic Asthmatics after Segmental Allergen Challenge." *The European Respiratory Journal: Official Journal of the European Society for Clinical Respiratory Physiology* 23 (6): 876–84.
- Pipkin, Matthew E., Jilian A. Sacks, Fernando Cruz-Guilloty, Mathias G. Lichtenheld, Michael J. Bevan, and Anjana Rao. 2010. "Interleukin-2 and Inflammation Induce Distinct Transcriptional Programs That Promote the Differentiation of Effector Cytolytic T Cells." *Immunity* 32 (1): 79–90.
- Platzer, Barbara, Madeleine Stout, and Edda Fiebiger. 2015. "Functions of Dendritic-Cell-Bound IgE in Allergy." *Molecular Immunology* 68 (2 Pt A): 116–19.

- Poliseno, Laura, Leonardo Salmena, Jiangwen Zhang, Brett Carver, William J. Haveman, and Pier Paolo Pandolfi. 2010. "A Coding-Independent Function of Gene and Pseudogene mRNAs Regulates Tumour Biology." *Nature* 465 (7301): 1033–38.
- Ponting, Chris P., and Wilfried Haerty. 2022. "Genome-Wide Analysis of Human Long Noncoding RNAs: A Provocative Review." *Annual Review of Genomics and Human Genetics*, April. <https://doi.org/10.1146/annurev-genom-112921-123710>.
- Popsicle: A Suite of Population Scale Analysis Tools for Single-Cell Genomics Data Including Implementation of Demuxlet / Freemuxlet Methods and Auxiliary Tools*. n.d. Github. Accessed May 14, 2023. <https://github.com/statgen/popsicle>.
- Qiao, Yong, Changliang Peng, Ji Li, Dongjin Wu, and Xiuwen Wang. n.d. "LncRNA MALAT1 Is Neuroprotective in a Rat Model of Spinal Cord Ischemia-Reperfusion Injury Through miR-204 Regulation." *Current Neurovascular Research* 15 (3): 211–19. Accessed March 7, 2022.
- Qi, Zhihong, Fang Wang, Guotao Yu, Di Wang, Yingpeng Yao, Menghao You, Jingjing Liu, et al. 2021. "SRSF1 Serves as a Critical Posttranscriptional Regulator at the Late Stage of Thymocyte Development." *Science Advances* 7 (16). <https://doi.org/10.1126/sciadv.abf0753>.
- Queiroz, Rayner M. L., Tom Smith, Eneko Villanueva, Maria Marti-Solano, Mie Monti, Mariavittoria Pizzinga, Dan-Mircea Mirea, et al. 2019. "Comprehensive Identification of RNA-Protein Interactions in Any Organism Using Orthogonal Organic Phase Separation (OOPS)." *Nature Biotechnology* 37 (2): 169–78.

- Quinlan, Aaron R. 2014. “BEDTools: The Swiss-Army Tool for Genome Feature Analysis.” *Current Protocols in Bioinformatics / Editorial Board, Andreas D. Baxevanis ... [et Al.]* 47 (September): 11.12.1–34.
- Raghavan, Arvind, Rachel L. Robison, Jennifer McNabb, Cameron R. Miller, Darlisha A. Williams, and Paul R. Bohjanen. 2001. “HuA and Tristetraprolin Are Induced Following T Cell Activation and Display Distinct but Overlapping RNA Binding Specificities *.” *The Journal of Biological Chemistry* 276 (51): 47958–65.
- Raundhal, Mahesh, Christina Morse, Anupriya Khare, Timothy B. Oriss, Jadranka Milosevic, John Trudeau, Rachael Huff, et al. 2015. “High IFN- γ and Low SLPI Mark Severe Asthma in Mice and Humans.” *The Journal of Clinical Investigation* 125 (8): 3037–50.
- Ricciardolo, Fabio L. M., Valentina Sorbello, Anna Folino, Fabio Gallo, Gian Mario Massaglia, Gabriella Favatà, Salvatore Conticello, et al. 2017. “Identification of IL-17F/frequent Exacerbator Endotype in Asthma.” *The Journal of Allergy and Clinical Immunology* 140 (2): 395–406.
- Rothrock, Caryn R., Amy E. House, and Kristen W. Lynch. 2005. “HnRNP L Represses Exon Splicing via a Regulated Exonic Splicing Silencer.” *The EMBO Journal* 24 (15): 2792–2802.
- Roth, Theodore L., Cristina Puig-Saus, Ruby Yu, Eric Shifrut, Julia Carnevale, P. Jonathan Li, Joseph Hiatt, et al. 2018. “Reprogramming Human T Cell Function and Specificity with Non-Viral Genome Targeting.” *Nature* 559 (7714): 405–9.

- Roychoudhuri, Rahul, David Clever, Peng Li, Yoshiyuki Wakabayashi, Kylie M. Quinn, Christopher A. Klebanoff, Yun Ji, et al. 2016. “BACH2 Regulates CD8(+) T Cell Differentiation by Controlling Access of AP-1 Factors to Enhancers.” *Nature Immunology* 17 (7): 851–60.
- Salerno, Fiamma, Sander Engels, Maartje van den Biggelaar, Floris P. J. van Alphen, Aurelie Guislain, Wanqi Zhao, Deborah L. Hodge, et al. 2018. “Translational Repression of Pre-Formed Cytokine-Encoding mRNA Prevents Chronic Activation of Memory T Cells.” *Nature Immunology* 19 (8): 828–37.
- Sandberg, Rickard, Joel R. Neilson, Arup Sarma, Phillip A. Sharp, and Christopher B. Burge. 2008. “Proliferating Cells Express mRNAs with Shortened 3' Untranslated Regions and Fewer microRNA Target Sites.” *Science* 320 (5883): 1643–47.
- Saradna, Arjun, Danh C. Do, Shruthi Kumar, Qing-Ling Fu, and Peisong Gao. 2018. “Macrophage Polarization and Allergic Asthma.” *Translational Research: The Journal of Laboratory and Clinical Medicine* 191 (January): 1–14.
- Schumann, Kathrin, Steven Lin, Eric Boyer, Dimitre R. Simeonov, Meena Subramaniam, Rachel E. Gate, Genevieve E. Haliburton, et al. 2015. “Generation of Knock-in Primary Human T Cells Using Cas9 Ribonucleoproteins.” *Proceedings of the National Academy of Sciences of the United States of America* 112 (33): 10437–42.
- Shankarling, Ganesh, Brian S. Cole, Michael J. Mallory, and Kristen W. Lynch. 2014. “Transcriptome-Wide RNA Interaction Profiling Reveals Physical and Functional Targets of hnRNP L in Human T Cells.” *Molecular and Cellular Biology* 34 (1): 71–83.

- Shapiro, V. S., K. E. Truitt, J. B. Imboden, and A. Weiss. 1997-7. “CD28 Mediates Transcriptional Upregulation of the Interleukin-2 (IL-2) Promoter through a Composite Element Containing the CD28RE and NF-IL-2B AP-1 Sites.” *Molecular and Cellular Biology* 17 (7): 4051–58.
- Shehata, Hesham M., Shahzada Khan, Elise Chen, Patrick E. Fields, Richard A. Flavell, and Shomyseh Sanjabi. 2018. “Lack of Sprouty 1 and 2 Enhances Survival of Effector CD8+ T Cells and Yields More Protective Memory Cells.” *Proceedings of the National Academy of Sciences of the United States of America* 115 (38): E8939–47.
- Shi, Charlie Y., Elena R. Kingston, Benjamin Kleaveland, Daniel H. Lin, Michael W. Stubna, and David P. Bartel. 2020. “The ZSWIM8 Ubiquitin Ligase Mediates Target-Directed microRNA Degradation.” *Science* 370 (6523). <https://doi.org/10.1126/science.abc9359>.
- Shui, Xiaolong, Shaomin Chen, Jinti Lin, Jianzhong Kong, Chengwei Zhou, and Jiaozhen Wu. 2019. “Knockdown of lncRNA NEAT1 Inhibits Th17/CD4+ T Cell Differentiation through Reducing the STAT3 Protein Level.” *Journal of Cellular Physiology* 234 (12): 22477–84.
- Shulman, Ziv, and Noam Stern-Ginossar. 2020. “The RNA Modification N6-Methyladenosine as a Novel Regulator of the Immune System.” *Nature Immunology* 21 (5): 501–12.
- Siddiqui, Sana, Kristina Johansson, Alex Joo, Luke R. Bonser, Kyung Duk Koh, Olivier Le Tonqueze, Samaneh Bolourchi, et al. 2021. “Epithelial miR-141 Regulates IL-13-Induced Airway Mucus Production.” *JCI Insight* 6 (5). <https://doi.org/10.1172/jci.insight.139019>.

- Siracusa, Mark C., Brian S. Kim, Jonathan M. Spergel, and David Artis. 2013. "Basophils and Allergic Inflammation." *The Journal of Allergy and Clinical Immunology* 132 (4): 789–801; quiz 788.
- Stellato, Cristiana, Matthew M. Gubin, Joseph D. Magee, Xi Fang, Jinshui Fan, Danielle M. Tartar, Jing Chen, et al. 2011. "Coordinate Regulation of GATA-3 and Th2 Cytokine Gene Expression by the RNA-Binding Protein HuR." *Journal of Immunology* 187 (1): 441–49.
- Strazza, Marianne, and Adam Mor. 2017. "Consider the Chemokines: A Review of the Interplay Between Chemokines and T Cell Subset Function." *Discovery Medicine* 24 (130): 31–39.
- Stuart, Tim, Andrew Butler, Paul Hoffman, Christoph Hafemeister, Efthymia Papalexi, William M. Mauck 3rd, Yuhao Hao, Marlon Stoeckius, Peter Smibert, and Rahul Satija. 2019. "Comprehensive Integration of Single-Cell Data." *Cell* 177 (7): 1888–1902.e21.
- Su, Kai, Nannan Wang, Qianqian Shao, Hao Liu, Bao Zhao, and Shiyin Ma. 2021. "The Role of a ceRNA Regulatory Network Based on lncRNA MALAT1 Site in Cancer Progression." *Biomedicine & Pharmacotherapy = Biomedecine & Pharmacotherapie* 137 (May): 111389.
- Suresh, M., J. K. Whitmire, L. E. Harrington, C. P. Larsen, T. C. Pearson, J. D. Altman, and R. Ahmed. 2001. "Role of CD28-B7 Interactions in Generation and Maintenance of CD8 T Cell Memory." *Journal of Immunology* 167 (10): 5565–73.

- Tanaka, Satoshi, and Kazuyuki Furuta. 2021. "Roles of IgE and Histamine in Mast Cell Maturation." *Cells* 10 (8). <https://doi.org/10.3390/cells10082170>.
- Tang, Monica, Brett M. Elicker, Travis Henry, David S. Gierada, Mark L. Schiebler, Brendan K. Huang, Michael C. Peters, et al. 2022. "Mucus Plugs Persist in Asthma, and Changes in Mucus Plugs Associate with Changes in Airflow over Time." *American Journal of Respiratory and Critical Care Medicine* 205 (9): 1036–45.
- Tavernier, S. J., V. Athanasopoulos, P. Verloo, G. Behrens, J. Staal, D. J. Bogaert, L. Naesens, et al. 2019. "A Human Immune Dysregulation Syndrome Characterized by Severe Hyperinflammation with a Homozygous Nonsense Roquin-1 Mutation." *Nature Communications* 10 (1): 4779.
- Till, S. J., S. R. Durham, K. Rajakulasingam, M. Humbert, D. Huston, R. Dickason, A. B. Kay, and C. J. Corrigan. 1998. "Allergen-Induced Proliferation and Interleukin-5 Production by Bronchoalveolar Lavage and Blood T Cells after Segmental Allergen Challenge." *American Journal of Respiratory and Critical Care Medicine* 158 (2): 404–11.
- Tong, Jiyu, Guangchao Cao, Ting Zhang, Esen Sefik, Maria Carolina Amezcuca Vesely, James P. Broughton, Shu Zhu, et al. 2018. "m6A mRNA Methylation Sustains Treg Suppressive Functions." *Cell Research* 28 (2): 253–56.
- Toumi, Ryma, Yevgeniy Yuzefpolskiy, Adithya Vegaraju, Hanxi Xiao, Kendall A. Smith, Surojit Sarkar, and Vandana Kalia. 2022. "Autocrine and Paracrine IL-2 Signals

Collaborate to Regulate Distinct Phases of CD8 T Cell Memory.” *Cell Reports* 39 (2): 110632.

Trendel, Jakob, Thomas Schwarzl, Rastislav Horos, Ananth Prakash, Alex Bateman, Matthias W. Hentze, and Jeroen Krijgsveld. 2019. “The Human RNA-Binding Proteome and Its Dynamics during Translational Arrest.” *Cell* 176 (1-2): 391–403.e19.

Tripathi, Vidisha, Jonathan D. Ellis, Zhen Shen, David Y. Song, Qun Pan, Andrew T. Watt, Susan M. Freier, et al. 2010. “The Nuclear-Retained Noncoding RNA MALAT1 Regulates Alternative Splicing by Modulating SR Splicing Factor Phosphorylation.” *Molecular Cell* 39 (6): 925–38.

Uehata, Takuya, Hidenori Iwasaki, Alexis Vandenbon, Kazufumi Matsushita, Eduardo Hernandez-Cuellar, Kanako Kuniyoshi, Takashi Satoh, et al. 2013. “Malt1-Induced Cleavage of Regnase-1 in CD4(+) Helper T Cells Regulates Immune Activation.” *Cell* 153 (5): 1036–49.

Ule, Jernej, Kirk Jensen, Aldo Mele, and Robert B. Darnell. 2005. “CLIP: A Method for Identifying Protein-RNA Interaction Sites in Living Cells.” *Methods* 37 (4): 376–86.

Urdaneta, Erika C., Carlos H. Vieira-Vieira, Timon Hick, Hans-Herrmann Wessels, Davide Figini, Rebecca Moschall, Jan Medenbach, et al. 2019. “Purification of Cross-Linked RNA-Protein Complexes by Phenol-Toluol Extraction.” *Nature Communications* 10 (1): 990.

Vandenberghe, P., J. Verwilghen, F. Van Vaeck, and J. L. Ceuppens. 1993. “Ligation of the CD5 or CD28 Molecules on Resting Human T Cells Induces Expression of the Early

Activation Antigen CD69 by a Calcium- and Tyrosine Kinase-Dependent Mechanism.”
Immunology 78 (2): 210–17.

Van der Auwera, Geraldine A., Mauricio O. Carneiro, Christopher Hartl, Ryan Poplin,
Guillermo Del Angel, Ami Levy-Moonshine, Tadeusz Jordan, et al. 2013. “From FastQ
Data to High Confidence Variant Calls: The Genome Analysis Toolkit Best Practices
Pipeline.” *Current Protocols in Bioinformatics / Editorial Board, Andreas D.*
Baxevanis ... [et Al.] 43 (1110): 11.10.1–11.10.33.

Van Nostrand, Eric L., Gabriel A. Pratt, Alexander A. Shishkin, Chelsea Gelboin-Burkhart,
Mark Y. Fang, Balaji Sundararaman, Steven M. Blue, et al. 2016. “Robust
Transcriptome-Wide Discovery of RNA-Binding Protein Binding Sites with Enhanced
CLIP (eCLIP).” *Nature Methods* 13 (6): 508–14.

Vogel, Katharina U., Stephanie L. Edlmann, Katharina M. Jeltsch, Arianna Bertossi, Klaus
Heger, Gitta A. Heinz, Jessica Zöllner, et al. 2013. “Roquin Paralogs 1 and 2 Redundantly
Repress the Icos and Ox40 Costimulator mRNAs and Control Follicular Helper T Cell
Differentiation.” *Immunity* 38 (4): 655–68.

Wang, Qing-Ming, Guang-Yu Lian, Yuan Song, Yan-Fang Huang, and Yi Gong. 2019.
“LncRNA MALAT1 Promotes Tumorigenesis and Immune Escape of Diffuse Large B
Cell Lymphoma by Sponging miR-195.” *Life Sciences* 231 (August): 116335.

Wang, Xiao, Zhike Lu, Adrian Gomez, Gary C. Hon, Yanan Yue, Dali Han, Ye Fu, et al.
2014. “N6-Methyladenosine-Dependent Regulation of Messenger RNA Stability.”
Nature 505 (7481): 117–20.

- Wang, Yaping, Peng Wu, Rufeng Lin, Liucheng Rong, Yao Xue, and Yongjun Fang. 2015. “LncRNA NALT Interaction with NOTCH1 Promoted Cell Proliferation in Pediatric T Cell Acute Lymphoblastic Leukemia.” *Scientific Reports* 5 (September): 13749.
- Wei, Jun, Lingyun Long, Wenting Zheng, Yogesh Dhungana, Seon Ah Lim, Cliff Guy, Yanyan Wang, et al. 2019. “Targeting REGNASE-1 Programs Long-Lived Effector T Cells for Cancer Therapy.” *Nature* 576 (7787): 471–76.
- Welten, Suzanne P. M., Anke Redeker, Kees L. M. C. Franken, Jennifer D. Oduro, Ferry Ossendorp, Luka Čičin-Šain, Cornelis J. M. Melief, Peter Aichele, and Ramon Arens. 2015. “The Viral Context Instructs the Redundancy of Costimulatory Pathways in Driving CD8(+) T Cell Expansion.” *eLife* 4 (August).
<https://doi.org/10.7554/eLife.07486>.
- Wenzel, Sally, Mario Castro, Jonathan Corren, Jorge Maspero, Lin Wang, Bingzhi Zhang, Gianluca Pirozzi, et al. 2016. “Dupilumab Efficacy and Safety in Adults with Uncontrolled Persistent Asthma despite Use of Medium-to-High-Dose Inhaled Corticosteroids plus a Long-Acting β 2 Agonist: A Randomised Double-Blind Placebo-Controlled Pivotal Phase 2b Dose-Ranging Trial.” *The Lancet* 388 (10039): 31–44.
- Wheeler, Benjamin D., John D. Gagnon, Wandi S. Zhu, Priscila Muñoz-Sandoval, Simon K. Wong, Dimitre R. Simeonov, Zhongmei Li, et al. 2023. “The lncRNA Malat1 Inhibits miR-15/16 to Enhance Cytotoxic T Cell Activation and Memory Cell Formation.” *bioRxiv*. <https://doi.org/10.1101/2023.04.14.536843>.

- Wherry, E. John, and Rafi Ahmed. 2004. "Memory CD8 T-Cell Differentiation during Viral Infection." *Journal of Virology* 78 (11): 5535–45.
- Whyte, Carly E., Kailash Singh, Oliver T. Burton, Meryem Aloulou, Lubna Kouser, Rafael Valente Veiga, Amy Dashwood, et al. 2022. "Context-Dependent Effects of IL-2 Rewire Immunity into Distinct Cellular Circuits." *The Journal of Experimental Medicine* 219 (7). <https://doi.org/10.1084/jem.20212391>.
- Wigton, Eric J., Yohei Mikami, Ryan J. McMonigle, Carlos A. Castellanos, Adam K. Wade-Vallance, Simon K. Zhou, Robin Kageyama, et al. 2021. "MicroRNA-Directed Pathway Discovery Elucidates an miR-221/222-Mediated Regulatory Circuit in Class Switch Recombination." *The Journal of Experimental Medicine* 218 (11). <https://doi.org/10.1084/jem.20201422>.
- Wilusz, Jeremy E., Susan M. Freier, and David L. Spector. 2008. "3' End Processing of a Long Nuclear-Retained Noncoding RNA Yields a tRNA-like Cytoplasmic RNA." *Cell* 135 (5): 919–32.
- Wilusz, Jeremy E., Hongjae Sunwoo, and David L. Spector. 2009. "Long Noncoding RNAs: Functional Surprises from the RNA World." *Genes & Development* 23 (13): 1494–1504.
- Winzen, Reinhard, Basant Kumar Thakur, Oliver Dittrich-Breiholz, Meera Shah, Natalie Redich, Sonam Dhamija, Michael Kracht, and Helmut Holtmann. 2007. "Functional Analysis of KSRP Interaction with the AU-Rich Element of Interleukin-8 and Identification of Inflammatory mRNA Targets." *Molecular and Cellular Biology* 27 (23): 8388–8400.

- Wojciechowski, Sara, Pulak Tripathi, Tristan Bourdeau, Luis Acero, H. Leighton Grimes, Jonathan D. Katz, Fred D. Finkelman, and David A. Hildeman. 2007. "Bim/Bcl-2 Balance Is Critical for Maintaining Naive and Memory T Cell Homeostasis." *The Journal of Experimental Medicine* 204 (7): 1665–75.
- Wu, Jian, Hanlu Zhang, Yang Zheng, Xiangyuan Jin, Mingyang Liu, Shuang Li, Qi Zhao, et al. 2018. "The Long Noncoding RNA MALAT1 Induces Tolerogenic Dendritic Cells and Regulatory T Cells via miR155/Dendritic Cell-Specific Intercellular Adhesion Molecule-3 Grabbing Nonintegrin/IL10 Axis." *Frontiers in Immunology* 9 (August): 1847.
- Wu, Yuxuan, Dan Liang, Yinghua Wang, Meizhu Bai, Wei Tang, Shiming Bao, Zhiqiang Yan, Dangsheng Li, and Jinsong Li. 2013. "Correction of a Genetic Disease in Mouse via Use of CRISPR-Cas9." *Cell Stem Cell* 13 (6): 659–62.
- Xiao, Haibing, Kun Tang, Peijun Liu, Ke Chen, Junhui Hu, Jin Zeng, Wei Xiao, et al. 2015. "LncRNA MALAT1 Functions as a Competing Endogenous RNA to Regulate ZEB2 Expression by Sponging miR-200s in Clear Cell Kidney Carcinoma." *Oncotarget* 6 (35): 38005–15.
- Xie, Chengxia, Shengjie Wang, He Zhang, Yalan Zhu, Pengjun Jiang, Shiya Shi, Yanjun Si, and Jie Chen. 2023. "Lnc-AIFM2-1 Promotes HBV Immune Escape by Acting as a ceRNA for miR-330-3p to Regulate CD244 Expression." *Frontiers in Immunology* 14 (February): 1121795.

- Xie, Haibiao, Xinhui Liao, Zhicong Chen, Yuan Fang, Anbang He, Yucheng Zhong, Qunjun Gao, et al. 2017. “LncRNA MALAT1 Inhibits Apoptosis and Promotes Invasion by Antagonizing miR-125b in Bladder Cancer Cells.” *Journal of Cancer* 8 (18): 3803–11.
- Xu, Jichuan, Jian Xu, Xinyuan Liu, and Jianxin Jiang. 2022. “The Role of lncRNA-Mediated ceRNA Regulatory Networks in Pancreatic Cancer.” *Cell Death Discovery* 8 (1): 287.
- Yang, Liang-Zhong, Yang Wang, Si-Qi Li, Run-Wen Yao, Peng-Fei Luan, Huang Wu, Gordon G. Carmichael, and Ling-Ling Chen. 2019. “Dynamic Imaging of RNA in Living Cells by CRISPR-Cas13 Systems.” *Molecular Cell* 76 (6): 981–97.e7.
- Yang, Wen-Lan, Weinan Qiu, Ting Zhang, Kai Xu, Zi-Juan Gu, Yu Zhou, Heng-Ji Xu, et al. 2023. “Nsun2 Coupling with RoRyt Shapes the Fate of Th17 Cells and Promotes Colitis.” *Nature Communications* 14 (1): 863.
- Yao, Yingpeng, Wenhui Guo, Jingjing Chen, Pingting Guo, Guotao Yu, Juanjuan Liu, Fang Wang, et al. 2018. “Long Noncoding RNA Malat1 Is Not Essential for T Cell Development and Response to LCMV Infection.” *RNA Biology* 15 (12): 1477–86.
- Yao, Yingpeng, Ying Yang, Wenhui Guo, Lifan Xu, Menghao You, Yi-Chang Zhang, Zhen Sun, et al. 2021. “METTL3-Dependent m6A Modification Programs T Follicular Helper Cell Differentiation.” *Nature Communications* 12 (1): 1333.
- Zaman, Mohammad Mahabub-Uz, Kazuya Masuda, Kishan Kumar Nyati, Praveen Kumar Dubey, Barry Ripley, Kai Wang, Jaya Prakash Chalise, Mitsuru Higa, Hamza Hanieh, and Tadamitsu Kishimoto. 2016. “Arid5a Exacerbates IFN- γ -Mediated Septic Shock by

Stabilizing T-Bet mRNA.” *Proceedings of the National Academy of Sciences of the United States of America* 113 (41): 11543–48.

Zhang, Lei, Keming Zhang, Wenjie Fang, Hang Li, Yingfang Li, Weiwei Jiang, Dongying Hu, et al. 2020. “CircRNA-1806 Decreases T Cell Apoptosis and Prolongs Survival of Mice After Cryptococcal Infection by Sponging miRNA-126.” *Frontiers in Microbiology* 11 (November): 596440.

Zhang, Yanyan, Baohua Li, Qiang Bai, Pengcheng Wang, Gang Wei, Zhirong Li, Li Hu, et al. 2021. “The lncRNA Snhg1-Vps13D Vesicle Trafficking System Promotes Memory CD8 T Cell Establishment via Regulating the Dual Effects of IL-7 Signaling.” *Signal Transduction and Targeted Therapy* 6 (1): 126.

Zhang, Zhongfu, Jieqing Chen, Zhongshuang Zhu, Zhongqing Zhu, Xinhui Liao, Jianting Wu, Jianli Cheng, Xintao Zhang, Hongbing Mei, and Guosheng Yang. 2020. “CRISPR-Cas13-Mediated Knockdown of lncRNA-GACAT3 Inhibited Cell Proliferation and Motility, and Induced Apoptosis by Increasing p21, Bax, and E-Cadherin Expression in Bladder Cancer.” *Frontiers in Molecular Biosciences* 7: 627774.

Zhao, Hanfei, Ying Liu, Lixia Wang, Gang Jin, Xiaocui Zhao, Jing Xu, Guangyue Zhang, Yuying Ma, Na Yin, and Min Peng. 2021. “Genome-Wide Fitness Gene Identification Reveals Roquin as a Potent Suppressor of CD8 T Cell Expansion and Anti-Tumor Immunity.” *Cell Reports* 37 (10): 110083.

Zhao, Lianhe, Jiajia Wang, Yanyan Li, Tingrui Song, Yang Wu, Shuangfang Fang, Dechao Bu, et al. 2021. “NONCODEV6: An Updated Database Dedicated to Long Non-Coding

RNA Annotation in Both Animals and Plants.” *Nucleic Acids Research* 49 (D1): D165–71.

Zhao, Ping, Meng-Meng Ji, Ying Fang, Xiao Li, Hong-Mei Yi, Zi-Xun Yan, Shu Cheng, et al. 2021. “A Novel lncRNA TCLlnc1 Promotes Peripheral T Cell Lymphoma Progression through Acting as a Modular Scaffold of HNRNPD and YBX1 Complexes.” *Cell Death & Disease* 12 (4): 321.

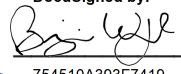
Zheng, Simin, Bao Q. Vuong, Bharat Vaidyanathan, Jia-Yu Lin, Feng-Ting Huang, and Jayanta Chaudhuri. 2015. “Non-Coding RNA Generated Following Lariat Debranching Mediates Targeting of AID to DNA.” *Cell* 161 (4): 762–73.

Zhou, Jing, Xingli Zhang, Jiajia Hu, Rihao Qu, Zhibin Yu, Hao Xu, Huifang Chen, et al. 2021. “m⁶A Demethylase ALKBH5 Controls CD4⁺ T Cell Pathogenicity and Promotes Autoimmunity.” *Science Advances* 7 (25). <https://doi.org/10.1126/sciadv.abg0470>.

Publishing Agreement

It is the policy of the University to encourage open access and broad distribution of all theses, dissertations, and manuscripts. The Graduate Division will facilitate the distribution of UCSF theses, dissertations, and manuscripts to the UCSF Library for open access and distribution. UCSF will make such theses, dissertations, and manuscripts accessible to the public and will take reasonable steps to preserve these works in perpetuity.

I hereby grant the non-exclusive, perpetual right to The Regents of the University of California to reproduce, publicly display, distribute, preserve, and publish copies of my thesis, dissertation, or manuscript in any form or media, now existing or later derived, including access online for teaching, research, and public service purposes.

DocuSigned by:

754510A393F7419... Author Signature

5/19/2023
Date